Application of capacitor commutated converters in multi-infeed HVDC-schemes

by
Magne Meisingset

A thesis
submitted to the Faculty of Graduate Studies
in partial fulfilment of the requirements for the
degree of Doctor of Philosophy

at

The University of Manitoba,
Department of
Electrical and Computer Engineering

Winnipeg, Manitoba, Canada

THE UNIVERSITY OF MANITOBA

FACULTY OF GRADUATE STUDIES

*****

COPYRIGHT PERMISSION PAGE

APPLICATION OF CAPACITOR COMMUTATED CONVERTERS IN MULTI-INFEED HVDC-SCHEMES

BY

MAGNE MEISINGSET

A Thesis/Practicum submitted to the Faculty of Graduate Studies of The University of Manitoba in partial fulfillment of the requirements of the degree

of

DOCTOR OF PHILOSOPHY

ACKNOWLEDGEMENTS

The author expresses his sincere gratitude to his advisor throughout this work, Prof. A.M. Golé. I have greatly appreciated the opportunity to gain knowledge of his expertise in the field of HVDC and power electronics. Professor Golé has not only been an inspiring supervisor, but has through his pleasant personality and wide-ranging knowledge made this time a very enjoyable one.

I gratefully acknowledge my employer, Statnett SF - The Norwegian Power Grid Company in Oslo, for the financial support to this work.

The author appreciates the technical assistance provided by D. Brandt of Brandt and Rashwan Consultants Inc., R.S. Burton of Teshmont Consultants Inc., in Winnipeg and T.R. Time of Statnett SF in Oslo. My colleagues, both professors and graduate students, at the Department of Electrical and Computer Engineering at the University of Manitoba also deserve many thanks for their helpfulness.

I am grateful to my new friends in Winnipeg, Erik, Eilef, Veronica, Milton, Vanya, Debbie and Gratton, who have given me a very enjoyable social life. By introducing me to Canadian culture, politics and history, Erik and Eilef made my time in Canada more interesting and informative, also in fields other than science. It has also been enjoyable to be a part of the F.C. Winnipeg and A.F.F. soccer teams. I thank the Thorne-Tjomslands for hosting me during my first week in Winnipeg.

Special thanks are extended to my family in Norway and Australia. Finally, I want to thank Åsne, for her support and patience during the time I worked on this thesis.

Magne Meisingset

Winnipeg, May 2000

ABSTRACT

The capacitor commutated converter (CCC) is a new type of HVDC converter topology which shows promise for use in long distance transmission via cables. This technology is, thus, a potential candidate for use in HVDC transmission across large bodies of water. This thesis investigates the suitability of CCC in such applications using electromagnetic transient simulation.

An analytical formulation is first developed, which is used to investigate the steady-state behaviour of both the CCC and the conventional HVDC converter. The results indicate that the CCC is superior to the conventional in terms of stability margin when operated in power control.

Two new control strategies are developed because the traditional control strategy was found unsuitable in long cable HVDC-transmission. The suitability of the CCC-inverter in a long cable HVDC-scheme was examined for both control options.

Ac-filters at near-unity-power-factor converters, such as the CCC, require some mechanism of on-line tuning due to their sensitivity to detuning effects. An active filter, based on a voltage source converter, is developed to ensure satisfactory filtering performance.

Finally, the suitability of the CCC-inverter is investigated in a network configuration where two HVDC-links are feeding power into a common ac-network. The multi-infeed HVDC-scheme under study is a simplified representation of the existing and planned HVDC-connections in Norway. The results indicated that the presence of the CCC-inverter does not have an uniformly favourable impact on the multi-infeed HVDC scheme's performance. The scheme demonstrated, nevertheless, satisfactory transient performance regardless of the converter type employed at the inverter.

TABLE OF CONTENTS

Chapter 1

INTRODUCTION

1.1 DEREGULATION AND POWER MARKETS

In the recent decade, many parts of the world have experienced a fundamental re-structuring of their electricity industry involving de-regulation and realisation of competitive power markets [6]. The de-regulation divides former publicly-owned vertically-integrated power utilities into a generation part and a transmission part, because these two business sectors may have conflicting interests in a power market environment. The generation companies are now subject to competition with the view to increase efficiency. The Nordic countries provide a good example of this world-wide trend as this process took place already in the early 1990s, starting with Norway in 1991. The Nordic Power Exchange, Nord Pool ASA, is the first international electricity exchange and organises today a well-functioning power market [30] with participants from most countries in the region. One may, however, wonder if an integrated and sustainable development of the entire power system infrastructure is achievable in such a deregulated environment.

This new environment has opened new opportunities for the generation companies since they now are driven by profit-maximising, as the market is free of government regulation. Generation companies in Norway have therefore been aware of the possibility that it could be profitable to access the higher-priced central European market through long submarine HVDC-cables across the North Sea.

Several HVDC-schemes connecting Norway to Germany and the Netherlands, are currently in the planning stage which involve cable lengths of roughly 600 km. These cable-lengths are more than

twice the length of the world's longest HVDC-cable today; the Baltic Cable which runs between Sweden and Germany. Although these extremely long cable HVDC-projects are not expected to generate insurmountable technical problems, there are aspects that require special attention. One of the challenges is to design a control system which masters the unique characteristic of the large dc cable capacitance between the rectifier and the inverter.

1.2 MAIN FOCUS

Today's power networks are becoming highly interconnected partly due to the deregulated environment in the electricity industry. HVDC-transmission is a particularly interesting concept in this regard, since it allows the transfer of power between non-synchronous ac networks through long submarine cables. Ac networks which contain dc-infeed from several HVDC transmission links in electrical vicinity of each other, are termed as multi-infeed HVDC-schemes throughout this thesis. Several problems may arise in such multi-infeed schemes. They include interactions between the dc-links due to the low impedance between the inverter ac buses as well as transient problems such as contiguous commutation failures. The problems are expected to be worse when the receiving ac network is weak and the dc lines consist of long cables.

Conventional HVDC converters have a serious limitation in that they rely on the ac network voltage for the turn-off of the thyristor valves. The robustness of the ac network is therefore of critical importance for proper operation of such converters. Disturbances to the ac network caused by transients in one of the dc infeeds can cause serious problems for the other infeeds. Buseman [7] introduced already in 1954 an HVDC-topology, which utilises series capacitors for generating a portion of the voltage required for thyristor valve commutation. This HVDC-converter topology is referred to as the Capacitor Commutated Converter (CCC) and has been reported on by several other authors [9,11,12,13]. Other types of artificially commutated converters have also been discussed in literature [8,10]. The CCC converter, which only recently have been made available

by manufacurers, appears much less dependent on the ac network strength and on other network disturbances for successful valve commutation. Therefore, it should offer an attractive alternative to conventional dc transmission in multi-infeed HVDC-schemes.

The main focus of this thesis is therefore to investigate the suitability of CCC-inverters in long cable multi-infeed HVDC-schemes is beneficial. This topic was chosen due to the author's affiliation, The Norwegian Power Grid Company (Statnett SF). Appendix 1 provides a brief explanation of frequently used technical terms related to HVDC and power electronics in the thesis.

1.3 OVERVIEW OF THE REPORT

Chapter 2 gives a general introduction to the concept of Capacitor Commutated Converter (CCC). The CCC is basicly a conventional HVDC converter modified with the addition of series capacitors between the transformer and the valve in each phase. Advantages and disadvantages related to the CCC compared to the conventional converter are briefly pointed out.

Chapter 3 examines the operation characteristics of the CCC and serves as an introduction to later chapters where the converter is used in long cable single- and multi-infeed HVDC schemes. The steady-state behaviour of a 6-pulse CCC-inverter of 800 MW power rating is examined by an analytical formulation, which involves 18 variables and 14 non-linear equations. Four variables need to be pre-specified and the Newton-Raphson iterative technique is applied to reach a steady-state solution. This formulation is implemented a Fortran program which is designed to also present parametric plots. A parametric plot consists of a number of succeeding steady-state solutions where one of the pre-specified variables (in this case the dc-current) is slightly increased from one solution to the next. The maximum dc-power capacity and other variables of interest are plotted both for the CCC and for the conventional converter.

The CCC inverter configuration is, thereafter, modelled and simulated in an electromagnetic

transient simulation program in order to validate the results from the analytical formulation. This type of study integrates the non-linear differential equations, presents time-domain results and is thus a better representation of the real system. The principal operation of the CCC-inverter is first described while operating in apparent extinction angle control. Then, the steady-state value of several quantities are recorded at different levels of dc-current and compared to the corresponding results obtained from the analytical formulation. The analytical and simulated results agree well, which validates the CCC steady-state equations as well as the accuracy of the simulation model.

Chapter 4 describes the modelling of two 1200 MW long cable single-infeed HVDC schemes with different converter types employed at their inverters. The first alternative has conventional inverters, whereas the second uses CCC-type inverters. Both schemes terminate in a very weak receiving ac-network. The modelling includes converters, ac network equivalent, converter transformers, ac-filters, dc-cable, thyristor valve firing scheme and controls. Design considerations for the series capacitance (only for the CCC) and its surge arrestor are also included. An algorithm is developed for both apparent and real extinction angle measurement at the CCC-inverter. The traditional control with current control at the rectifier and extinction angle control at the inverter, is found unsuited in such long cable HVDC-applications. Two new control options are therefore developed to handle the unique characteristics of the large cable capacitance.

Chapter 5 investigates the transient behaviour of the conventional and the CCC single-infeed HVDC schemes, developed in the previous chapter, when various fault and disturbances are applied on the inverter side. The schemes' performance are examined for both control options with the view to determine if the presence of CCC-inverters in long cable dc transmission is beneficial.

Chapter 6 explains why ac-filters at CCC-buses require some mechanism of on-line tuning to keep the filters tuned to their targeted harmonic frequencies. An active filter based on a voltage source converter (VSC), using IGBTs as switching devices, is developed to meet this requirement.

The filter targets only the most significant characteristic harmonics, e.g. the 11th and the 13th. The filter design is described in detail including its topology, controls and coupling filter to the ac-network. The operation of the filter is illustrated by removing the harmonic currents generated by a current source. The rating of the filter depends primarily on the amount of harmonic current to be removed and the expected degree of de-tuning in the coupling filters. The filter output voltage is limited by the maximum voltage rating of the IGBT switching devices in the VSC. This voltage is boosted up by a transformer in order to achieve harmonic removal at the converter bus voltage. The active filter is investigated at a CCC-inverter in a 1200 MW long cable HVDC-scheme. The active filter demonstrates satisfactory filtering performance and shows no adverse impact on the operation of the HVDC-scheme. The proposed filter should therefore be attractive in the view of the expected application of near-unity-power-factor converters such as the CCC.

Chapter 7 describes the modelling of three multi-infeed long cable HVDC schemes, each being a simplified representation of the existing and planned HVDC-connections in the Norwegian power grid. Each alternative consists of a 1200 MW and a 1600 MW HVDC-connection feeding power into a weak ac-network, but with different combinations of inverter types. *The conventional multi-infeed HVDC alternative employs conventional inverters in both dc-links, the mixed alternative is a mix of the conventional (1600 MW link) and the CCC (1200 MW link) types, whereas the CCC multi-infeed alternative uses CCC-inverters in both dc-links.* The conventional and CCC single-infeed dc-links, developed in Chapter 4, are employed in the multi-infeed alternatives. The two additional dc-links are generated by simply scaling up the 1200 MW links to 1600 MW power rating. The 1200 MW and the 1600 MW links thus demonstrate identical pu-behaviour when they use the same inverter type. It is necessary to modify the control settings in the mixed and CCC multi-infeed alternatives in comparison to those of the single-infeed configuration, in order to achieve satisfactory performance. These modifications depend on the electrical coupling between their inverter terminals.

Chapter 8 investigates the performance of the three multi-infeed HVDC alternatives, described in the previous chapter, under transient conditions such as faults, load rejections and set-point changes in the control system. The multi-infeed alternatives are examined both when their inverters share a common ac-bus and when they are connected by a transmission line. It is therefore evident that events (e.g. commutation failures or simply adjustments of the control settings) occurring in one link, also affect the commutation voltage at the other inverter. In other words, the performance of each HVDC-link mutually affects the other link since the two practically share the same inverter commutation bus voltage. Such interactions may deteriorate the performance of the overall multi-infeed scheme in comparison to a situation where each HVDC-scheme operates separately. It is surmised that the presence of CCC inverter in one or both of the dc links would lessen this deterioration. The primary objective is thus to evaluate whether the presence of CCC inverters improves the performance of long cable multi-infeed HVDC-schemes.

Chapter 9 makes concluding remarks and suggestions for future work.

All electromagnetic transients simulations throughout the work presented in this thesis are performed using PCSCAD/EMTDC [44] version 2.00. This program is developed by Manitoba HVDC Research Centre Inc. and has the capability to model and simulate virtually any conceivable power system and its associated controls. This feature is essential in order to investigate the behaviour of the HVDC-schemes, associated controls and active filter in sufficient detail. The program is used worldwide by universities, research companies and utilities, and is presently one of the most powerful tool for transient simulation of power systems.

Chapter 2

THE CAPACITOR COMMUTATED CONVERTER

The Capacitor Commutated Converter (CCC) shown in Fig. 2.1, is constructed as a conventional converter modified with the addition of a series capacitor between the transformer and the valve in each phase. The dc-current flows through the capacitor in each phase in either forward or reverse direction depending on whether the thyristor in the upper or lower part of the bridge is conducting. The CCC utilises these series capacitors for generating some of the voltage required for thyristor valve commutation. This converter is therefore expected to be much less dependent on the ac network strength for successful valve commutation and less susceptible to commutation failure due to network disturbances.

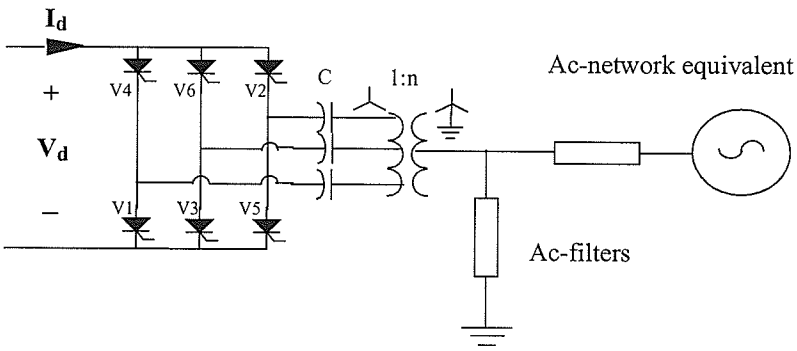

Figure 2.1 The CCC HVDC inverter.

Referring to Fig. 2.2, the minimum firing angle CONVα_{min} for a conventional converter is typically 5 degrees, because some amount of voltage across the valves is required to guarantee a successful turn-on of the thyristor valves. The nominal firing angle is usually is about 15 degrees. The region between these values is used as a control margin, e.g. to temporarily increase the dc-

voltage to maintain rated dc-current. The maximum firing angle (or minimum extinction angle $CCC\gamma_{min}$) for the inverter mode is unable to go beyond 180 degrees, because it would lead to commutation failure.

In the CCC it is necessary to distinguish between the apparent- (γ_{app}) and the real extinction angle (γ_{real}). In the conventional HVDC converter, the extinction angle γ is defined as the electrical angle corresponding to the time at which the valve turns off to the positive zero-crossing of the line-to-line voltage at the ac converter bus. However, in the case of the CCC this measurement does not take into account the capacitor voltage and is therefore not a measure of the real extinction angle. It is therefore referred to as the apparent extinction angle (γ_{app}). Due to its reliance on the additional capacitor voltage the CCC has, contrary to the conventional, the ability to operate at a firing angle ($CCC\alpha_{min}$) or at an extinction angle ($CCC\gamma_{min}$) at very small or even negative angles with the choice of suitable series capacitors. The CCC has, thus, the ability to produce reactive power both in the rectifier and the inverter operation mode. Apparent extinction angle control is therefore a convenient way of controlling the reactive power consumption to a minimum level.

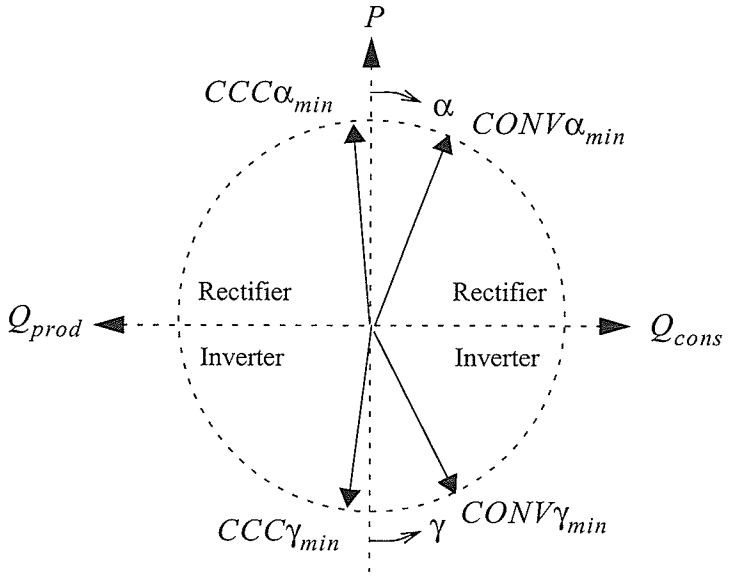

Figure 2.2 P-Q operating chart for the conventional and the CCC HVDC converter.

The real extinction angle (γ_{real}) on the other hand is defined as the electrical angle corresponding to the time at which the valve turns off to the positive zero-crossing of the line-to-line commutation voltage. It is of course larger than apparent extinction angle (γ_{app}) as the commutation voltage lags the converter bus voltage due to the voltage drop across the series capacitor. The real extinction angle (γ_{real}) will therefore increase with an increase in the dc-current. This inherent feature of the CCC is beneficial whenever voltage reductions occur at the ac converter bus, as it brings the converter further away from commutation failure.

The real extinction angle (γ_{real}) will however approach the apparent extinction angle (γ_{app}) if the converter is operated at reduced dc-power (i.e. reduced dc-current). It must always exceed the minimum allowed commutation margin, which typically is 15 degrees. This means that the converter must be controlled at a higher apparent extinction angle (γ_{app}) at low dc-power operation.

One major disadvantage of the CCC, is however that the voltage stress on the valves is increased. It is therefore practical to limit the minimum capacitor size so that the additional valve stress is limited to approximately 10 % over that of the conventional.

Some of the most important advantages and disadvantages using the CCC-topology compared to the conventional are listed below:

Advantages:

- The reactive power compensation is typically close to 50 % of the rated dc power in a conventional converter. Full load rejection can, thus, cause critical overvoltages because of large installed Mvar in the filters, particularly in weak ac-networks. The apparent extinction angle γ_{app} in a CCC may be zero or even negative, which means the converter would in fact produce reactive power. The need for reactive compensation may therefore be greatly reduced and the filters may concentrate only on harmonic elimination. Over-

voltage caused by a load rejection is therefore not a critical problem any more. The need for switching of filter/shunt capacitor banks according to the dc-power transfer, is therefore avoided in the CCC.

- The $d\gamma/dI_d$ characteristic is negative for the conventional converter. This may represent a critical problem in schemes where the dc-link is a long cable and inverter is connected to a weak ac-network. The occurrence of a fault in the inverter ac-network, results in an increased inverter dc-current (I_d) when the large cable capacitance starts discharging. The negative $d\gamma/dI_d$ characteristic can therefore cause commutation failure with lowering of the network voltage in such HVDC-schemes. The $d\gamma/dI_d$ characteristic of the CCC is significantly less negative and could even become positive in strong ac-networks. This indicates that the CCC is more robust against such a fault.
- The Maximum Available Power (MAP) [12,13,16,21] is larger and occurs at a higher value of dc-current. This results in a larger margin to commutation failure, since we know that points on the power curve beyond the MAP are unstable, assuming dc-power control.
- The converter transformer rating is reduced since the reactive power consumption in the converter is greatly reduced.
- Three-phase short circuit faults in the ac network, which are severe disturbance for the conventional converter, appear less harmful for the CCC.
- One of the problems associated with series compensation in ac networks is the possibility of ferro-resonance. This phenomenon occurs when a light loading or a load rejection combined with the presence of a non-linear resonant interaction between the magnetic circuit of a transformer with a series capacitance. Fig. 2.3 shows that there is no current flow in the series capacitance during a load rejection (i.e. a converter blocking) of the CCC. Hence there is no occurrence of ferro-resonance between the converter transformers and the series capacitance.

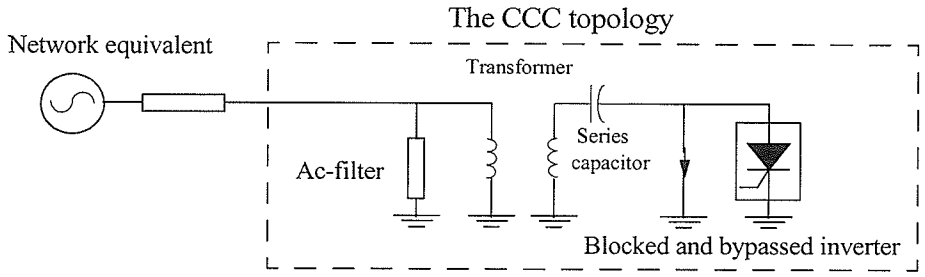

Figure 2.3 Load rejection of the CCC.

- The Controlled Series Capacitor Converter (CSCC) [13] is another type of series compensated HVDC-converter which has similar steady-state and transient behaviour as the CCC. The danger of ferro-resonance is of concern in this topology, because the series capacitor is located on the ac network side of the converter transformers. The CCC is, in the view of the ferro-resonance problem, therefore favourable in comparison to the CSCC.

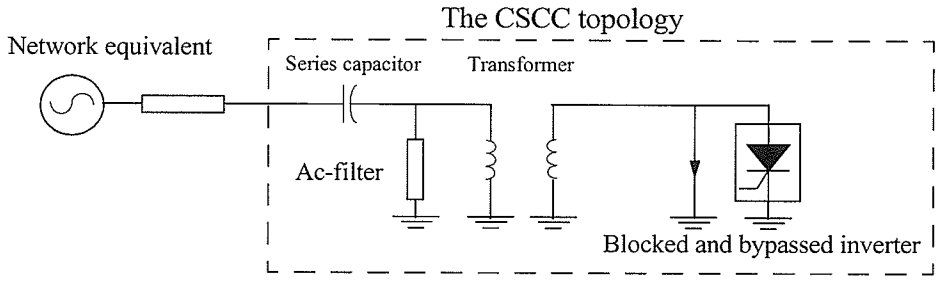

Figure 2.4 Load rejection of the CSCC.

- The valve short-circuit current is significantly reduced in the CCC compared to the conventional converter during rectifier operation.

Drawbacks:

- The commutating capacitors represent an additional cost in the CCC compared to the conventional converter.
- The valve voltage stresses are higher (10 %) than those for a conventional converter, which means larger valve rating and thus higher costs.
- The polarity of the capacitor voltage results in a larger driving voltage across the

transformer leakage reactance during the commutation interval. This leads to a smaller overlap angle and therefore a somewhat higher harmonic content in the ac-current compared to the conventional converter.

- As mentioned earlier, the ac-filters are mainly required for harmonic elimination and not for reactive power supply. This reduces the Mvar-value of the filter to a very small value, which results in a narrow passband. To keep the filter tuned as e.g. aging may slightly change the resonant frequency, continuously tunable filters or active filters are required. Even with tunable filters, a minimum value of reactive power may be necessary in order to provide sufficient bandwidth.
- Single phase faults may introduce dc-components in the capacitor voltages.
- Unbalanced commutation voltages may lead to asymmetry in valve currents, which may accumulate capacitor charge and over-voltage.
- Because of their stored energy, the series capacitors may cause additional dynamic performance deterioration during transients.

Chapter 3

ANALYSIS OF THE CCC-INVERTER

This chapter investigates the steady-state behaviour of the CCC as well as the conventional converter using an analytical formulation. The results from the analytical study are then confirmed using detailed electromagnetic transient simulation. In the example analysed, a 6-pulse 800 MW (V_d=500 kV, I_d=1.6 kA) inverter is connected to an ac-network, represented by a thevenin equivalent. The nominal frequency used throughout this work is the European 50 Hz standard. This chapter serves as an introduction to the consequent parts of the thesis where both converter-types will be applied in long cable single-infeed and multi-infeed HVDC-schemes.

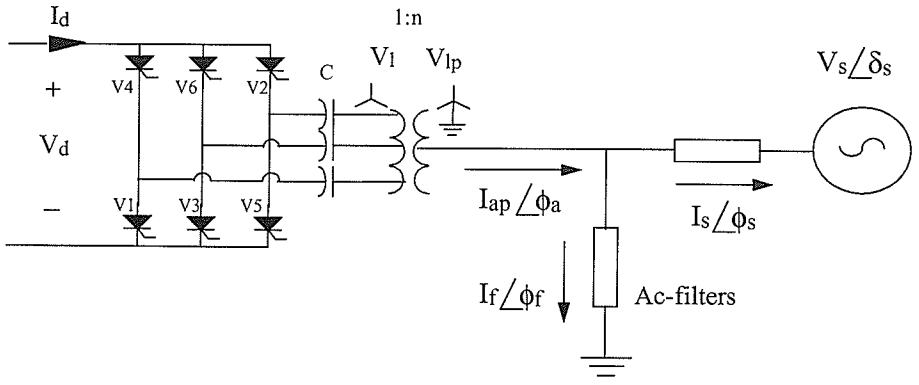

Figure 3.1 CCC-inverter connected to an ac-network.

3.1 THEORETICAL STEADY-STATE PERFORMANCE

As part of this research, an analytical formulation was developed for the CCC. This section uses the analytical formulation to investigate and compare the steady-state behaviour of the CCC and the conventional HVDC converters. Note that the analysis is based on fundamental frequency

quantities only, and does not include any dynamic impact neither from the inverter controls nor from the ac-network.

3.1.1 The model

The steady-state model of the circuit in Fig. 3.1 is presented below by using vector and matrix notation. The model is defined by 14 power flow equations and 18 unknown variables, which can be put into vector form:

$$\bar{x} = \left[V_d, I_d, \alpha, \gamma_{app}, \mu, \Delta v_1, \Delta v_2, B, n, V_{lp}, I_{ap}, \phi_a, I_f, \phi_f, I_s, \phi_s, V_s, \delta_s\right]^t$$

These variables correspond to the following quantities in the CCC-inverter:

I_d, V_d	Dc current and voltage.
$\alpha, \gamma_{app}, \mu$	Firing angle, apparent extinction angle and overlap angle for the bridge.
$\Delta v_1, \Delta v_2$	Increase in capacitor voltages during the overlap interval for incoming and outgoing phase, respectively.
B	Constant resulting from the solution of the overlap differential equation
n	Turns ratio of transformer (primary/valve side)
V_{lp}	Transformer primary side ac line-to-line voltage
$I_{ap}\angle\phi_a$	Magnitude and phase of ac current in transformer (primary side)
$I_f\angle\phi_f$	Magnitude and phase of current in ac-filter (flowing towards earth)
$I_s\angle\phi_s$	Magnitude and phase of system current from the converter to the network
$V_s\angle\delta_s$	Magnitude and phase of network equivalent voltage

$$\bar{f}(\bar{x}) = [f_1, f_2, \ldots, f_{14}]^t$$

Steady-state operating points are therefore solutions to the equation:

$$\bar{f}(\bar{x}) = 0$$

The 14 equations are derived in Appendix 2 and are listed in the following:

$$f_1(\bar{x}) = \left[\frac{I_d}{2} + \frac{V_{lp}\cdot\omega\cdot\cos\alpha}{n\sqrt{2}(\omega_o^2-\omega^2)L}\right]\cos\left(\frac{\omega_o}{\omega}\mu\right) + B\sin\left(\frac{\omega_o}{\omega}\mu\right) + \frac{I_d}{2} + \frac{V_{lp}\cdot\omega\cdot\cos(\alpha+\mu)}{n\sqrt{2}(\omega_o^2-\omega^2)L} \quad (3.1)$$

$$f_2(\bar{x}) = B + \frac{\pi I_d}{3\frac{\omega}{\omega_o}} - \frac{\Delta v_2}{2\omega_o L} + \frac{E\omega_o}{2(\omega_o^2-\omega^2)L}\sin\alpha \quad (3.2)$$

$$f_3(\bar{x}) = \left[\frac{-I_d}{2} - \frac{V_{lp}\omega\cos\alpha}{n\sqrt{2}(\omega_o^2-\omega^2)L}\right]\sin\left(\frac{\omega_o}{\omega}\mu\right) + B\cos\left(\frac{\omega_o}{\omega}\mu\right) + \frac{V_{lp}\omega_o\sin(\alpha+\mu)}{n\sqrt{2}(\omega_o^2-\omega^2)L} + \frac{\frac{2I_d\pi}{3\omega C} - \Delta v_1}{2\omega_o L} \quad (3.3)$$

$$f_4(\bar{x}) = \Delta v_1 + \Delta v_2 - \frac{I_d\mu}{\omega C} \quad (3.4)$$

$$f_5(\bar{x}) = V_d + \frac{3}{\pi}\cdot\frac{\sqrt{2}V_{lp}}{n}\cdot\left[\frac{\cos\alpha+\cos(\alpha+\mu)}{2}\right] + \left[\frac{3}{\pi}(\Delta v_2 - \Delta v_1)\cdot\left(\frac{\pi}{3}-\frac{\mu}{4}\right)\right] \quad (3.5)$$

$$f_6(\bar{x}) = nI_{ap} - \frac{\sqrt{6}}{\pi}I_d \quad (3.6)$$

$$f_7(\bar{x}) = \cos\phi_a + \frac{\cos\alpha}{2} + \frac{\cos(\alpha+\mu)}{2} \quad (3.7)$$

$$f_8(\bar{x}) = \pi - \alpha - \mu - \gamma_{app} \quad (3.8)$$

The second term in (3.5) is identical to the expression for the dc-voltage in a conventional converter. There are two contributions from the series capacitance having an impact on the dc-voltage; the most significant one is already represented in the second term because the capacitance lowers the overlap angle μ and thereby increases the dc-voltage. The contribution from the third term is negligibly small and is caused by a difference between the charging of the in-coming capacitor Δv_1 and the out-going capacitor Δv_2 during the overlap interval. Some simplification in the formulation can be achieved if this term is ignored.

The six remaining equations below are obtained by applying Ohm and Kirchoff's laws at the ac-

network side of the transformer. This leads initially to three additional equations in complex form, each of which are divided into two equations based on their real- and imaginary part.

$$f_9(\bar{x}) = V_{lp} - V_s\cos\delta_s - \sqrt{3}(R_sI_s\cos\phi_s - X_sI_s\sin\phi_s) \tag{3.9}$$

$$f_{10}(\bar{x}) = -V_s\sin\delta_s - \sqrt{3}(R_sI_s\sin\phi_s + X_sI_s\cos\phi_s) \tag{3.10}$$

$$f_{11}(\bar{x}) = I_s\cos\phi_s - I_{ap}\cos\phi_a + I_f\cos\phi_f \tag{3.11}$$

$$f_{12}(\bar{x}) = I_s\sin\phi_s - I_{ap}\sin\phi_a + I_f\sin\phi_f \tag{3.12}$$

$$f_{13}(\bar{x}) = \frac{V_{lp}G_f}{\sqrt{3}} - I_f\cos\phi_f \tag{3.13}$$

$$f_{14}(\bar{x}) = \frac{V_{lp}B_f}{\sqrt{3}} - I_f\sin\phi_f \tag{3.14}$$

The real extinction angle γ_{real} is of course larger than apparent extinction angle γ_{app} because the real commutation voltage is the sum of the line-to-line ac bus voltage and the series capacitor voltages. Solving the above-listed equations calculates the apparent extinction angle, but not the real extinction angle. It is also an interesting quantity because it is a good measure of the margin to commutation failure. The real extinction angle is therefore found by solving equation 3.15 where γ_{real} is the only unknown variable, using an iterative technique.

$$\frac{\sqrt{2}V_{lp}}{n}\cdot\sin(\alpha+\mu+\gamma_{real}) + \frac{2\pi I_d}{3\omega C} - \Delta v_1 - \frac{I_d\gamma_{real}}{\omega C} = 0 \tag{3.15}$$

3.1.2 The Newton-Raphson Method

In the equations above representing the CCC system shown in Fig. 3.1, there are 18 unknown variables but only 14 equations. Four variables need therefore to be pre-specified in order to reach a solution. When the number of unknowns is reduced to 14, the numerical solution can be obtained by using an iterative technique, such as the Newton-Raphson method. The convergence criterion

chosen for the iteration ensures that voltage, current and angle variables have a minimum accuracy of 0.01 kV, 0.01 kA and 0.01 degrees respectively. Algebraically, the Newton-Raphson method derives from the familiar Taylor series expansion of a function in the neighbourhood of an operation point;

$$f(x) = f(x_0) + \frac{\partial}{\partial x} f(x_0)\Delta x + \frac{1}{2!}\left[\frac{\partial^2}{\partial x^2} f(x_0)\right]\Delta x^2 + \ldots + \frac{1}{n!}\left[\frac{\partial^n}{\partial x^n} f(x_0)\right]\Delta x^n$$

Terms beyond the second one are usually negligible, which leads to the following simplified equation:

$$f(x) \approx f(x_0) + \frac{\partial}{\partial x} f(x_0)\Delta x = f(x_0) + J(x_0)\Delta x$$

The various elements in the Jacobian matrix may be expressed as:

$$J = \begin{bmatrix} \frac{\partial}{\partial V_d} f_1 & \frac{\partial}{\partial I_d} f_1 & \cdots & \frac{\partial}{\partial \delta_s} f_1 \\ \frac{\partial}{\partial V_d} f_2 & \frac{\partial}{\partial I_d} f_2 & \cdots & \frac{\partial}{\partial \delta_s} f_2 \\ \cdots & \cdots & \cdots & \cdots \\ \frac{\partial}{\partial V_d} f_{14} & \frac{\partial}{\partial I_d} f_{14} & \cdots & \frac{\partial}{\partial \delta_s} f_{14} \end{bmatrix}$$

Initially, a guess of the state vector x_0 is required in order to start the iteration process. The elements of f(x) are very close to zero when the steady-state solution of x is reached. We use this fact to calculate a correction term $\Delta x = -[J(x_0)]^{-1} f(x_0)$ which brings the state vector $x = x_0 + \Delta x$ closer to the final solution. This is repeated in an iteration-process until the convergence criterion is satisfied. The described iteration method is implemented in a Fortran program, which is designed to also present parametric plots. A parametric plot consists of a number of succeeding steady-state solutions where one of the pre-specified variables (in this case the dc-current) is slightly increased

from one solution to the next.

3.1.3 Analytical approach

Three main approaches to analyse the steady-state behaviour of a single-infeed HVDC-converter have been proposed in the past. One approach presented by Ainsworth et al. [14] in 1980, is known as the Maximum Power Curve (MPC) method and is based on the concept of Maximum Available Power (MAP). The second approach known as the Voltage Stability Factor (VSF) method, was first presented by Hammad et al. [15] in 1984. Both approaches use system sensitivity to small changes in controlling quantities as a measure of system stability. Frankén and Andersson proved in 1990 [16] that the stability limit obtained by the MPC and the VSF methods coincide in the power control operating mode. Aik and Andersson have in the recent years extended the VSF [20] and MPC methods [21] into the multi-infeed situation. Nayak [17,18] introduced in 1993 a third approach, the Control Sensitivity Index (CSI). This method calculates the change in an important system variable caused by an incremental change in the controlled variable. The CSI can be calculated for different control modes and provides therefore, unlike the MPC and the VSF methods, also valuable information in the design of the controller.

Common for these methods is that they study steady-state phenomena in the time-scale after actions of the HVDC-controls but prior to the response of voltage controlling equipment such as transformer tap-changers, synchronous machines and SVCs in the ac-network.

The MPC method of analysis, which assumes constant inverter extinction angle control, is used in obtaining the results presented in the next section.

3.1.4 Results

A base case solution is required in order to obtain a parametric plot. In this case, V_d=500 kV, I_d=1.6 kA, γ_{app}=20.4 degrees and V_{lp}=300 kV are chosen as the pre-specified variables. The base case solution represents the rated condition and is indicated in the plots by a dashed line. In each

parametric plot, where a particular variable is plotted as a function of I_d, the transformer turns ratio n and the network equivalent voltage V_s are held constant at the values found in the base case solution. Each parametric plot consists of a number of succeeding solutions where I_d, γ_{app}, n and V_s are the pre-specified variables and where I_d is slightly increased from one solution to the next. The technical data for each component in the configuration in Fig. 3.1 are given in Appendix 3. Such parametric plots has been calculated for the conventional and the CCC inverter with four different values SCR, which is a measure of the of the ac-network strength. We will first investigate the impact of SCR on the behaviour for each converter type.

The Short-Circuit-Ratio (SCR) and the Effective-SCR (ESCR), defined in Appendix 4, are measures of the ac-network strength vis-a-vis the transmitted dc power. A large SCR (or ESCR) implies a strong ac-network and results in a small impedance for the ac-network equivalent.

An HVDC inverter's power factor improves when the extinction angle γ becomes smaller. However, the probability of commutation failure increases as γ gets smaller and a compromise is usually chosen close to 20 degrees. The base case solution for the CCC-inverter is selected so that the inverter operates at a constant apparent extinction angle (γ_{app}) of 2 degrees, which means that it consumes only a small amount of reactive power. This value of γ_{app} corresponds to a real extinction angle (γ_{real}) of 20.4 degrees with the selected component ratings. The conventional inverter also operates at an extinction angle of 20.4 degrees so that a consistent comparison between the two converter types can be made. The presented curves show how the inverter will behave if a transient event, such as an ac-fault, moves its dc-current away from the rated operating point.

The conventional inverter is first analysed by using the same equations as those of the CCC-inverter. This is possible by selecting a negligibly small series capacitor impedance. The behaviour of the conventional inverter is examined for different levels of ac-network strength by varying the

SCR. The ac-filters connected to the inverter bus have 440 Mvar reactive power installed, which is 55 % of the rated dc-power. The pre-specified variables for each of the four parametric plots are given Table 3.1.

Table 3.1 Pre-specified variables in the conventional inverter.

SCR	Pre-specified variables			
	I_d [kA]	γ [degrees]	n	V_S [kV]
3.05	0.1, .. , 3.0	20.4	0.6890	297.26
2.55	0.1, .. , 3.0	20.4	0.6890	300.54
2.05	0.1, .. , 3.0	20.4	0.6890	307.60
1.55	0.1, .. , 3.0	20.4	0.6890	324.48

Figure 3.2 shows the dc-voltage, the maximum power curve (MPC), the ac-voltage at the inverter bus and the overlap angle, respectively, as the dc-current is varied. The base case solution (rated condition) is indicated by the vertical dashed line at I_d =1.6 kA. Both the dc-voltage and the ac-bus voltage are maintained closer to their rated value when the ac-network is strong (i.e. SCR is large). The MPC-curve [13], is a plot of the dc-power versus the dc-current, which is easily calculated from Fig. 3.2 by multiplying V_d and I_d. It has the slope of an inverted parabola, with the peak indicating the Maximum Available Power (MAP) that can be transmitted in the converter. The concept of MAP was first introduced by Ainsworth [14] and is defined as the dc-power P_d, corresponding to a dc-current, I_{MAP}, where:

$$\frac{dP_d}{dI_d} = 0 \tag{3.16}$$

Beyond the MAP-condition, the power is decreasing with further increase in the dc-current. This happens because an increased dc-current causes a larger percentage drop in the inverter ac-voltage, resulting in a decrease in dc-power. This region of the curve represents unstable operating points if the dc-system is operated in the constant power mode. Consider a situation where the converter

operates in the stable region, but moves into the unstable region due to a transient event. The controller will attempt to increase the dc-power by increasing the current. This will, however, move the converter even further away from the initial operating point and the system is therefore unstable. The controller is in many cases equipped with a current order limit in order to maintain operation if such a scenario takes place. The MAP-condition is for this reason referred to as the stability limit of the ac/dc interconnection. Figure 3.2c shows that the converter operates in the unstable region for the lowest value of network strength examined SCR (i.e. SCR=1.55).

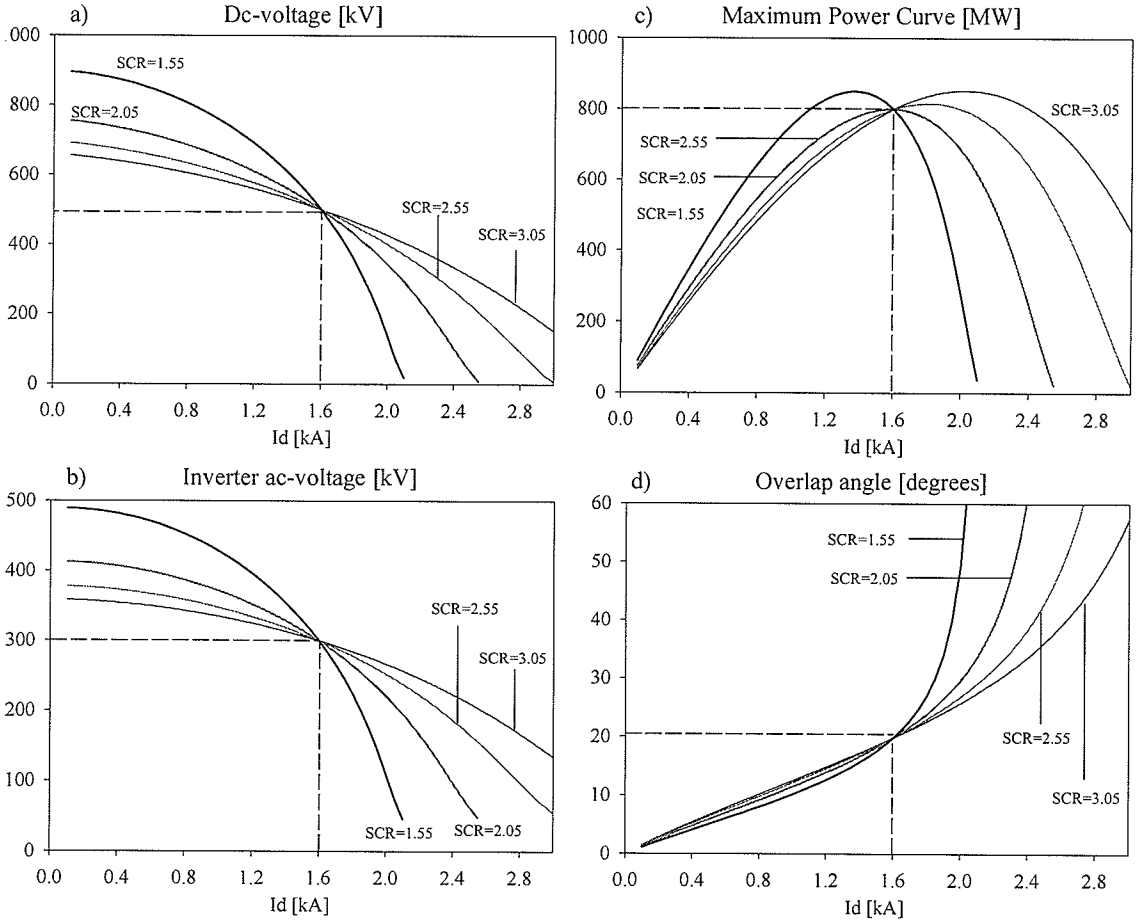

Figure 3.2 Parametric plots for the conventional inverter operating at γ=20.4 degrees.

A large SCR increases the I_{MAP}, which gives more stability margin since the stability limit is further away from the nominal operating point. As seen in Fig. 3.2d, the overlap angle increases as the dc-current increases regardless of the ac-network strength. This trend can be explained by the

lower availability of commutation voltage during the overlap interval as well the larger amount of current that has to be commutated between the valves at higher levels of dc-current. The SCR does not affect the overlap angle significantly for dc-currents up to the rated value of 1.6 kA. The overlap angle increases more rapidly for weak ac-networks for higher value of dc-current.

In the CCC-option, the reactive power consumption at the inverter bus is significantly reduced because the apparent extinction angle is controlled to two degrees. The installed reactive power is, thus, reduced to 116 Mvar, which is only 14.5 % of the rated dc-power. The parametric plots for the CCC-inverter are presented in Fig. 3.3 and the pre-specified variables related to each plot are given in Table 3.2. The component data for this option are identical to those of the conventional converter except for the lower Mvar in the ac-filters and the addition of a 48 μF series capacitor.

Table 3.2 Pre-specified variables in the CCC converter.

SCR	Pre-specified variables			
	I_d [kA]	γ_{app} [degrees]	n	V_S [kV]
3.05	0.1, .. , 3.0	2	0.7916	297.72
2.55	0.1, .. , 3.0	2	0.7916	301.08
2.05	0.1, .. , 3.0	2	0.7916	308.27
1.55	0.1, .. , 3.0	2	0.7916	325.23

Figure 3.3 shows the parametric plots obtained from the CCC-inverter for the same four different values of SCR. It is clearly seen that the SCR has a similar impact on the results as for the conventional inverter. Both the ac-bus voltage and the dc-voltage are maintained closer to their rated values as the SCR becomes larger. From the MPC plot, it is evident that both the stability limit I_{MAP} and the MAP becomes larger for stronger ac-network (i.e. large SCR). Similarly to the conventional converter, the SCR does not seem to affect the overlap angle for dc-currents below rated value. At higher values of dc-current, the rate-of-rise of the overlap angle becomes steeper for weak ac-networks.

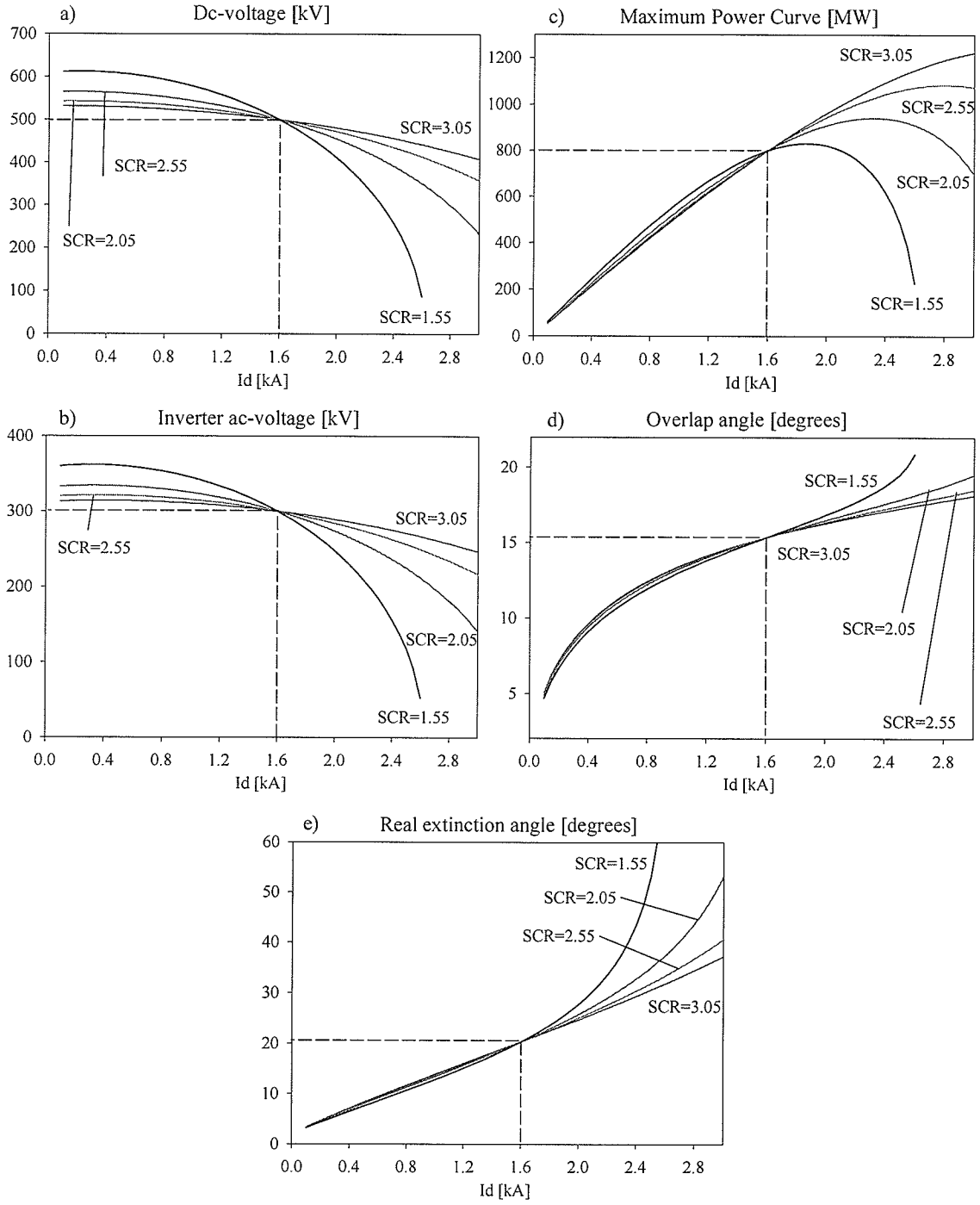

Figure 3.3 Parametric plots for the CCC inverter operating at γ_{pp} =2 degrees.

The real extinction angle, plotted in Fig. 3.3e, becomes larger at higher levels of dc-current because of the larger voltage drop across the series capacitor. The SCR does not have a significant impact on the real extinction angle for dc-currents lower than rated value. Above rated value, the

real extinction angle increases more rapidly for weaker ac-networks. Note that the real extinction angle declines from 20.4 degrees at rated conditions as the dc-current is reduced. Operation at real extinction angles below 15 degrees is not recommended due to high probability of commutation failure. The real extinction angle has reached this critical value when the dc-current is reduced to roughly 1.1 kA. It is therefore realised that the curves presented for the CCC-inverter are somewhat artificial for dc-currents lower than this value. The only way to operate at these low currents with a sufficient real extinction angle, is to increase the apparent extinction angle.

One of the objectives with this chapter was to compare the steady-state behaviour of the CCC and the conventional HVDC converters. A comparison between the two converter types is carried out in the following when the connected ac-network is relatively weak (i.e. SCR of 1.82). Values for the four pre-specified variables for each of the two parametric plots, are given in Table 3.3.

Table 3.3 Pre-specified variables in the steady-state base case solution.

Inverter type	Pre-specified variables			
	I_d [kA]	γ [degrees]	n	V_s [kV]
CCC	0.01, .. , 3.0	2 (=γ_{app})	0.7969	313.5
Conventional	0.01, .. , 3.0	20.4	0.6888	313.6

Figure 3.4 shows the dc-voltage, MAP, inverter ac-voltage and overlap angle for each inverter type plotted together. As seen from the curves for dc-voltage, the voltage regulation for the CCC is far more superior to that of the conventional option as evidenced by the flatness of the voltage profile. The CCC inverter ac-voltage is also maintained closer to the rated value in comparison to the conventional inverter. It is evident from the MPC that the CCC is superior to the conventional inverter in terms of dc-power capability. The plots clearly show that the CCC has both a higher MAP and a larger dc-current stability limit, compared to the conventional converter. Hence, the margin from the rated operation point to the stability limit is larger in the CCC-option, resulting in a more robust operation.

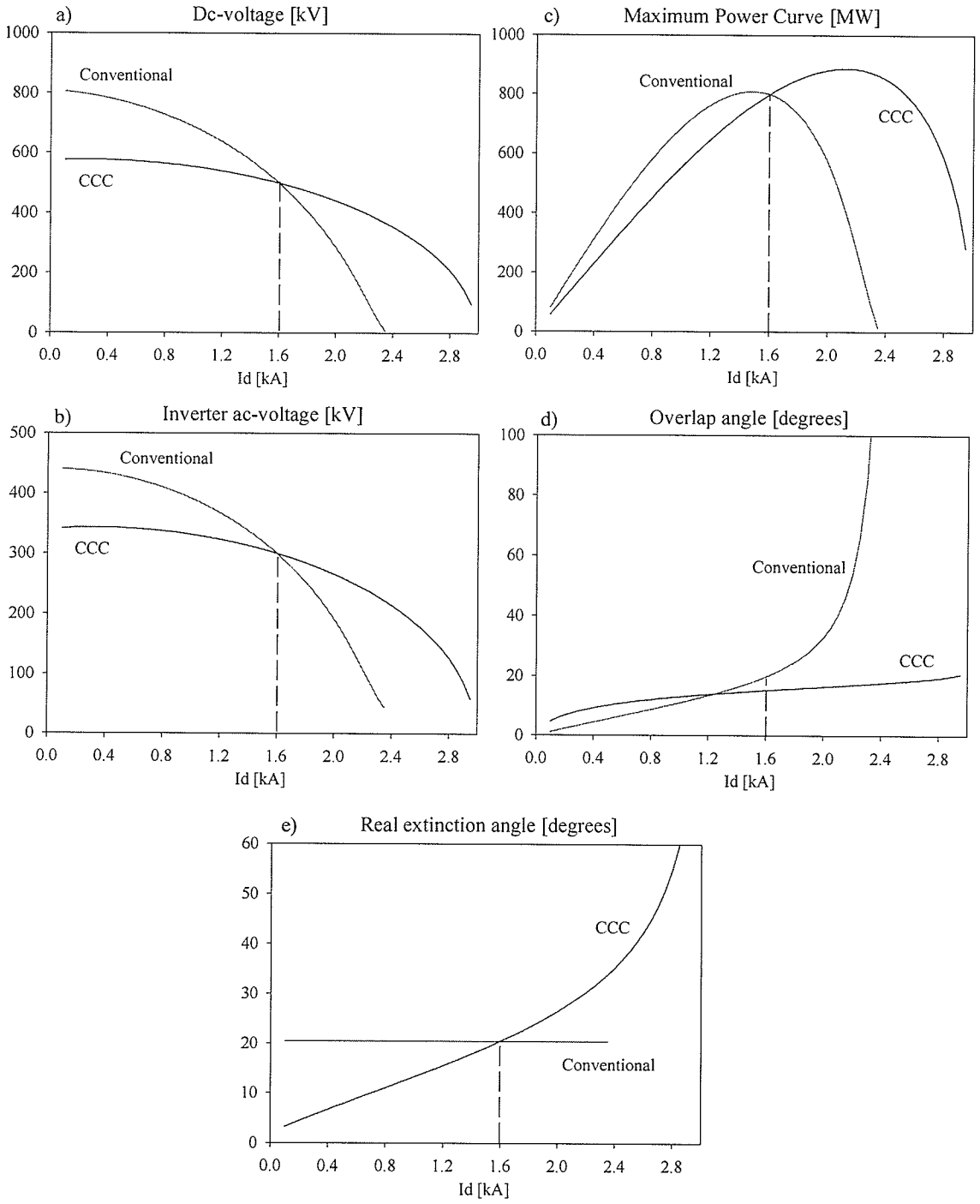

Figure 3.4 The conventional and the CCC inverter, operating at γ=20.4 and γ_{app}=2 degrees, respectively.

As may be seen from Fig. 3.4e, the natural tendency for the real extinction angle is to increase when the dc-current becomes larger. This can be explained by the larger voltage drop across the series capacitors results in a larger real extinction angle, since the apparent extinction angle is kept

constant by the controls. This characteristic of the CCC reduces the likelihood for commutation failure, particularly for long cables, where any lowering of the inverter ac-side voltage results in a surge of dc-current from the discharge of the cable capacitance.

In the case of the conventional inverter, the apparent and real extinction angles are identical and equal to the pre-specified 20.4 degrees. The extinction angle is therefore constant when the dc-current varies simply because it is pre-specified (i.e. constant extinction angle control mode). In the CCC-inverter, the real extinction angle increases from 20.4 degrees at rated conditions (I_d = 1.6 kA) when more current flows through the series capacitor.

The analytical formulation used here is based on steady-state equations at fundamental frequency. In order to make a more realistic investigation of the HVDC-schemes modelled in the forthcoming chapters of this thesis, a study using electromagnetic transient simulation is necessary. Such a simulation will also take into account the transient nature (gains, time-constants, limits, etc.) of the control system when various types of disturbances are applied in the ac-network.

3.2 SIMULATED STEADY-STATE PERFORMANCE

In order to validate the analytically obtained results in Section 3.1, the CCC and conventional inverter topologies are investigated using electromagnetic transient simulation. Such a study integrates the non-linear differential equations of the detailed formulation and presents time domain results. The method of solution is therefore completely different from that of the analytical formulation and closer to the behaviour of the real system.

A detailed model of the CCC-inverter showed in Fig. 3.1 is first developed in PSCAD/EMTDC in order to demonstrate the operating characteristics of the CCC, and then to validate the results obtained by the analytical formulation.

3.2.1 The model

Figure 3.5 shows a schematic diagram of the 800 MW (V_d=500kV, I_d=1.6kA) CCC-inverter model which was developed in PSCAD. In addition to the three-phase model of the circuit itself, a phase-locked-loop based firing logic, controls and extinction angle measurement are also modelled. The rectifier is for simplicity represented as a current-controlled voltage source whose PI-controller attempts to maintain the rated dc-current by adjusting the rectifier dc-voltage. The inverter is a 6-pulse bridge provided with series capacitors of 48 μF between the transformer and the thyristor valves. The CCC-inverter operates in apparent extinction angle control at two degrees using a PI-type controller. Algorithms for apparent and real extinction angle measurements are developed and they are described in detail in Section 4.8.

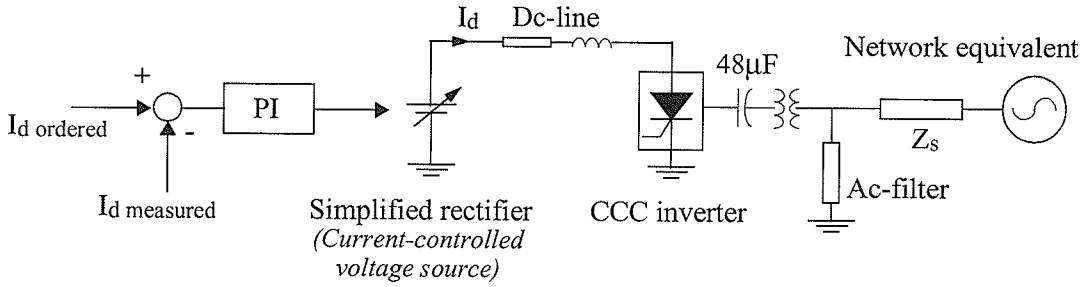

Figure 3.5 CCC-inverter in constant apparent extinction angle control.

The ac-network on the inverter side is represented by an RL-type equivalent with a SCR of 1.82 and a damping angle at fundamental frequency of 75 degrees. The RL-type equivalent which is explained in detail in Appendix 7, consists of the series-connection of a resistance and an inductance. The network equivalent impedance Z_s is calculated as in (3.17) where V_{lp} and P_d are the inverter ac-bus voltage and the converter's power rating, respectively.

$$Z_s = \frac{V_{lp}^{\,2}}{P_d \cdot SCR} = 15.998 + j59.707 \qquad (3.17)$$

The ac-network source voltage is fixed to 313.5 kV and the transformer turns ratio is pre-specified to 0.7969 (300 kV/376.5 kV), which are identical to those found in the base case of the CCC in

Table 3.3.

At the CCC-inverter's 300 kV ac-bus, there are first order bandpass filters to eliminate the characteristic harmonic components of 5th, 7th, 11th and 13th order, as well as a highpass filter for removal of higher order harmonics. Each of the four bandpass filters have a quality-factor of 2000 and provides 7.5 Mvar reactive power. This is an idealised situation since the quality-factor would be smaller in most installations. The highpass-filter which has its resonant frequency at the 18th harmonic, has a quality-factor of 100 and supplies 8.67 Mvar reactive power. The filter arrangement supplies hence 38.67 Mvar to each phase, which gives a total of 116 Mvar for all three phases or 14.5% of the rated dc-power.

The CCC operates in the apparent extinction angle control mode, which maintains the average value of the apparent extinction angle for all six valves to two degrees. By controlling the CCC-inverter to two degrees apparent extinction angle at rated dc-current and using identical setpoints for the network source voltage and the transformer ratio, the same steady-state solution as that of the analytical formulation should be found.

3.2.2 Operating waveforms at rated conditions

The CCC is investigated by presenting a few important quantities in phase A during steady-state operation at rated conditions. Figure 3.6 plots the operating waveforms for the transformer current, the series capacitor voltage, the commutating voltage and the inverter bus voltage in a time-frame of two cycles (i.e. 40 ms in a 50 Hz system). The top graph (a) shows the phase currents that flow from the inverter through the transformer (referred to its valve side) towards the ac-network. The current in phase A is positive when valve 4 conducts and negative when valve 1 conducts. Each valve conducts for 120 degrees in each cycle. If the overlap interval is ignored (ideal commutation), then the valve current is zero during the remaining part of each cycle. This behaviour is identical to that of the conventional converter [2].

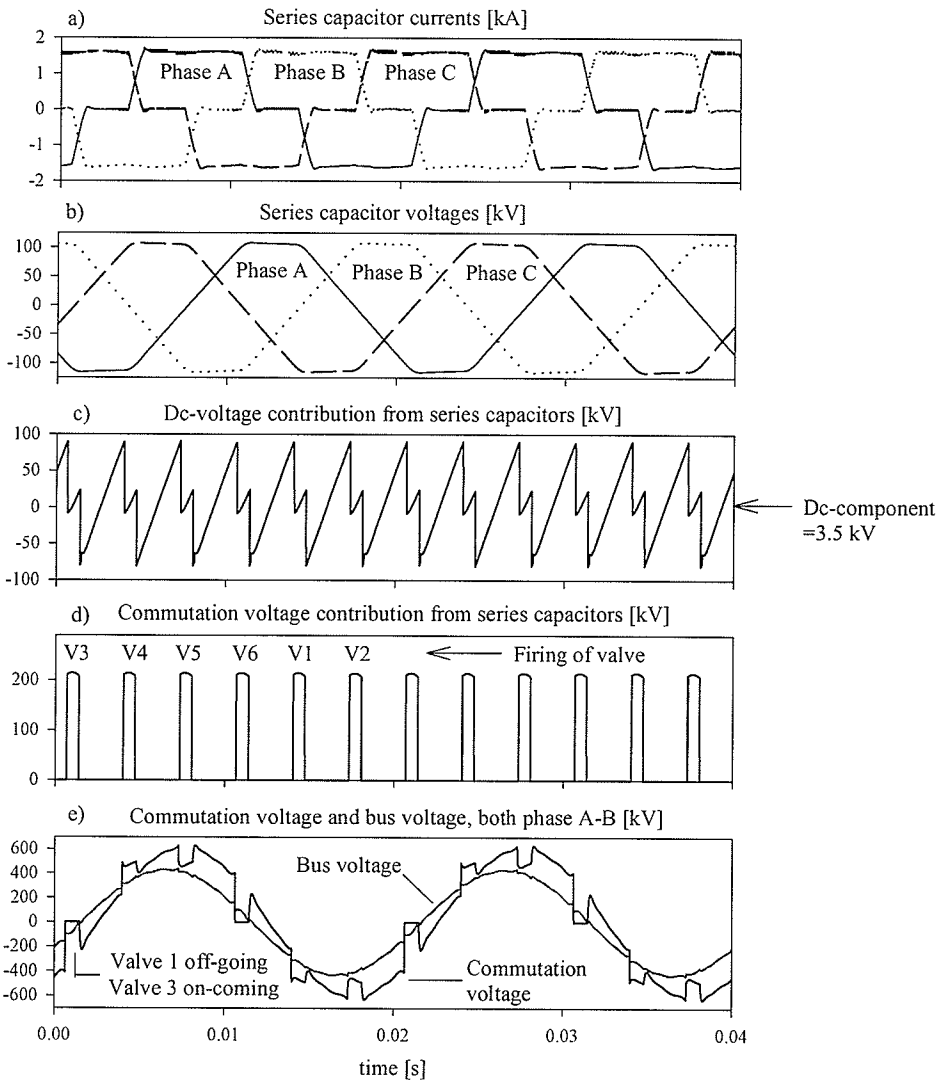

Figure 3.6 CCC 6-pulse operation waveforms.

The mid graph (b) plots the voltages across the series capacitors. The voltage across the capacitor in phase A is charging when a positive current is flowing (valve 4 conducts) and is discharging when a negative current is flowing (valve 1 conducts). There are two 60-degree intervals when neither valve 1 nor valve 4 is conducting. The voltage across the capacitor is maintained constant at its positive or negative peak value during those two intervals since no current is flowing in phase A. Graph c plots the contribution on the dc-voltage from the series capacitor voltages. It is evident that the contribution, which is given by the dc-component, is negligible (less than 1 %). Graph d shows that the series capacitors assists in the commutation process since they increase the

commutation voltage during the the overlap interval. Graph e shows the inverter bus voltage and the commutating voltage between phase A and B. It is evident that the commutating voltage lags the inverter bus voltage (due to the voltage across the series capacitor), which explains why the real extinction angle is larger than the apparent.

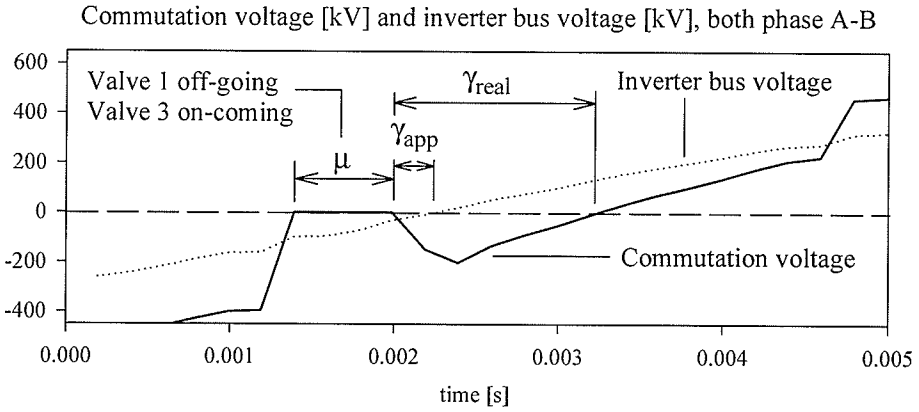

Figure 3.7 Real- and apparent extinction angle.

Figure 3.7 is simply a zoomed version of Fig. 3.6e around the commutation interval μ in which valve 3 takes over conduction for valve 1. As indicated in the graph, the real extinction angle (γ_{real}) for valve 1 is the angle corresponding to the instant when the valve ceases conduction until it becomes forward biased. Although the commutation voltage for valve 6 (V_{ab}) is plotted here, it is also the voltage that first would forward bias the off-going valve 1 after it has finished its conduction duty. Therefore, valve 1 becomes forward biased when the positive zero-crossing of the commutation voltage (V_{ab}) takes place. The apparent extinction angle (γ_{app}), on the other hand, is determined by the positive zero-crossing of the inverter bus voltage.

Operation at a relatively low apparent extinction angle (γ_{app}) and at the same time maintaining a sufficient commutation margin (γ_{real}) is thus possible as long as the inverter operates close to rated conditions. A larger apparent extinction angle (γ_{app}) is required for operation at lower values of dc-current in order to maintain the same margin to commutation failure.

3.2.3 Verification of the theoretical results

A number of steady-state solutions are obtained, for values of dc-current ranging from 0.6-2.6 kA, by the simulation model described in sub-section 3.2.1. Figure 3.8 plots these results together with the theoretical ones obtained by the analytical formulation in Fig. 3.4. The plotted quantities are dc-voltage, the Maximum Power Curve, the inverter bus voltage and the real extinction angle. The theoretical results are presented as a solid-drawn curve, whereas the simulated results are represented by individual crosshair symbols.

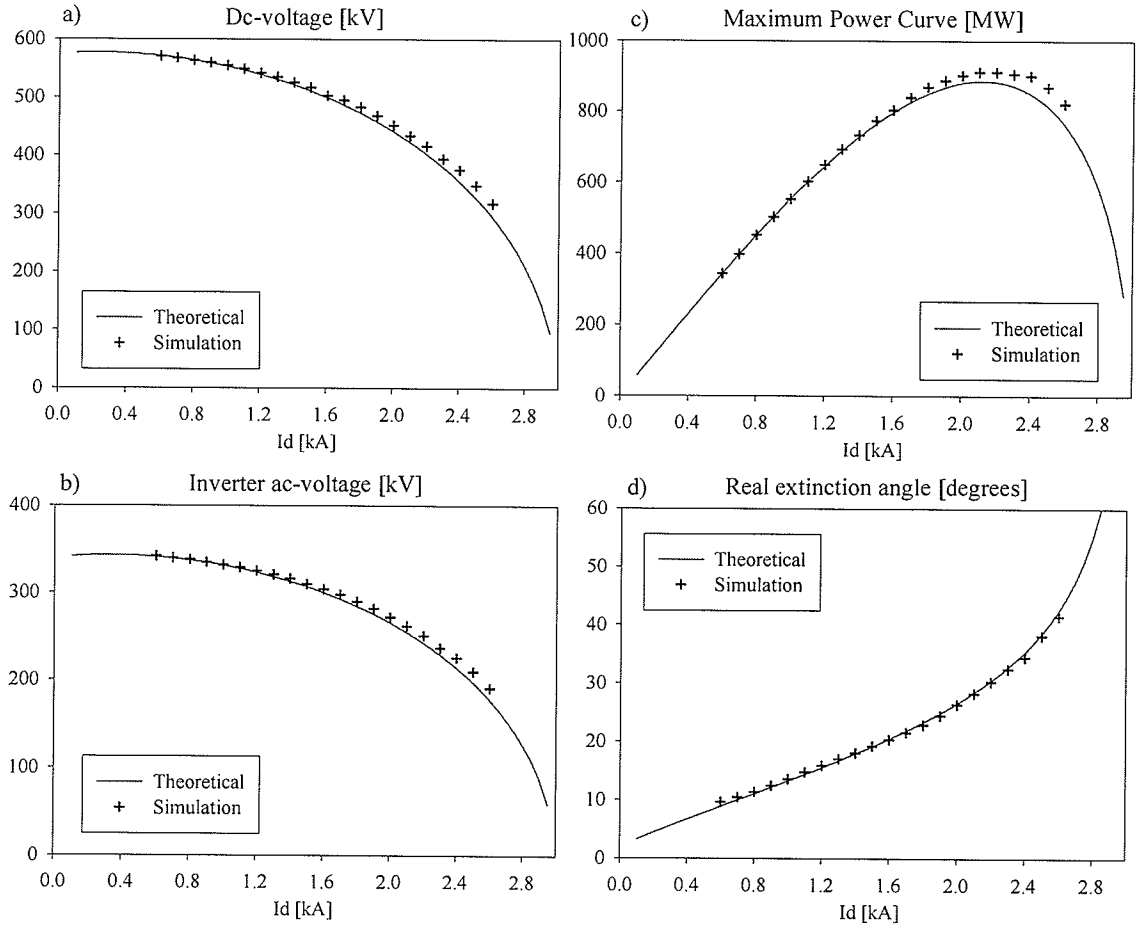

Figure 3.8 Comparison between theoretical and simulated steady-state results.

As may be seen from the graphs, the simulated results correspond quite well with the theoretical ones up to rated dc-current value. There is a small deviation in magnitude at dc-currents above rated value, but the two curves demonstrate a very similar trend.

The primary point to be recognised is that the simulated results and the theoretical results agree in general very well. It is therefore reasonable to conclude that the results acquired by the simulation model verify those obtained by the analytical formulation in the previous section. This indicates that the derived steady-state CCC-equations and the iteration algorithm have been correctly implemented in the Fortran-program. It also validates the accuracy of the electromagnetic transient simulation model (PSCAD/EMTDC) and its associated controls.

With this conclusion, the simulation model will be extended into a full-scale long cable single-infeed HVDC-scheme using either the conventional and the CCC converter type at the inverter end. These two schemes will thereafter be used to build multi-infeed HVDC-schemes, where two dc-links terminate in the same ac-network.

Chapter 4

MODELLING OF SINGLE-INFEED LONG CABLE HVDC SCHEMES

The objective of this and the succeeding chapter is to investigate the suitability of different inverter types in a long cable HVDC-scheme, terminating in a weak ac-network. The first alternative of such a single-infeed HVDC-scheme consists of conventional inverters, whereas the second uses CCC-type inverters. As pointed out later in this chapter, the traditional control option is unsuited in such long cable HVDC-applications. Two new control options have therefore been developed to handle the unique characteristics of the large cable capacitance. The two control methods are then evaluated for application both at the conventional and the CCC-inverter based HVDC scheme.

This chapter describes in detail the modelling of the HVDC-schemes, including their associated controls. The transient behaviour of the HVDC-schemes is evaluated in the next chapter.

4.1 THE SINGLE-INFEED HVDC-CONFIGURATION

The simple 6-pulse HVDC-scheme, developed in the previous chapter, is extended into a full 12-pulse HVDC-scheme of 1200 MW power rating. When a 6-pulse bridge is extended to a 12-pulse bridge, the transformer MVA, the capacitor reactance and the transformer voltage at the valve side must be reduced by half, in order to maintain the same inverter dc-voltage. This means that the capacitor size becomes twice as large. The two single-infeed HVDC alternatives developed are very similar with the exception that they have different inverter types:

- The conventional single-infeed HVDC-scheme employs conventional converters both at the rectifier and at the inverter.
- The CCC single-infeed HVDC-scheme uses a conventional rectifier and a CCC inverter.

The single-infeed scheme using CCC-inverters is illustrated in Fig. 4.1, where a conventional rectifier is connected to a CCC-inverter by a long dc-cable. The rectifier is connected to an infinitely strong ac-system whereas the inverter ac-system is relatively weak.

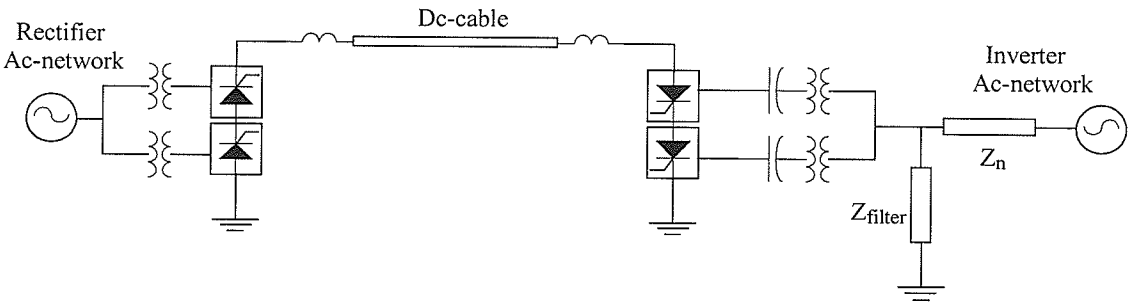

Figure 4.1 Single infeed CCC HVDC-scheme.

In the following sections, the modelling of the two single-infeed HVDC schemes are described in detail, including the inverter ac-network, dc-components and the two control options.

4.2 THE INVERTER AC-NETWORK

The ac-network on the inverter side is represented by an RRL-type equivalent with a short-circuit-ratio (SCR) equal to 2.05, which is a relatively weak network. The SCR is a measure of the ac-network strength vis-à-vis the transmitted dc power and is defined in Appendix 4. The damping angle is 85 degrees at fundamental frequency, resulting in a predominantly inductive equivalent. The ac-network equivalent Z_n may be calculated as in equation 4.1, where V_{lp} and P are the inverter ac-voltage and dc-power rating, respectively.

$$Z_n = \frac{V_{lp}^2}{P_{dc} \cdot SCR} \tag{4.1}$$

This RL-equivalent represents the ac-network at fundamental frequency. In order to make a better representation at higher frequencies, the ac-network is often modelled as an RRL-type equivalent.

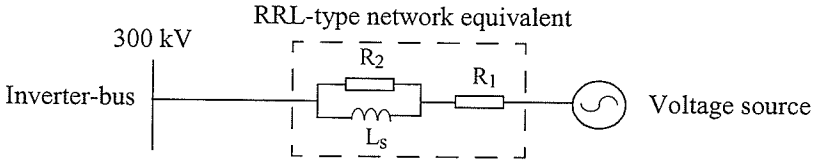

Figure 4.2 Ac-network equivalent of the RRL-type.

The RRL-equivalent, shown in Fig. 4.2, must of course satisfy (4.1) at fundamental frequency and is also specified to have a damping angle of 85 degrees inductive at the fundamental and at the third harmonic frequency. The frequency response (both magnitude and phase angle) is plotted in Appendix 7 for both the RL and the RRL-type equivalent. The two types of network equivalents exhibit different impedance characteristics in the high frequency range. It clearly illustrates that the RRL-equivalent impedance magnitude saturates at high frequencies as opposed to the RL-type which increases towards infinity. The so-called RLL is another type of equivalent that has the same problem. The RRL-type equivalent is selected because it is more suitable in a digital simulation with high frequency noise. The phase angle of both types of equivalents is 85 degrees inductive at fundamental frequency. For higher order harmonics, the RL-type becomes more inductive and the RRL-type changes towards a resistive impedance.

More complicated equivalents could be used if detailed information about the frequency response of the ac-network was available.

In each single-infeed alternative, it is assumed that the dc-power would be uni-directional from the strong sending end to the relatively weak receiving end. Each alternative has, however, different effective-short-circuit-ratio (ESCR) since the total reactive power generated in the filters and shunt capacitors at the inverter bus Q_c, is different in each alternative.

$$ESCR = SCR - \frac{Q_c}{P_{dc}} \tag{4.2}$$

The relationship between SCR and ESCR is given in (4.2), where Q_c is the Mvar-generation and

P_{dc} is the total rated dc-power in each single-infeed HVDC alternative.

Table 4.1 SCR and ESCR in each single-infeed HVDC alternative.

Single-infeed HVDC alternative	Power rating	Mvar-generation	SCR	ESCR
Conventional	1200 MW	660 Mvar	2.05	1.5
CCC	1200 MW	174 Mvar	2.05	1.905

As may be seen from Table 4.1, the ESCR for the CCC single-infeed HVDC alternative is significantly larger compared to the conventional, due to the fact that the CCC has a lower reactive power installation at its converter bus. This indicates that the CCC ought to have a superior performance over the conventional option. However, the additional dynamics associated with the series capacitors could compromise this expected improvement.

4.3 COMPONENTS

4.3.1 Converter transformers

The MVA-rating of the transformers at the conventional converter is somewhat larger (typically 1.20 pu) than the nominal dc power transmitted since the converter operates at a lagging power factor. In this design, the rating of the wye-wye and wye-delta connected transformers is set to 705 MVA each, which corresponds to a total transformer rating of 1.175 pu. The transformer rating in the case of the CCC converter is similarly set to 1.175 pu, although it is realised that it could potentially be lower on account of the better power factor. The turns ratio (secondary/primary) is set to 214.3/300 kV and 185/300 kV for the conventional and CCC inverter, respectively. The transformers' leakage reactance is 0.15 pu.

4.3.2 The CCC series capacitor with surge arrestor

The considerations made in this sub-section are of relevance only for the CCC and not for the conventional converter type. The series capacitance in a CCC is located between the converter transformer and the valves in each of the three phases. The capacitance value and its protection

level provided by a surge arrestor must be carefully selected, as is discussed in the following.

In each cycle, the series capacitor is linearly charged to a peak positive voltage and thereafter discharged to a peak negative value, as illustrated in Fig. 3.6. The capacitor value and the dc-current therefore detemine the peak voltage across the series capacitance in steady-state operation. A large capacitive impedance will therefore result in a larger real extinction angle if the converter is controlled to a given apparent extinction angle. This basically means that a small capacitance is required in order to achieve operation with a good power factor (small apparent extinction angle) and a sufficient real extinction angle. This results in a larger operating range because the dc-current can be reduced to a lower value before the real extinction angle approaches its 15 degree critical value.

However, the drawback of a large capacitive impedance is higher voltage stress on the valves, which results in higher valve insulation requirements and therefore higher cost. A small capacitive impedance, on the other hand, will not only lower the voltage stress on the valves, but also reduce the cost of the capacitor itself. Assuming constant current, its cost is reduced due to the inverse relationship between the MVA-rating and the capacitor size.

Therefore, a trade-off has to be made between the wish for flexible operation on one side and low voltage stress on the valves on the other. As in other publications [12,13], our choice is based on 10 % additional voltage stress on the valves compared to that of the conventional converter. In this design, a series capacitance of 144 μF was chosen for the 1200 MW HVDC-link. This introduces a limit of approximately 180 degrees on the maximum firing angle, which means that the inverter operates close to unity power factor and leading power factor operation is not possible.

In the case of severe transients like a surge of dc-current when the cable capacitance discharges, the series capacitors will be charged to high voltage levels. Each of the capacitors is therefore protected by a surge arrestor in order to limit its overvoltage. The selection of the protection level

of the surge arrestor is a matter of optimisation. The minimum voltage level is obviously directly defined by the steady-state capacitor peak voltage (about 55 kV), given by (A.4) in Appendix 2. It must also be able to carry the 25 % overcurrent allowed by the VDCOL, described in section 4.4.

One of the benefits with the CCC is that the presence of the series capacitance limits both the peak and the duration of the short circuit current compared to the conventional converter [12]. The reason for this is that the series capacitors rapidly charge because of the short circuit current and counteract the driving network voltage. A high protection level will therefore utilise this effect to its fullest. A high protection level will, however, also allow a higher voltage across the series capacitor and will thereby also increase the voltage stresses on the valves during transients. In this design, the voltage protection level of the surge arrestors is selected to 2.5 pu of the steady-state peak capacitor voltage at rated condition.

4.3.3 Long submarine dc-cable

The dc-link represents a long submarine cable with resistance of 0.01 Ω/km, inductance of 0.3 mH/km and capacitance of 0.38 μF/km, which is typical for a cable of 600 MW capacity. In each of the four single-infeed schemes, a 600 km long cable is used, which results in values of 3 Ω, 90 mH and 228 μF for resistance, inductance and capacitance respectively.

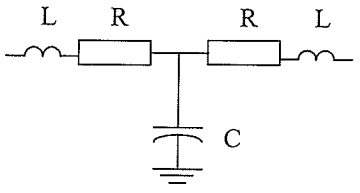

Figure 4.3 Dc-cable model.

In order to transfer 1200 MW it is necessary to use a scheme with two of these cables operated in parallel. These two cables are represented as one in the PSCAD/EMTDC-model, which means that the resistance and inductance must be halved whereas the capacitance must be doubled, compared to the data for the 600 MW cable. This results in values of 1.5 Ω, 45 mH and 456 μF for resistance,

inductance and capacitance respectively as shown in Table 4.2.

Table 4.2 Component values in the dc-cable model.

Dc-power	Resistance [Ω]	Inductance [mH]	Capacitance [μF]
1200 MW	1.5	45	452

4.3.4 The dc-smoothing inductor

The smoothing inductor is located at both the rectifier and inverter end of the dc-connection. It is a complex matter to choose a feasible size of this inductance. Its main purpose is to protect the converter against overvoltages caused by e.g. lightning and limit the dc-current during commutation failure. Care must be taken to avoid resonance (in particular at fundamental frequency) when selecting the inductance value. A value of 0.4 H is chosen for the smoothing inductor in both HVDC-alternatives, which meets these objectives.

4.3.5 The inverter ac-filters

Power electronic installations, such as HVDC-converters, generate a substantial amount of harmonics. Harmonic pollution may cause premature aging and degradation of performance (even misoperation) for various components in a power system. The allowable harmonic pollution is, in most countries, limited by indices in harmonic standards. HVDC-converters are hence equipped with filters at their ac-bus which target the harmonics generated under balanced conditions, the so-called characteristic harmonics. Both the CCC and the conventional inverter are therefore supplied with single-tuned bandpass (BP) filters to eliminate the characteristic harmonic components of 11th, 13th, 23rd and 25th order, as well as a highpass (HP) filter with cut-off frequency at the 36th harmonic for removal of higher order harmonics. The quality-factors for the BP-filters and for the HP-filter are 2000 and 100, respectively. Table 4.3 shows the installed Mvar in each of the four BP-filters as well as the HP-filter. Note that the values are for each phase, which means that the total three-phase Mvar-installation can be expressed by the following formula.

$$Total = 3 \cdot [4 \cdot BP + HP + capacitors] \tag{4.3}$$

It is realised that in an actual installation, multiple tuned filters may be employed. However, the selection of the single tuned filters used here does not affect the essential behaviour of the system.

Table 4.3 Installed Mvar in the ac-filters at each single-infeed scheme.

	Ac-filters		Shunt capacitors	Total
Dc-link	Bandpass	Highpass		
1200 MW Conventional	22.1	25.55	106.0 (or 11.25 μF)	660
1200 MW CCC	11.25	13.0	None	174

The total reactive power installation in the ac-filters at the conventional inverter bus is 55 % of its rated dc-power and is supplied from the filters and the shunt capacitors. The filters at the CCC-inverter bus have a reactive power installation of only 14.5 % of rated dc power because this converter type consumes significantly less reactive power. The single-tuned bandpass and highpass filters are shown in Fig. 4.4. Appendix 6 provides impedance plots for the two filter types and explains also which considerations that have to be made in order to make a suitable filter design. The concept of quality factor, bandwidth, installed Mvar and filtering performance as well as the relationship between them are explained in detail.

Figure 4.4 Single-tuned bandpass and highpass filter.

4.3.6 Dc-harmonics

The 12-pulse converter produces a dc-voltage waveform contains characteristic harmonics of 12n order (i.e. 12th, 24th, 36th, etc). In HVDC-schemes with an overhead dc-transmission line, these

harmonics may interfere with telecommunication circuits located in its close proximity. It is therefore important to minimise the magnitudes of the current harmonics on the dc transmission line. This is normally achieved by connecting a dc-filter at each end of the dc transmission line. This problem is, however, not of concern in HVDC-schemes using dc-cables because the fields generated by the harmonics are not in the proximity of any communication circuits. The HVDC-schemes are, for this reason, not equipped with any dc-filter.

4.4 THE CONTROLS

Although extremely long cable HVDC-connections are not expected to generate technical problems that could not be overcome, there are aspects that require special attention. One of the challenges is to design a control system which handles the unique characteristics of the large cable capacitance between the rectifier and the inverter.

4.4.1 Weaknesses of traditional controls

Many existing HVDC-schemes are operated in current control at the rectifier and extinction angle control at the inverter [1]. This is a convenient way of controlling the reactive consumption at the inverter to a minimum level without experiencing commutation failure. However, long cable HVDC schemes encounter problems when they are operated in this control mode. The large amount of energy stored in the cable capacitance is the source of the problem. Consider what happens when a disturbance occurs causing a reduction in the the ac inverter bus voltage. The inverter dc voltage V_{di} in (4.4), measured on the converter side of the smoothing inductor, will immediately decrease in accordance with the lowering of the commutation voltage V_c on the valve side of the transformer.

$$V_{di} = \frac{3\sqrt{2}}{\pi} V_c \cos\gamma - \frac{3\omega L}{\pi} I_d \qquad (4.4)$$

The voltage on the cable side of the smoothing inductor is maintained for a short time because the

large cable capacitance acts practically like a voltage source, as indicated in Figure 4.5. Now the cable starts to discharge through the smoothing inductor and the inverter into the ac-network. As a result, the commutation voltage decreases further due to the voltage drop through the transformer leakage reactance. The result may be commutation failure due to a rapid decrease in the extinction angle γ.

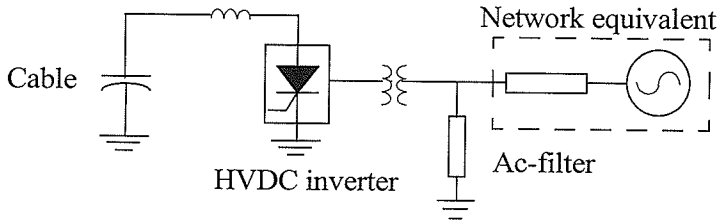

Figure 4.5 Long cable HVDC-scheme.

The above-discussed phenomenon is referred to as the negative resistance characteristic (higher current gives lower voltage) of the inverter as seen from the dc side when there is no fast-acting ac voltage control devices close to the inverter bus. The negative resistance is much less in the CCC compared to the conventional converter, because of the additional voltage generated across the series capacitor by the current from the discharging cable. It is therefore anticipated that the CCC inverter can be operated in the traditional extinction angle control mode for longer cable lengths in comparison to the conventional type. For extremely long cables, the inverter is unable to counteract the surge of current into the ac-network by control means (since the term $\cos\gamma$ is kept constant by the extinction angle controller) regardless of the converter type employed.

The rectifier controls the dc-current on its end of the cable and hence also the inverter current under steady-state conditions. This relationship between the two currents is however not present under transient conditions because of the presence of the large cable capacitance. The rectifier and the inverter control are therefore decoupled in the transient time scale. Even if the rectifier was equipped with a force retard capability, it would not succeed in decreasing the transient inverter

dc-current sufficiently.

The traditional control strategy is therefore unsuited for application in long cable HVDC-schemes, since the control system is unable to make counter-measures to reduce the surge of current following such a disturbance. Two alternative control options are developed in the following sub-section, which both handle this particular problem and result in acceptable transient performance.

4.4.2 Alternative control strategies

It is evident from the arguments made above, that a control strategy is required that maintains the dc voltage when the voltage drops in the ac-network. Equation (4.4) reveals that this can be achieved by keeping the term $V_c\cos\gamma$ constant. The inverter has to be operated at a higher nominal extinction angle so that the control system may counteract the ac voltage drop by decreasing the extinction angle and thereby keeping $V_c\cos\gamma$ constant. This is in literature [32] referred to as variable extinction angle control. Two possible control options are described in the following, that are similar to this technique. The first control option applies dc-current control at the inverter, whereas the second one uses dc-voltage control at the inverter.

Common for both control options is that the nominal extinction angle has to be somewhat larger than for extinction angle control, so that a control margin for lower extinction angles is available. Although this has advantages from the control point of view, there are a few drawbacks that should be pointed out. Operating at a poorer power factor requires a higher transformer MVA-rating. The increased reactive consumption at the inverter bus must be compensated by a larger Mvar installation in the ac-filters or shunt capacitors. A larger commutation voltage is required in order to attain the same dc-voltage as before, resulting in larger voltage stress on valves and thus a higher valve voltage rating.

4.4.3 Control option 1: Inverter in current control

Figure 4.6 shows the steady-state characteristics for the first proposed control option, termed as

control option 1, where the rectifier operates in voltage control (VC) and the inverter operates in current control (CC) during normal operation. This control option is used in both of the two different HVDC-schemes. There are, however, minor differences in setpoints of various limits, slopes and parameters between the scheme using CCC-type inverters and the scheme using conventional inverters.

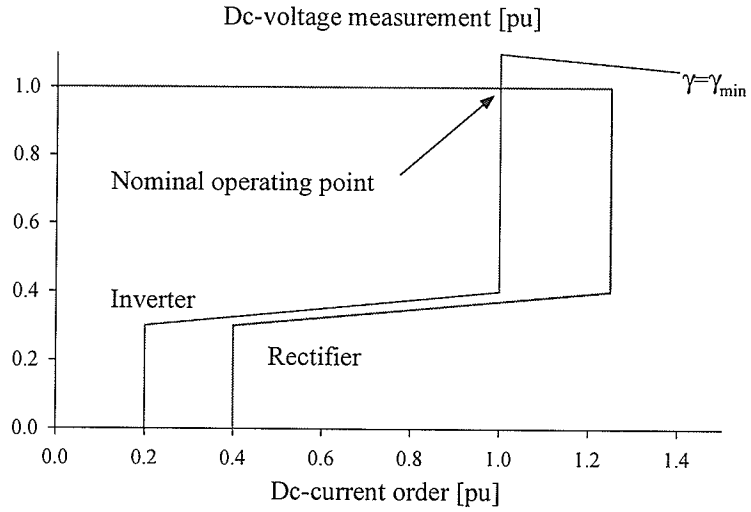

Figure 4.6 V/I characteristics for an HVDC-system with control option 1 (inverter in current control).

The rectifier controller has two possible operating modes, current control (CC) and voltage control (VC), as shown in Fig. 4.7. The VC operating mode is in charge during start-up where the rectifier dc-voltage order is ramped up to rated value, as well as in normal operation. Any transitions from VC to CC operating mode happen when the rectifier dc-current attempts to exceed 1.25 pu, which typically occurs when an ac-fault happens on the inverter side. The current order in the CC operating mode, both for the rectifier and the inverter, is calculated by the voltage-dependent-current-order-limiter (VDCOL). The VDCOL generates a current order which is dependent on the measured dc voltage, according to the characteristic shown in Fig. 4.7.

The VDCOL limits the current order during a lowering of the dc voltage as would happen in the case of an inverter side fault. This threshold voltage must be carefully selected and is chosen to be

40 % of the rated value in this design. As may be observed in Fig. 4.6, the corresponding current order is linearly reduced to 0.4 pu for dc-voltages lower than 30 % of rated value. The current order at the rectifier is somewhat higher than at the inverter. This difference in VDCOL current order between the rectifier and the inverter recharges the cable until the rectifier dc-voltage has reached its rated value, where its controls switch back to the VC operating mode.

A rapid recovery of the dc-power from an ac-fault requires a certain steepness in the rate of rise for both the current as well as for the voltage. If the current order generated from the VDCOL at both the rectifier and the inverter rise fast, then there may not be not sufficient current left to charge the cable. It is therefore critical that the current order at the rectifier is substantially larger than the order at the inverter in order to achieve an acceptible rate of rise in voltage. The two VDCOL-characteristics have to carefully designed so that a certain rate of rise in current order is obtained as the cable is being re-charged. The rate of rise in VDCOL current order output is limited by maximum slopes, one for increase and one for decrease. A slope of 15 kA/sec for increase corresponds to a rise in the VDCOL current order from zero to rated value during 160 ms. These slopes ensure that sudden jumps do not appear in the ordered current. A more rapid change is allowed for decrease than for increase, which is important to achieve a fast reduction of the current in the inverter valves during ac-faults on the inverter side.

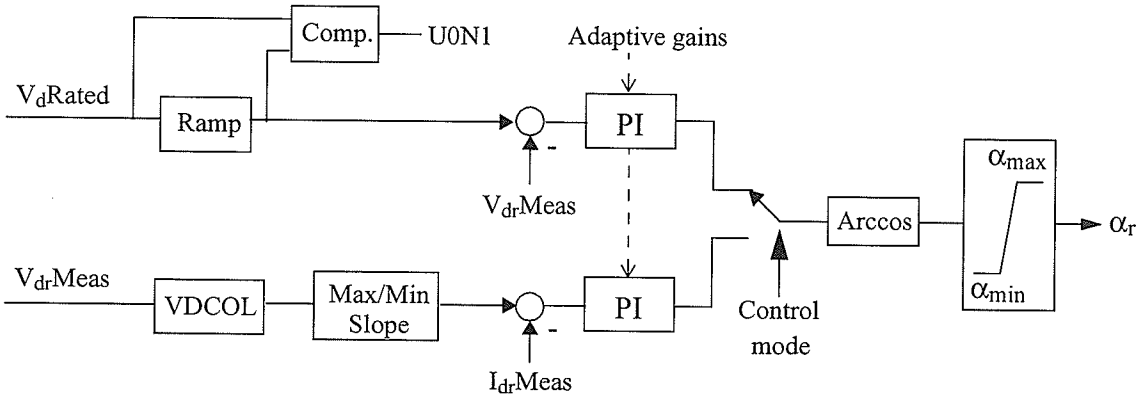

Figure 4.7 Rectifier controller.

The current controller gains at the rectifier are slowed down during the initial stage of the recovery process following such an ac-fault. This type of adaptive control reduces the gains once the ac-fault has been detected, which happens when the ac-voltage at the inverter drops below 0.77 pu. The slow controls result in a larger current peak at the rectifier. This leads to a much faster re-charging of the dc-cable once the fault has been cleared. The gains are brought back to normal values when the firing angle at the rectifier is approaching its pre-fault value. Values of 30 (conventional) and 45 (CCC) degrees were selected as the criterion at which the slow controls were disabled.

The control schemes do not allow the de-selected controller to saturate which may cause sudden jumps in the firing angle when the de-selected controller is put back in charge. This is achieved by choosing both the upper and lower limit of the de-selected controller equal to the firing angle calculated by the one in charge. Both PI-controllers in the rectifier control scheme calculate the dc-voltage order, which thereafter is re-calculated to the firing order (α_r).

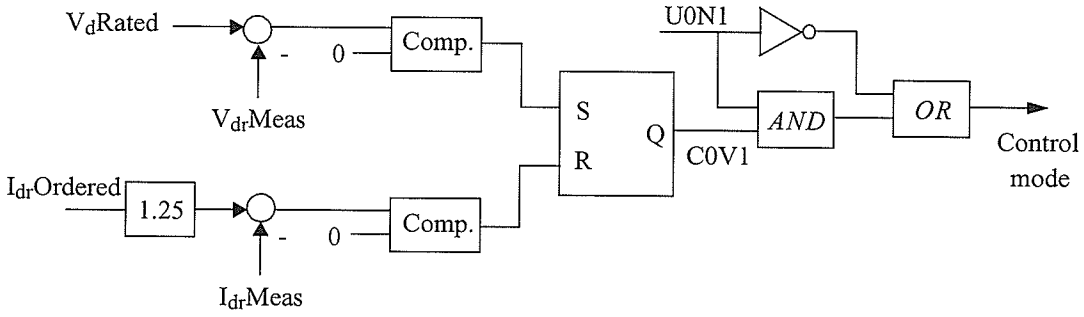

Figure 4.8 Rectifier controller mode logic.

Figure 4.8 illustrates in detail the logic which determines whether the rectifier control operates in VC or CC. The output of the SR-type flip-flop C0V1 is set during the VC operating mode. The output is reset if the rectifier dc-current attempts to exceed 1.25 pu, causing the controls to switch into CC. VC is brought back in charge when the rectifier dc-voltage has reached its rated value again. The signal U0N1 is reset during start-up so that the control-mode is forced to be set,

resulting in VC operating mode. During normal operation following the start-up, the control-mode signal is identical to C0V1 and hence CC operation is allowed if its criterion is met.

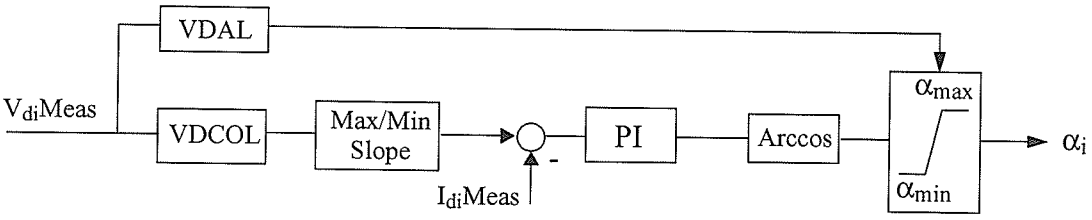

Figure 4.9 Inverter controller.

The inverter is always operating in the current control (CC) mode with a VDCOL as illustrated in Fig. 4.9. The controller-output is the firing angle α_i. Any lowering of ac-voltage at the inverter bus, typically caused by a fault, results in a surge of dc-current from the discharge of the cable capacitance. The current controller attempts to reduce this current by increasing alpha (i.e. reducing the extinction angle), which brings the inverter closer to commutation failure. The inverter is, thus, equipped with a voltage dependent maximum alpha-order limit (VDAL) in order to reduce the likelihood for commutation failure during such faults.

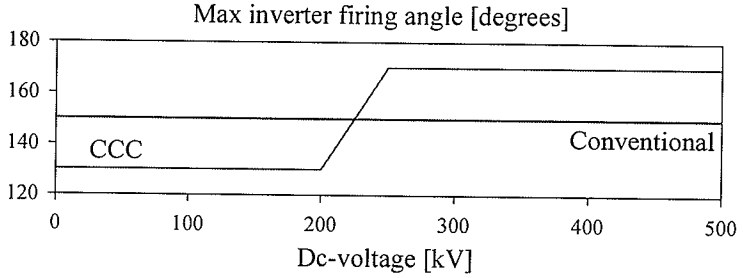

Figure 4.10 Voltage dependent maximum alpha order at the inverter.

The maximum firing angle is plotted as a function of ac-voltage in Fig. 4.10, which illustrates that the maximum alpha for the conventional inverter is constant at 150 degrees. The CCC inverter allows due to its commutating series capacitance firing angles up to 170 degrees. The maximum firing angle is reduced to 130 degrees for lower voltages. The selection of a maximum angle was

found to be an important feature in order to avoid commutation failure during faults at the inverter ac-bus for both types of inverters.

The controllers at both the rectifier and the inverter use pu-quantities - a standard feature in modern HVDC-schemes. This is convenient because the control system is independent of power rating, i.e. it can be used in schemes of different power rating and still demonstrate the same pu-behaviour. The non-linear arccos-function is introduced in order to cancel the non-linearity in the relationship between the dc-voltage and the firing angle (rectifier) or extinction angle (inverter), given in equation 4.4. This results in an almost linear response between the firing angle (or extinction angle) and the converter's dc-voltage.

As already mentioned, the rectifier may operate in voltage control or in current control, whereas the inverter is always in current control. Table A.3 in Appendix 8 gives an overview of the gains and time-constants in the PI-controllers in each of the two HVDC-schemes. The current order at each converter is provided with a maximum slope for increase as well as decrease. The tuning of the controls, i.e. gains, VDCOL-characteristics, VDCOL-slopes and firing order limits, are made on a trial and error basis with the view to optimise the converter's performance under various faults and disturbances.

4.4.4 Control option 2: Inverter in voltage control

Control option 2 is the other proposed control system and its V/I characteristics are showed in Fig. 4.11. This control option follows many of the same principles as control option 1, described in the previous sub-section. The most significant change is that the rectifier now operates in current control (CC), whereas the inverter normally operates in voltage control (VC) but switches into current control (CC) during ac-faults on the inverter side. This control option is used in both of the HVDC-schemes. Similarly to the settings in control option 1, there are minor differences in setpoints of various limits, slopes and parameters between the scheme using CCC-type inverters

and the scheme using conventional inverters.

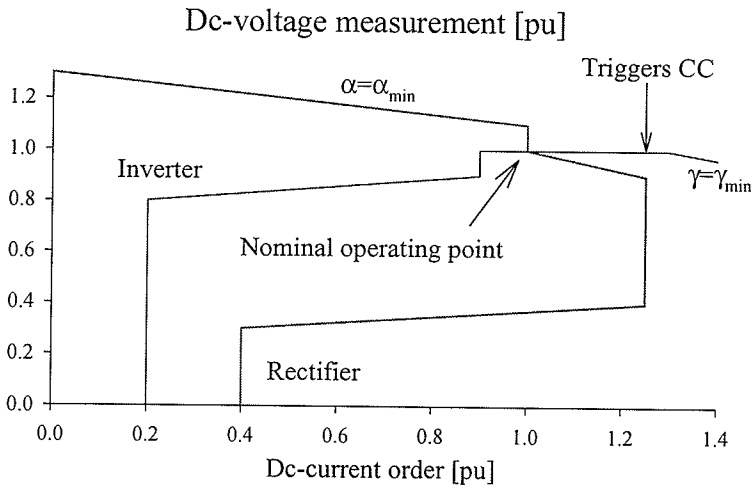

Figure 4.11 V/I characteristics for an HVDC-system with control option 2 (inverter in voltage control).

The VDCOL-characteristic in control option 2 is somewhat different than in control option 1. The most important change is that the inverter current order is kept at 0.2 pu until 0.8 pu voltage is reached. A much larger current order is now available to charge the cable, which results in a more rapid rise of voltage. The rise of the inverter current from 0.2 pu to rated value takes place as the cable voltage is increased further from 0.8 pu to 0.9 pu. Table A.4 in Appendix 8 gives an overview of the gains and time-constants in the PI-controllers in each of the two HVDC-schemes.

The transition from VC to CC at the inverter takes place when dc-current attempts to exceed 1.25 pu. Thus, it is possible that both the rectifier and the inverter are simultaneously operating in CC. It must, however, be realised that this is not a steady-state situation. VC is brought back in charge when the inverter dc-voltage has reached its rated value again.

The maximum firing angle at the conventional inverter is set to 150 degrees in order to ensure some margin to commutation failure. The CCC inverter has a voltage dependent maximum alpha-order which ranges from 130 to 170 degrees.

4.5 OPERATING POINT

To ensure successful firing, a minimum firing angle (α) of about 5 degrees is required at the rectifier, so that a sufficient positive voltage across the valve exists at the time of firing. It is, for control flexibility, customary to maintain a steady-state firing angle within a tolerance band around 15 degrees. The choice of extinction angle (γ), at the inverter represents a trade-off between low Mvar consumption (low γ), and low risk of commutation failure (high γ). The voltage source in the inverter ac-network is adjusted so that the extinction angle (γ_{real} in the CCC-inverter) becomes 22 degrees. Tap-changer control at the converter transformers is normally used to keep the firing angle and the extinction angle within their desired range, whenever they exceed their tolerance band for more than a few seconds [4]. The transformers are typically tapped with the occurrence of a lasting change in the ac-network. Due to the slow nature of the tap changer control, the instantaneous control response is provided by the controls. Tap-changer control is not included in the controls modelled here because the transient behaviour investigated takes place in a shorter time-scale.

4.6 THE CCC-INVERTER VALVE FIRING SCHEME

There are two conditions required to be fulfilled for the thyristor valve to attain the conduction state. In addition to be forward biased (positive anode-cathode voltage), a firing signal has to be present at the gate. Each valve conducts for 120 degrees during each cycle and ceases conducting when the valve current reaches zero.

Table 4.4 Commutation voltage for each thyristor valve.

Upper bridge valves	Valve 4 (c-a)	Valve 6 (a-b)	Valve 2 (b-c)
Lower bridge valves	Valve 1 (a-c)	Valve 3 (b-a)	Valve 5 (c-b)

Table 4.4 shows, in brackets, which line-to-line voltage that commutates each valve in the bridge. For each valve, a phase-locked-loop (PLL) generates a triangular signal which increases linearly from zero to one during every cycle [19]. The PLL makes sure that these signals have identical

frequency and phase as its corresponding line-to-line ac-voltage at the inverter bus. The desired firing angle, generated by the controls, is transferred into a value between zero (0 degrees) and one (360 degrees). A firing signal is sent to each valve when its triangular signal becomes larger than the firing signal.

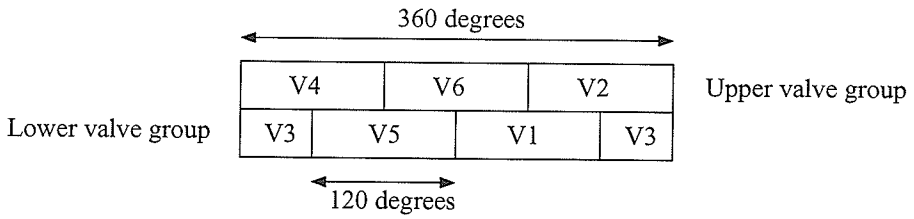

Figure 4.12 Thyristor valve conduction sequence.

Figure 4.12 illustrates in a simplified way the conduction sequence for the valves both in the upper and bottom part of the bridge during one cycle. Note that there are series inductances in the circuit, which introduces an overlap interval. During the overlap, both the in-coming and the off-going valve are conducting. The overlap interval is ignored in this illustration.

The firing of the valves in the conventional converter is less complicated, because a standard PSCAD/EMTDC converter model is used. It is simply supplied with the three-phase bus voltage measurement and the ordered firing angle. The model determines internally which valves conduct on the basis of these inputs.

4.7 VALVE BLOCKING AND BYPASSING

It is customary to include valve blocking and bypass capability in converters since this is required in order to start and stop operation in an HVDC-scheme. The valve blocking interrupts the firing signals to all the valves in the bridge. This could lead to continuous conduction in the last conduction valves, which would place the ac-voltage on the dc-cable and cause dc current to flow in the converter transformers. To avoid this, the current is normally commutated from the last conduction valves to a bypass valve and thereafter to a bypass switch. In this design, a valve

blocking and a simplified bypass-scheme have been implemented at the inverter. Instead of using a separate bypass valve, the bypass is formed by firing the valves in one of the main bridge arms.

4.8 APPARENT- AND REAL EXTINCTION ANGLE MEASUREMENT

The apparent extinction angle γ_{app} is defined as the electrical angle corresponding to the time at which a valve turns off to the positive zero-crossing of the corresponding line-to-line *voltage at the ac bus*. The critical harmonic components of this voltage have been eliminated by the ac-filters. Higher order harmonic components may, especially during transients, cause the voltage to have more than one positive zero-crossing in each cycle. The extinction angle measurement for that particular cycle, would in these cases be too inaccurate. To avoid this problem, a first-order highpass-filter with a gain of 1.0 and a time-constant of 0.5 ms (cut-off frequency of 318 Hz) is used to eliminate these higher order harmonic components. The filtered voltage has only one positive zero-crossing in each cycle, which would make the extinction angle measurement more accurate. Note, however that the highpass-filter introduces a time-delay which causes the filtered voltage to lag the bus voltage by 8.93 degrees. Hence, we have to subtract 8.93 degrees in order to obtain the correct measurement of the apparent extinction angle.

The real extinction angle γ_{real} is defined as the electrical angle corresponding to the time at which the valve turns off to the positive zero-crossing of the corresponding line-to-line *commutating voltage*. This is the voltage on the valve side of the capacitors and is a quite distorted sinusoidal waveform, which is caused by the 6 overlap intervals in each cycle. This may be observed in the bottom graph of Figure 3.6. Consider the commutation voltage between phase A and B. During the overlap interval when valve 1 is off-going and valve 3 is in-coming in the lower part of the bridge, the commutation voltage is forced from a negative value to approximately zero. The commutation voltage is similarly forced close to zero from a positive value 180 degrees later, when valve 6 takes over for valve 4 in the upper part of the bridge. These two occurrences should not be detected as a

positive and negative zero-crossing respectively. A positive zero-crossing would be detected if the commutating voltage goes positive during the first overlap case, which indeed could be happening if the voltage drop across the off-going and in-coming valves are not equal. It is necessary to ensure that this is not detected as a positive zero-crossing because it is not the one we are looking for and it would result in an inaccurate real extinction angle measurement.

To keep this from happening, an improved zero-crossing detection block is developed for the commutation voltage, where an additional criteria has to be fulfilled in order to detect a zero-crossing. It is no longer sufficient that the voltage goes from a negative value to a positive one, but the positive value also has to be larger than a certain limit (which is chosen to be 0.1). The block detects negative zero-crossings by a similar algorithm. Depending on the nature of the positive zero-crossing, this additional criteria may introduce an error of one timestep in the detection of the zero-crossing. The selected 50 μs timestep could thus result in a 0.9 degree error in the real extinction angle measurement for an individual valve. It is, however, unlikely that the error is introduced for more than one valve at the same time. Both the apparent- and the real extinction angle measurements are taken as the average value of the 6 valves in the inverter. The maximum expected error in the average real extinction angle therefore becomes 0.9/6 = 0.15 degrees.

4.9 START-UP PROCEDURE

The detailed sequences used for starting and stopping of HVDC-schemes vary depending on the manufacturer as each of them use their own components and equipment. Thus, the rise of voltage, current and power is tailored to each individual application. The HVDC-schemes discussed here require special attention because of the long dc cable involved.

In control option 1, both the rectifier and the inverter are initially blocked for 90 ms. This is done because the converter bus voltage needs time to reach steady-state after the converter is connected. Another reason is that the phase-locked-loop needs some time to lock to the ac-network voltage.

As in all HVDC-schemes, either the rectifier or the inverter must be started first. The rectifier is selected to be deblocked 10 ms before the inverter. After the rectifier is deblocked, its dc-voltage starts to build up. The inverter is still blocked and bypassed, which effectively apply a short-circuit on the dc-side. This ensures that the rectifier dc-voltage has gained a positive value when the inverter deblocks. The rectifier controls are forced to be in voltage control mode during the ramping of the dc-voltage order up to the rated value. The voltage order is built up by a rate of rise of 3000 kV pr. second, which means that the rated voltage of 500 kV is reached after 1/6th of a second. The current order at the inverter is determined by its VDCOL, resulting in a 0.25 pu current order until the dc-voltage has reached a setpoint of 30 % of rated value. The current order is thereafter gradually increased to 1.0 pu which is reached at 40 % dc-voltage.

The start-up procedure for control option 2 is also based on de-blocking the rectifier before the inverter. Both converters are, however, operated in current control, which basically means that the start-up procedure is very similar to the recovery process following an ac-fault occurrence with the exception of use of adaptive rectifier control.

Chapter 5

TRANSIENT BEHAVIOUR OF SINGLE-INFEED LONG CABLE HVDC-SCHEMES

The primary focus in this chapter is to evaluate the suitability of CCC-inverters in long cable HVDC-schemes which terminate in a weak ac-network. This is done by investigating the transient performance of the two single-infeed HVDC-schemes modelled in the previous chapter, using electromagnetic transient simulation. This evaluation was made for each of the two control options developed in the previous chapter. The performance of each scheme was examined when various faults were applied in the inverter ac network and when setpoint changes were made in the controls.

It is important that the transient behaviour of the HVDC-scheme is such that the stability of the overall system is maintained. A phenomena that plays an important role in this context is the commutation failure, i.e. failure to turn off a thyristor valve [29]. When the current (e.g. in an off-going valve in the upper part of a bridge) is brought to zero during the overlap interval, the valve requires a certain negative voltage time area in order to acquire a forward blocking capability. The required turn-off time for a thyristor valve is typically 400-500 μs, which corresponds to 7.2-9.0 degrees in a 50 Hz system. Commutation failure will occur if the valve has not established its forward-blocking capability before the positive zero-crossing of the valve voltage takes place. This phenomenon is therefore much more likely to occur at the inverter than at the rectifier, since the valve becomes forward biased shortly after it has finished its conduction duty. The commutation failure may be triggered by a sudden voltage reduction in the inverter ac-voltage and results in continuing conduction in the off-going valve. If the commutation between the valves in the lower

part of the bridge continues as normal, then there will be a 120 degree interval during the next cycle, where the bridge is short-circuited on the dc-side. The dc-current will increase and the dc-cable starts discharging through the valve pair that is by-passing the bridge. During the time the dc-voltage is zero, no dc-power will be transmitted in the HVDC-scheme. This might impose a severe disturbance on the ac-network that could lead to subsequent commutation failure, particularly if the ac-network is weak. It is therefore of great importance that HVDC-schemes are designed to withstand disturbances in the ac-network.

The results from several types of disturbances are presented and discussed in the following sections. The last section makes a final evaluation of the two inverter types and the two control options on the basis of the obtained results. The presented results for the CCC single-infeed HVDC alternative are obtained with surge arrestors across its series capacitors.

5.1 INVERTER LOAD REJECTION

An HVDC-converter, including the CCC, normally consumes reactive power both when operating as a rectifier and as an inverter. The amount of reactive power consumed at the converter bus increases with the transformer reactance as well as with an increased firing angle (rectifier) or extinction angle (inverter). The conventional converter normally consumes reactive power in the range of 0.5-0.6 pu of the transmitted dc-power. The corresponding amount for a CCC-type converter is, due to its ability to operate at a lower extinction angles, significantly less (about 0.15 pu). The installed Mvar in ac-filters and capacitor banks is thus significantly less at the CCC-converter bus compared to the conventional.

A sudden change in active dc-power transmitted, for instance caused by an inverter load rejection, therefore results in a change in the reactive power consumed at the converter bus. The immediate surplus of reactive power will temporarily raise the bus voltage particularly if the ac-network is weak. This temporary overvoltage can be reduced within 200-600 ms [22] by the generator

excitation system in ac-networks where the converter bus is located in close proximity to generator infeed. If the generators are remotely located from the converter bus, then the overvoltages can be sustained for many seconds. The use of fast acting voltage-regulating equipment close to the converter bus, such as static var compensators (SVCs), is one way to reduce the overvoltages in such a case.

The HVDC-schemes under study have neither generators nor SVCs in close proximity to their inverter bus. This results in a permanent overvoltage in the ac-network after a load rejection of the inverter. The load rejection is applied by the formation of a bypass-pair in the inverter valves. The steady-state overvoltage resulting from the blocking of the CCC-inverter is recorded to 350.5 kV (i.e. 1.17 pu), as shown in Fig. 5.1. This overvoltage is significantly smaller than that generated by the blocking of the conventional inverter 448.5 kV (1.50 pu), which is plotted in Fig. 5.2. These results are valid regardless of the control option that is used. The load rejection overvoltage can also be calculated theoretically, simply using the ac-network voltage magnitude, the impedance of the network equivalent and the filter impedance (including any shunt capacitors) at fundamental frequency, as indicated in (5.1).

$$Overvoltage = V_s \cdot \frac{Z_{filter}}{Z_{filter} + Z_{network}} \tag{5.1}$$

The theoretical overvoltages were calculated to 352.0 kV (i.e. 1.17 pu) and 450.5 kV (1.50 pu) respectively for the CCC and the conventional inverter. This means that the simulated and the theoretical results agree very well. These overvoltages will be less if saturation effects in the converter transformer are included in the model.

The presence of the CCC lowers the load rejection overvoltage simply due to the smaller amount of Mvar installed at its inverter bus. The presence of a CCC-inverter has therefore a favourable impact on the ac-network for this particular disturbance, when compared to the conventional type.

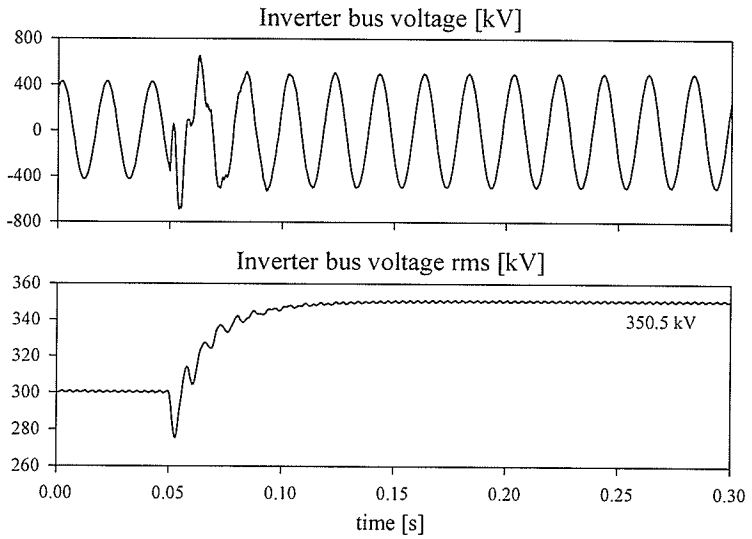

Figure 5.1 Overvoltage following a CCC inverter block using control option 1.

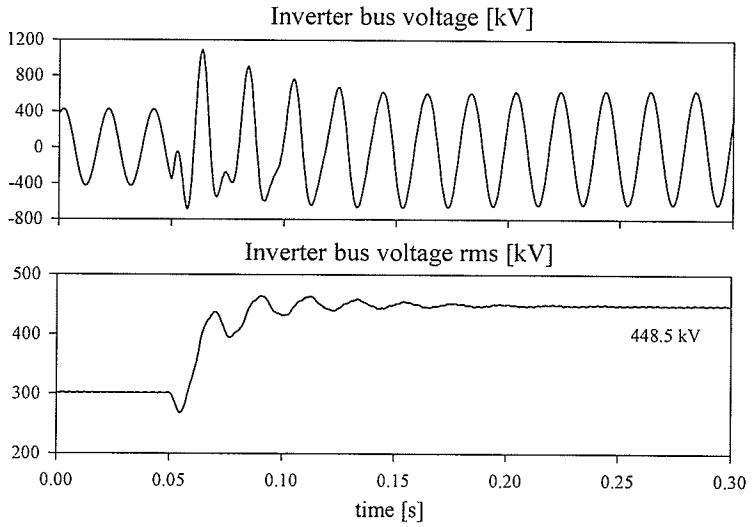

Figure 5.2 Overvoltage following a conventional inverter block using control option 1.

5.2 PHASE SHIFT IN THE AC-NETWORK VOLTAGE SOURCE

The next disturbance investigated is a sudden phase shift in the ac-network source voltage. This simulates a phase shift due to sudden changes in the load close to the inverter bus. Such a phase shifts can result in a sudden decrease of the extinction angle, and thus lead to commutation failure. The phase shift due to an inductive load-increase results in a similar response from the controls as a negative phase shift in the source voltage. The increase of a capacitive load and a positive phase

shift also trigger similar actions in the controls. The source voltage lags the inverter bus voltage during steady-state operation.

The application of a phase shift in the leading direction (positive) in the source voltage also causes the phase angle in the inverter bus voltage to move in the same direction. The phase-locked-loop based valve firing scheme needs, due to its time-constant, some time to lock back to the bus voltage. The phase-locked-loop signal lags its corresponding inverter bus voltage during this period of time, which means that the valves are fired later than they should have been. In other words, the real firing angle is larger than the ordered firing angle output of the controls, simply because the valve firing instants are related to the phase-locked-loop signal and not to the bus voltage. This basically means that the dc-voltage appearing at the inverter becomes transiently larger than the ordered firing angle "asks for". The increased inverter dc-voltage reduces the inverter dc-current below rated value. These events occur in the transient time-scale immediately after the positive phase shift in the source voltage has been applied.

The secondary response to this disturbance takes place in the control system. Let us first consider control option 1 where the inverter operates in current control. The controller now attempts to increase the dc-current back to rated value by lowering the firing angle. A similar response in the firing angle was observed when the HVDC-scheme was operated by control option 2. In this case, the voltage controller at the inverter attempts to bring the inverter dc-voltage down to rated value by lowering the firing angle. The secondary response to a positive phase shift in the voltage source, is thus to decrease the firing angle.

A similar argument can be made on the application of a negative phase shift in the voltage source, except now the inverter bus voltage lags the phase-locked-loop signal transiently. This results in a smaller real firing angle than the ordered firing angle. The response by the controls is, in this case, to increase the firing angle.

Table 5.1 presents the maximum phase shifts both in the leading (positive) and lagging (negative) direction that could be applied in the voltage source without causing commutation failure for each single-infeed HVDC alternative. The results show clearly that the CCC is able to withstand a significantly larger phase shift in the lagging (negative) direction compared to the conventional converter regardless of the control option employed. As explained above, the negative phase shift results in a larger dc-current and the control response is to increase the firing angle. This will clearly reduce the extinction angle and thereby also reducing the margin to commutation failure for both converter types.

Table 5.1 Maximum and minimum phase shifts [degrees] in the ac-network voltage.

Single-infeed HVDC alternative			
Control option 1		Control option 2	
Conv.	CCC	Conv.	CCC
+20/-7	+10/-41	+15/-6	+11/-34

The impact of the increased dc-current on the commutation margin is however much worse for the conventional than for the CCC converter. An increased dc-current in the conventional converter leads to a larger overlap interval which in turn reduces the extinction angle. As explained in earlier chapters, the presence of the series capacitors in the CCC assists in the commutation process. The capacitor in both the off-going and the on-coming phase are charged with a polarity that increases the commutation voltage during the overlap interval. An increased dc-current would result in additional availability of series capacitor voltage, and therefore assist even more in the commutation process. This is the reason why the CCC was observed to withstand a substantially larger negative phase shift in comparison to the conventional converter type.

A phase shift in the leading (positive) direction is, due the above-mentioned reasons, expected to be a less critical disturbance to the conventional converter, compared to a negative phase shift. The lowering of the dc-current, generated by the positive phase shift, decreases the overlap interval and

should hence increase the margin to commutation failure. The results presented for the conventional converter agree with this theory since they show that a larger positive than a negative phase shift is possible without causing commutation failure. The results presented for the CCC converter show the opposite behaviour; that it is able to withstand a smaller positive than negative phase shift. The CCC converter is, in other words, more sensitive to a positive than a negative phase shift in the source voltage. The decreased dc-current generated by the positive phase shift, results in a reduced series capacitor voltage and thus less assistance in the commutation process.

From the results it is evident that the CCC converter is significantly more robust against a negative phase shift in the source voltage compared to the conventional type. The negative phase shift triggers a similar control response as an inductive load-increase, which is the most common type of load. The performance of the CCC is therefore superior in comparison to that of the conventional type for this particular disturbance. The conventional converter is, however, more capable of withstanding a positive phase shift in the voltage source. The positive phase shift is, however, considered to be less relevant in comparison to the negative phase shift.

5.3 ROBUSTNESS AGAINST REMOTE AC-FAULTS

The recovery performance of the each single-infeed HVDC alternative are investigated when two types of remote faults are applied in the inverter ac-network. A remote fault is, in this context, defined as a fault occurring electrically distant from the converter bus. The remote faults are, due to the primarily inductive impedance of transmission lines, simulated by connecting a shunt reactor at the inverter bus, as illustrated in Fig. 5.3. The minimum value of fault inductance under which the system remains operating without commutation failure, is identified by trial and error. Any fault with more severity (lower inductance) than this limiting value causes commutation failure. Because a low inductance corresponds to a more severe fault, the lower the limiting inductance, the more robust is the scheme. The results are obtained using a fault clearance time

ranging from 40 to 200 ms. The critical inductances obtained are identical regardless of which clearance time that is selected within this range. The clearance time will, however, have an impact on the recovery performance if the remote fault is severe enough to cause commutation failure and subsequent discharge of the dc-cable.

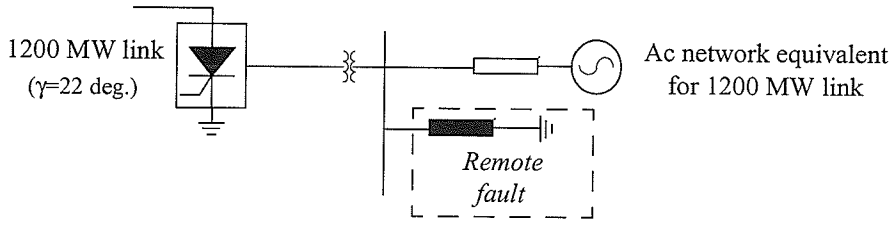

Figure 5.3 A remote fault applied in a single-infeed HVDC-scheme.

5.3.1. Single-phase to ground fault

The HVDC-schemes' robustness against a single-phase to ground remote fault in the inverter ac-network, is investigated. This particular type of fault accounts for about 85 % [5] of all faults that occur in overhead lines and it is, in literature [29], considered to be more severe than a three-phase fault in terms of commutation failure. The reason for this is due to the fact that the single-phase faults result, contrary to the balanced three-phase fault, in phase-shifts in the zero-crossings of the commutating voltages. These phase-shifts decrease the commutation margin for some of the thyristor valves and increase it for other valves.

Table 5.2 Limiting (minimum) inductance simulating a single-phase remote fault.

Single-infeed HVDC alternative			
Control option 1		Control option 2	
Conv.	CCC	Conv.	CCC
0.75 H	1.04 H	0.77 H	0.79 H

The results do not support this theory since all the schemes demonstrate a larger degree of robustness against the single-phase fault (Table 5.2) in comparison to the three-phase fault (Table 5.3). The reason could be the presence of the large cable capacitance since the single-phase fault

results in a smaller lowering of the dc-voltage and thus also in a smaller discharge current from the cable.

The results for the single-phase fault demonstrate two main findings. Firstly, the conventional converter is more robust against this type of remote fault in comparison to the CCC for both control options. This may be explained by the fact that an imbalance in the series capacitor voltages will generate problems for the commutation process of the CCC. Secondly, that one control option is not generally superior to the other.

5.3.2. Three-phase to ground fault

The HVDC-schemes' robustness against a balanced three-phase to ground remote fault in the inverter ac-network, is investigated in the following. This type of fault is considered more severe than a single-phase fault for long cable dc transmission and its transient performance is therefore analysed more thoroughly.

The steady-state impact of such a disturbance is first investigated theoretically. The results show that the application of the remote fault causes the inverter ac-bus voltage to drop in magnitude and its phase angle to move in the leading direction. Both these effects bring the inverter closer to commutation failure. They happen immediately and occur at both converter types, but to a larger extent for the conventional compared to the CCC. The theoretical results therefore indicate that the CCC should be more robust against this type of remote fault in comparison to the conventional converter.

Let us consider the immediate impact caused by the remote fault prior to any actions taken by the controls (i.e. the firing angle remains constant). The drop in the inverter ac-voltage magnitude clearly increases the overlap angle and hence increases the likelihood of commutation failure. The positive phase shift in the ac-voltage takes place instantaneously whereas the phase-locked-loop (PLL) based valve firing scheme needs, due to its time-constant, a certain time to lock on to the ac-

voltage again. The ac-voltage leads its PLL-signal during this period of time, which means that the real firing angle is larger than the ordered firing angle. A larger real firing angle at the inverter results in a smaller commutation margin since the valves become forward biased sooner after they cease conducting. Both the two above-mentioned effects are thus bad from the commutation point of view, but they have opposite impact on the inverter dc-voltage. The drop in magnitude permanently reduces the dc-voltage, whereas the positive phase-shift temporarily increases the dc-voltage.

Table 5.3 Limiting (minimum) inductance simulating a three-phase remote fault.

Single-infeed HVDC alternative			
Control option 1		Control option 2	
Conv.	CCC	Conv.	CCC
1.22 H	1.16 H	1.36 H	1.06 H

From the simulation results, it is clear that the dominant impact is due to the drop in magnitude, since the natural response from the controls is to compensate for the reduction in dc-voltage by increasing the ordered firing angle. This is reasonable because the positive phase-shift has no impact on the commutation process once the PLL has locked on to the voltage again.

The results presented in Table 5.3 show that the CCC is able to withstand a significantly more severe remote fault than the conventional type. This result is expected since the CCC allows a much larger firing angle compared to the conventional inverter and there is no voltage imbalance between the series capacitors. Each of the two single-infeed HVDC alternatives demonstrates similar fault performance for both control options.

Figure 5.4 illustrates the performance of the CCC single-infeed HVDC-scheme operated in control option1, when it is subjected to a severe (L=1.16 H) three-phase remote fault at its inverter bus. The inverter bus voltage is suppressed during the fault causing a significant increase in the dc-

current. The rectifier switches from voltage to current control. The current controller at the inverter attempts to reduce the current to rated value (2.4 kA) by increasing its firing angle. The firing angle hits its 170 degree ceiling and sits there until the fault is cleared. The real extinction angle is transiently reduced to 7.5 deg. shortly after the application of the fault at 50 ms.

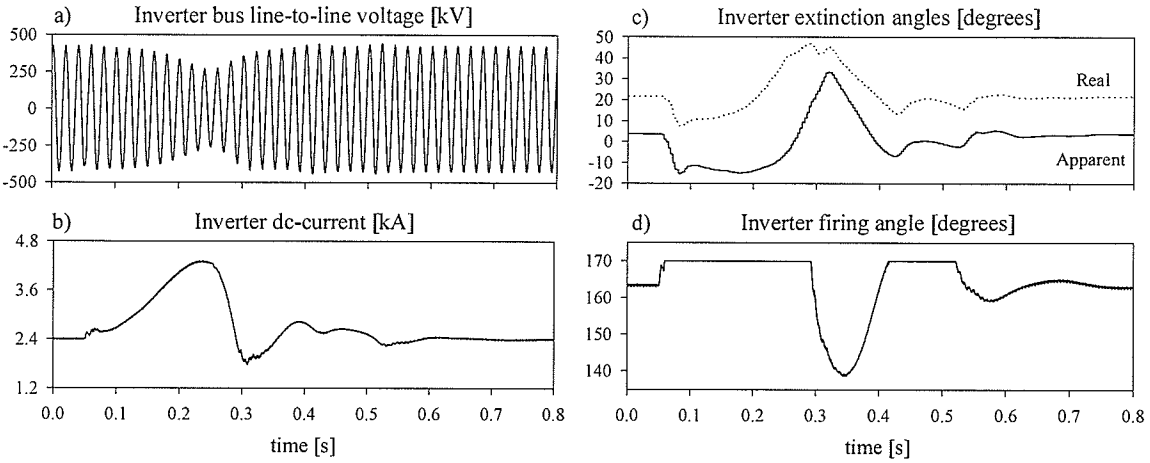

Figure 5.4 A three-phase remote fault applied at the CCC single-infeed HVDC scheme.

5.4 RECOVERY FROM CLOSE-IN AC-FAULTS

Commutation failure and succeeding discharge of the cable into the inverter ac-network is often unavoidable if the ac-fault takes place electrically very close to the converter bus. Power-recovery of HVDC-schemes is usually more difficult and slower for weak ac-networks in comparison to strong networks. Fast recovery is, however, more critical for weak networks in order to maintain stability, because they are less capable of withstanding the temporary deficit of power.

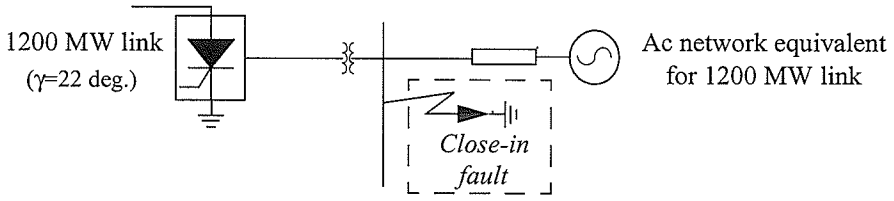

Figure 5.5 A close-in fault applied in a single-infeed HVDC scheme.

The recovery performance is investigated when a 50 ms single-phase and a three-phase to ground fault are applied at the ac inverter bus in each single-infeed HVDC alternative. The clearance time

is mainly determined by the relay detection time and breaker switching time. The latter obviously depends on the type of breaker used. The selected fault clearance (50 ms) requires state-of-the-art equipment both for relays and breakers. The recovery time is defined as the time from fault clearing to the instant at which 90 % of the pre-fault dc-power is restored.

5.4.1. Single-phase to ground fault

The recovery performance was investigated when a 50 ms single-phase to ground fault was applied at the ac inverter bus in the HVDC-schemes. Table 5.4 shows the recovery time and dc-current peak at the rectifier as well as the inverter for each single-infeed HVDC-alternative for both types of controls. It is evident that control option 1 results in a quicker power recovery in comparison to control option 2.

Table 5.4 Recovery performance following a single-phase to ground close-in fault.

	Single-infeed HVDC alternative			
	Control option 1		Control option 2	
Inverter type:	Conv.	CCC	Conv.	CCC
Recovery time	145 ms	240 ms	170 ms	300 ms
Rectifier current peak	7.9 kA	5.5 kA	10.4 kA	5.3 kA
Inverter current peak	18.0 kA	17.6 kA	17.9 kA	17.3 kA

Figure 5.6 shows the performance following the fault of both the conventional (solid-drawn) and the CCC (dashed) single-infeed HVDC alternative when they are operated by control option 1. The results show that the CCC demonstrates a slower recovery than the conventional type for both control options. The rectifier peak dc-current is somewhat lower for the single-infeed HVDC alternatives using CCC-inverters, which is favourable since it lowers the current stress on the valves. The reason for this behaviour can be explained by the settings in the current controller at the rectifier. The controller in CCC single-infeed HVDC alternative is not slowed down as much as in the conventional alternative. The controller in the CCC alternative is therefore more capable

of reducing the rectifier current by increasing its firing angle.

The single-phase to ground fault is, in general, considered to be less severe than three-phase faults in terms of power system stability. This type of unbalanced fault can, however, be particularly critical for the CCC since it may generate imbalance in the series capacitor voltages which may result in performance deterioration during transients. The surge arresters will however limit any imbalances from reaching extreme values.

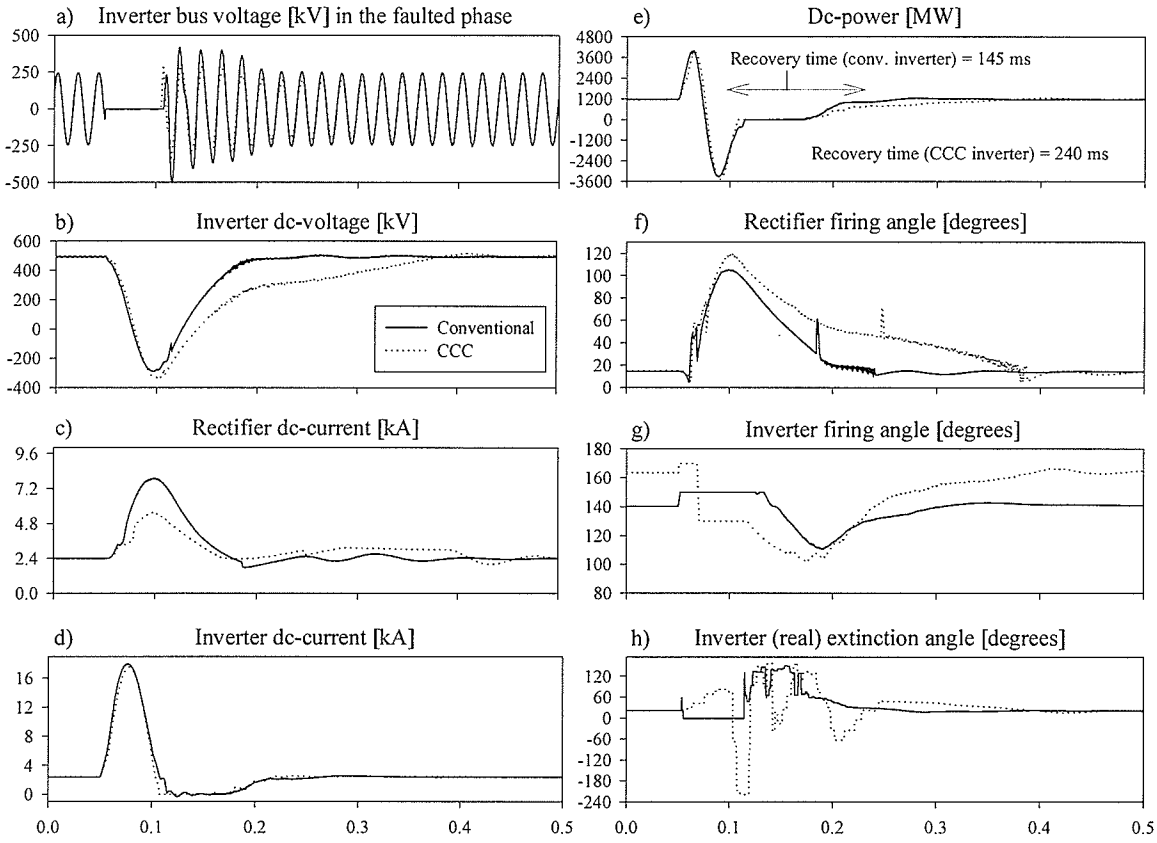

Figure 5.6 Single-phase to ground fault applied at the inverter bus in the conventional and CCC single-infeed HVDC alternative using control option 1 (inverter in current control).

5.4.2. Three-phase to ground fault

The recovery performance was investigated when a 50 ms three-phase to ground fault was applied at the ac inverter bus in each of the single-infeed HVDC-alternatives. Table 5.5 presents the recovery time and dc-current peak at the rectifier as well as at the inverter. The results show that

the use of CCC-inverters has the effect of lowering the transient peak in both the rectifier and the inverter dc-current. This is favourable since it reduces the current stress on the valves. Each alternative demonstrates a recovery time that falls within 300 ms for both types of control option, which is considered acceptable since most HVDC-schemes recover within 100 to 300 ms. Recovery times up to 500 ms may be required [22] if the ac-network is weak. The recovery time of the CCC single-infeed HVDC-scheme operated in control option 1, is 90 ms. This rapid recovery is quite remarkable particularly in the view of the weak ac-network. Control option 1 demonstrates a more rapid recovery of the dc-power transmitted for both single-infeed HVDC alternatives.

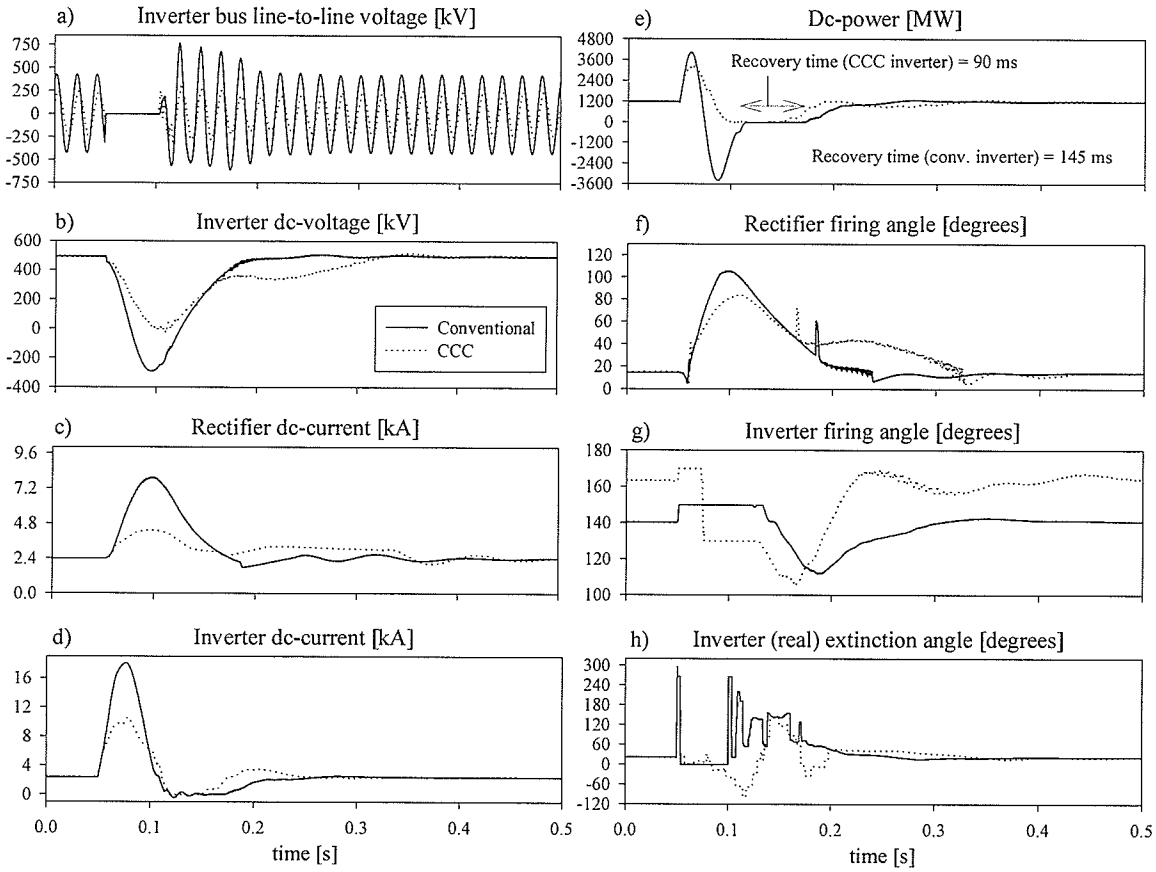

Figure 5.7 Three-phase to ground fault applied at the inverter bus in the conventional and CCC single-infeed HVDC alternative using control option 1 (inverter in current control).

Figure 5.7 shows the performance following the fault of both the conventional (solid-drawn) and the CCC (dashed) single-infeed HVDC alternative when they are operated by control option 1.

From the results, it is evident that the CCC alternative demonstrates a quicker recovery than the conventional when operated by this control option. Figure 5.7a clearly shows that the conventional alternative has a much higher temporary overvoltage after fault clearance in comparison to the CCC-alternative. The surge of current into the ac-network, given by the inverter dc-current, is reduced from 18.1 kA (7.5 pu) in the conventional option to 10.6 kA (or 4.4 pu) in the CCC-option. The results for control option 2 are very similar. Figure 5.7e, shows that the dc-power becomes negative after the fault in the conventional single-infeed alternative. As the dc-current is always positive, the negative power is a consequence of the dc-voltage being negative. With a sustained line-to-line short-circuit as happens during a commutation failure, the ac-voltage gets applied to the dc-side resulting in this negative value, as seen in Fig. 5.7b. The dc-power remains positive in the CCC alternative because the additional capacitor voltages have a phase relationship, such that the resulting dc-voltage, although low in magnitude, does not become negative for the operating conditions considered here.

Table 5.5 Recovery performance following a three-phase to ground close-in fault.

	Single-infeed HVDC alternative			
	Control option 1		Control option 2	
Inverter type:	Conv.	CCC	Conv.	CCC
Recovery time	145 ms	90 ms	165 ms	185 ms
Rectifier current peak	7.9 kA	4.3 kA	10.4 kA	4.2 kA
Inverter current peak	18.1 kA	10.6 kA	17.4 kA	10.9 kA

5.4.3. Parameters sensitive for recovery enhancement

The recovery performance for close-in faults or any other fault, depends on the characteristics of the ac and dc systems as well as the settings in the control system. It is necessary to perform a careful tuning of the controls so that the HVDC-schemes demonstrate good performance for all faults and disturbances analysed. The tuning is done with the objective to optimise the performance following a three-phase fault since this is considered to be the most severe type of

fault in terms of power system stability. First of all, the allowable rate of restoration must be carefully chosen in order to avoid new commutation failures from occurring during the recovery process. The large energy storage in the dc-cable capacitance results in an HVDC-scheme with high inertia, which must be handled gently in order to ensure successful recovery. The presence of a weak ac-network at the inverter side is another factor which requires a relatively slow recovery from the fault. A rapid power recovery will quickly increase the reactive power drawn from the ac-network, which may generate large fluctuations in the ac-voltage. This can result in unsuccessful recovery due to commutation failure. It may therefore be necessary to slow down the rate-of-rise of power during the recovery.

As explained in section 4.4, the control system is designed with a trade-off between the rate-of-rise of voltage and current in order to achieve a rapid recovery. This is a crucial point in the design of a suitable control system. In addition to the gains, several other control parameters have significant impact on the recovery performance, such as the adaptive rectifier control, limited allowable change in the VDCOL-current order and the maximum inverter firing angle. The impact from the setting of each of these parameters on the HVDC-scheme's performance is discussed below.

A reduction of the rectifier controller gains was found necessary in order to achieve good performance. The reduction of the gains is done by a certain factor ranging from 5 to 2.5 for the HVDC-scheme alternatives. This slow control mode is enabled once the ac-fault has been detected, and is disabled at the end of the recovery when the rectifier firing angle approaches its nominal value again. The use of this type of adaptive control results in a more rapid recovery, but also results in a larger dc-current peak at the rectifier.

The allowable change in the VDCOL-current order, at both the rectifier and the inverter, is limited by a maximum slope for increase and decrease. A relatively low slope for decrease is important to achieve a rapid recovery. This ensures that the current order has not dropped to its minimum valve

at the moment the fault is cleared where the recovery process starts. The slope is also important in order to make a step-change of the dc-current from 1 to 0.01 pu without causing commutation failure. A steeper slope for current order decrease is suitable for the conventional converter in comparison to the CCC. This may be explained by the fact that the series capacitors in the CCC represent additional inertia that needs to be handled with care. The slope related to increase is roughly the same for both converter types and significantly smaller than the slope related to decrease.

The setting of the maximum allowable firing angle also have a major impact on the results, which is to be expected. The natural response from the controls is to increase the firing angle in order to limit the surge of current when the cable discharges, which reduces the inverter's margin to commutation failure. The maximum firing angle for the conventional converter is set to 150 degrees. The CCC-inverter has the ability to operate at much larger firing angles. In this design, a dc voltage-dependent maximum firing angle limit is used, which ranges from 130 degrees at low dc voltages to 170 degrees at large voltages. These limits result in higher robustness against remote ac-faults and negative phase-shifts in the network voltage compared to larger values.

5.5 SETPOINT CHANGES IN THE DC-CONTROLS

A step change is made to the dc-current order at rated conditions to evaluate the robustness of the schemes to set-point changes in the controls. This essentially means a step-change in the ordered dc-power.

Table 5.6 Maximum step-change in the dc-current order.

Single-infeed HVDC alternative			
Control option 1		Control option 2	
Conv.	CCC	Conv.	CCC
+16 % -99 %	+24 % -99 %	+14 % -99 %	+20 % -99 %

Table 5.6 shows the maximum step-changes that could be made without causing commutation failure for each single-infeed HVDC alternative. A generally accepted performance level is that the HVDC-schemes should follow an instantaneous ±10 % change in order. All the alternatives meet this specification, albeit with varying margins.

The results demonstrate two major findings. Firstly, a slightly larger percentage step-increase is possible for both single-infeed HVDC-alternatives if operated by control option 1 instead of control option 2. Secondly, that the CCC-inverter type is superior to the conventional since the former allows a larger step-increase in the dc current compared to the latter converter type. Each single-infeed HVDC-alternative allows a 99 % reduction of the dc-current from rated conditions. This means that sudden current reductions which are required for protective strategies can easily be accommodated in all the single-infeed alternatives. The maximum allowable change of the VDCOL dc-current order has to be relatively low in order to make such a large step-decrease in the dc-current without causing commutation failure.

The results are highly dependent on the settings in the control, particularly the maximum allowable change in the VDCOL dc-current order. With the settings selected here, it is evident that the CCC-inverter based single-infeed HVDC alternative demonstrate superior performance.

5.6 IMPACT OF SURGE ARRESTORS

The impact of the use of surge arresters across the series capacitors is examined by investigating the transient performance of the CCC single-infeed HVDC-alternative with and without surge arrestors across the series capacitors. Figure 5.8 plots the behaviour of the two options together when a three-phase to ground fault is applied at their inverter ac bus. The performance of the CCC single-infeed HVDC scheme is plotted in solid-drawn graphs, whereas the performance without surge arrestors is plotted in dashed graphs. The graphs clearly identifies two improvements in the performance due to the presence of the surge arresters:

- Reduction of the dc-current peak at both the rectifier and the inverter.
- Reduction of the recovery time.

These two findings hold true for both control option. The only deterioration observed by the addition of surge arresters is longer recovery time for single-phase to ground faults. This finding is somewhat surprising because the surge arresters limit any imbalance between the series capacitor voltages and should therefore improve in the commutation process. The performance with and without surge arresters are very similar for phase-shifts in the network voltage, remote faults and for setpoint changes in the controls.

It is therefore reasonable to conclude that the option with surge arrestors included across the series capacitors demonstrate, in general, the better performance.

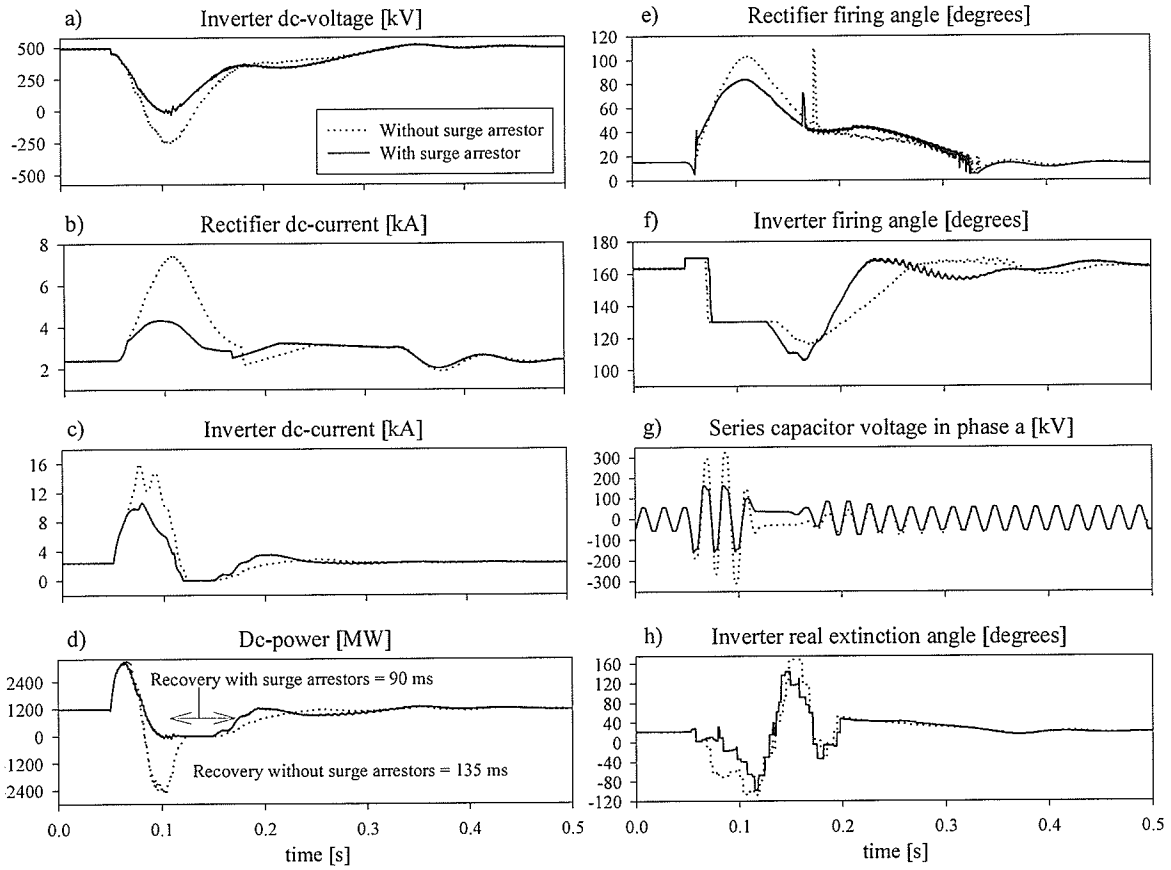

Figure 5.8 Three-phase to ground close-in fault applied at the inverter bus in the CCC single-infeed HVDC alternative using control option 1 (inverter in current control).

5.7 PERFORMANCE EVALUATION SUMMARY

The occurrence of faults on a dc-cable is very rare and is therefore not included in the investigation of the transient performance. The evaluation of the converter types and the control options in this section are carried out with surge arrestors included across the series capacitors in the CCC-inverters. From the results it is also clear that the use of control option 1 leads to superior performance in comparison to control option 2 for most of the faults investigated, as outlined in the following.

- Consistently better recovery times for both three-phase and single-phase to ground faults.
- The conventional single-infeed HVDC alternative exhibits significantly better performance if operated by control option 1 after the application of a negative phase shift in the network voltage. The CCC single-infeed alternative is, however, slightly most robust against this phase shift when it is operated by control option 2.
- Significantly larger negative phase shift in the network voltage possible for the CCC-inverter based single-infeed HVDC-alternative.
- A slightly larger increase of setpoint value for the dc-current is possible.

The main objective of the chapter was to investigate the suitability of CCC-inverters in long cable HVDC-schemes terminating in weak ac-networks. The improvements in the performance, due to the use of CCC-inverters, (with surge arresters across the series capacitors) are listed in the following:

- The CCC requires less reactive power installed at its converter bus, which results in a significantly smaller overvoltage following an inverter load rejection.
- A much larger negative phase-shift in the network voltage is possible at the CCC-inverter for both control options.
- The CCC-inverter is able to withstand a more severe three-phase to ground remote fault for both control options.
- The CCC has a significantly lower dc-current peak at the inverter for three-phase to ground close-in faults for both control options.
- The CCC has considerably shorter recovery after three-phase faults when operated by control option 1.

However, the application of a CCC-inverter in this type of HVDC-scheme results in performance deterioration following the occurrence of unbalanced faults:

- The HVDC-scheme, based on CCC-inverters, exhibit a longer recovery time after single-phase to ground close-in faults for both control options.
- The HVDC-scheme based on CCC-inverters is less robust against single-phase to ground remote faults for both control options.

Unbalanced faults introduce a certain imbalance between the series capacitor voltages in the CCC-inverter, which may generate problems for its commutation process. This may explain the performance deterioration that was observed.

The HVDC-scheme alternatives demonstrate very similar performance for the remaining faults and disturbances examined. With the exception of single-phase to ground faults (remote and close-in), it is therefore evident that the CCC-inverter based HVDC-scheme has the better performance.

Chapter 6

ACTIVE FILTERING

This chapter discusses the application of an ac side active filter in HVDC schemes involving capacitor commutated converters like the CCC or CSCC [13]. A suitable topology and control algorithm is developed to achieve the necessary objective of filtering the lower order characteristic harmonics. The dependence of the filter's rating on parameters such as the extent of de-tuning of its passive elements is investigated. The performance of this filter in a capacitor commutated converter application is then evaluated using an electromagnetic transient simulation program. One concern is the possibility of adverse interactions taking place between the dc-controls and active filter.

6.1 INTRODUCTION

One particular advantage of the capacitor commutated converters is that they require a much smaller amount of reactive power support in comparison with conventional converters. In conventional HVDC transmission, the ac filters not only absorb the current harmonics, but they also provide a major component of the reactive power support.

6.1.1 The case of active filter at CCC-buses

For the reasons discussed above, the filters in the CCC and CSCC options are required primarily for harmonic elimination and provide only a very small amount of reactive power. When the filters have a low Mvar rating, they also have a narrow pass-band, which makes them more sensitive to detuning effects. Some mechanism of on-line tuning is therefore necessary in order to keep the

filter in tune during frequency drift or when component values change due to aging or failure of capacitor cans. This re-tuning can be realised with the use of active filters that utilise active devices to synthesise the appropriate voltage or current waveforms, which result in harmonic removal from the system. Another alternative [25] is the use of continuously tuned inductors.

6.1.2 Background

Although proposed earlier by Wong et al. [24], active filters for HVDC-applications have only recently been considered [23] due to the availability of high-frequency active switching devices such as Insulated Gate Bipolar Transistors (IGBTs). Active filters have also been proposed for harmonic removal and reactive compensation in distribution systems [28].

Because of the larger voltage and current ratings, the introduction of active filters in HVDC transmission has been somewhat slower. The first application was for filtering on the dc side [25]. It is relatively easy to introduce the active filter on the dc side because of the small harmonic content (other elements such as the smoothing reactance also provide some harmonic mitigation) and due to the fact that there is no fundamental frequency current that flows through the filter.

However, for use in ac side applications at the converter bus, some special considerations are required on account of the potentially larger voltage and current ratings. One problem with IGBT and other high-power switching devices is the difficulty of series connection that imposes a limit on the maximum voltage rating. Thus, the active elements may require a transformer interface to the power system so that voltage ratings of the switching devices are not exceeded. Another requirement is to ensure that the switching frequency of the devices is limited so that excessive switching losses and the associated thermal problems are avoided. It must also be realised that the control system plays an important role in the performance of the active filter. It must have an acceptable dynamic response and not have any adverse control interaction with the HVDC system.

The active filter discussed here (see Fig. 6.1) is specifically for application at CCC converter buses

and is thus different in topology from that described by Plaisant and Reeve [26]. Their approach eliminated harmonics of all orders and used a coupling filter that blocked any fundamental frequency current. Our approach targets only the most significant harmonics (11th and 13th) with the view to minimise the switching frequency of the IGBT devices. The coupling filter is tuned to the harmonics targeted for elimination and also provides a portion of the reactive power requirement of the converter (approx. 10-15 % of the rated dc-power in a typical CCC installation)

The design principles for the proposed filter are discussed in the following sections. The ensuing design and its proper operation at a CCC converter station are then verified using electromagnetic transient simulation.

6.2 THE PROPOSED ACTIVE FILTER

A simplified diagram of the proposed active filter application is shown in Fig. 6.1. The filter consists of an active controlled voltage source, based on the forced commutation Pulse-Width-Modulation (PWM) technique, in series with a passive coupling filter. The coupling filter serves two purposes:

- It provides a low-impedance path for the harmonics that are to be removed, and thereby lowers the effort required by the active source. This results in lower ratings in the filter.
- It also creates a high-impedance path to the fundamental frequency component of ac-voltage, thereby shielding the active components from the full brunt of the ac-voltage magnitude.

The active source is continuously adjusted by the control system, described in section 6.3, to inject harmonic currents into the converter bus, eliminating the low order characteristic harmonics in the bus voltage waveform.

In lower voltage active filter applications [27], a current source is used instead of a voltage source. However, current-reference PWM converters vary their frequency of switching depending on load

conditions and are generally considered less suitable for high power applications. The active source may be controlled to remove several harmonics simultaneously. This means however that the switching frequency must be large. An upper bound on the harmonics targeted for removal is imposed by the maximum allowable switching frequency.

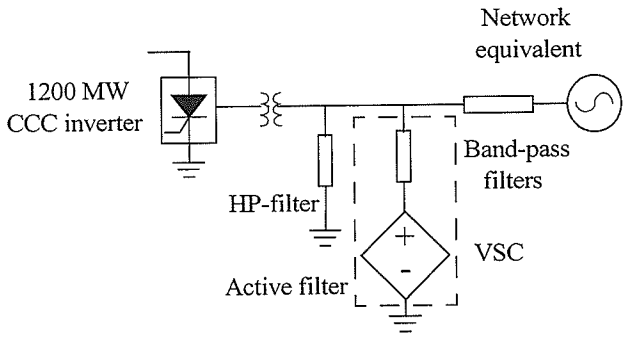

Figure 6.1 Active filter used in a CCC HVDC-scheme.

The active source is constructed using a Voltage Source Converter (VSC). Any arbitrary waveform can be generated using the PWM technique, as depicted in Fig. 6.2. The reference waveform to be generated (shown as a sine wave, but could be any other waveshape) is compared with a high-frequency triangular wave or carrier in Fig. 6.2a. When the reference waveform is larger than the carrier, the VSC connects the output to the positive dc-voltage, and when smaller, to the negative dc-voltage, as shown in Fig. 6.2b. Thus, the average magnitude of the reference over one period of the carrier is represented in the pulse-width of the output waveform. When higher order components (equal to or larger than the carrier frequency) are removed from the PWM waveform, the reference waveform is re-produced. Thus, the higher the carrier frequency, the more accurate is this representation. This is because the original waveform is sampled more often and also because the high-frequency components are easily removed by the natural low-pass filtering effect of the system components. However, a larger carrier frequency represents additional switching losses, and is therefore usually limited to less than 10 kHz with the present day high-power switching devices.

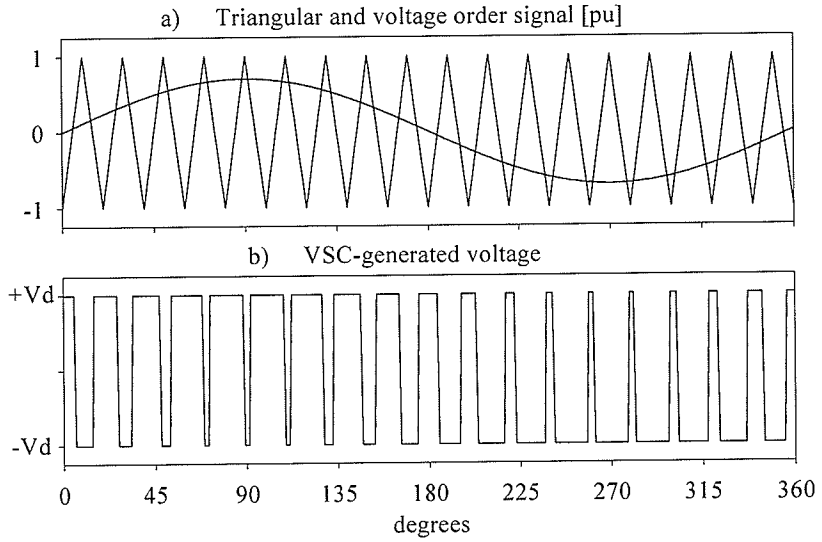

Figure 6.2 The concept of sinusoidal Pulse-Width-Modulation.

6.3 IMPLEMENTATION OF THE ACTIVE FILTER

The active filter presented in the previous section is designed to absorb the 11th and the 13th harmonic currents, generated by a 1200 MW CCC HVDC converter as well as to provide a portion of the reactive power requirement at the converter bus. The primary operation of the filter is investigated using electromagnetic transient simulation, where the converter is modelled as a simple current source.

6.3.1 The topology

The configuration of the active filter is illustrated in detail in Fig. 6.3. The filter consists of an IGBT-based three-phase VSC with a dc-voltage source of ±Vd. When an IGBT is turned on, either the IGBT or its diode in anti-parallel conducts depending on the direction of the output current. The diodes are not a part of a protection scheme, such as a snubber circuit. The mid-point of the dc-source is grounded to allow zero-sequence current to flow into the filter. The dc-voltage is supplied by a low-power rectifier connected to the ac-bus. The power generated at fundamental frequency in the filter is negligible because the coupling filter blocks fundamental frequency current from entering the ac-network. The power at the harmonic frequencies is also negligible

because the filter injects currents so that the harmonic voltages at the bus become zero. The filter generates an output voltage whose dominant harmonic components are equal both in frequency and phase to those of the voltage-order signal, calculated by the control system.

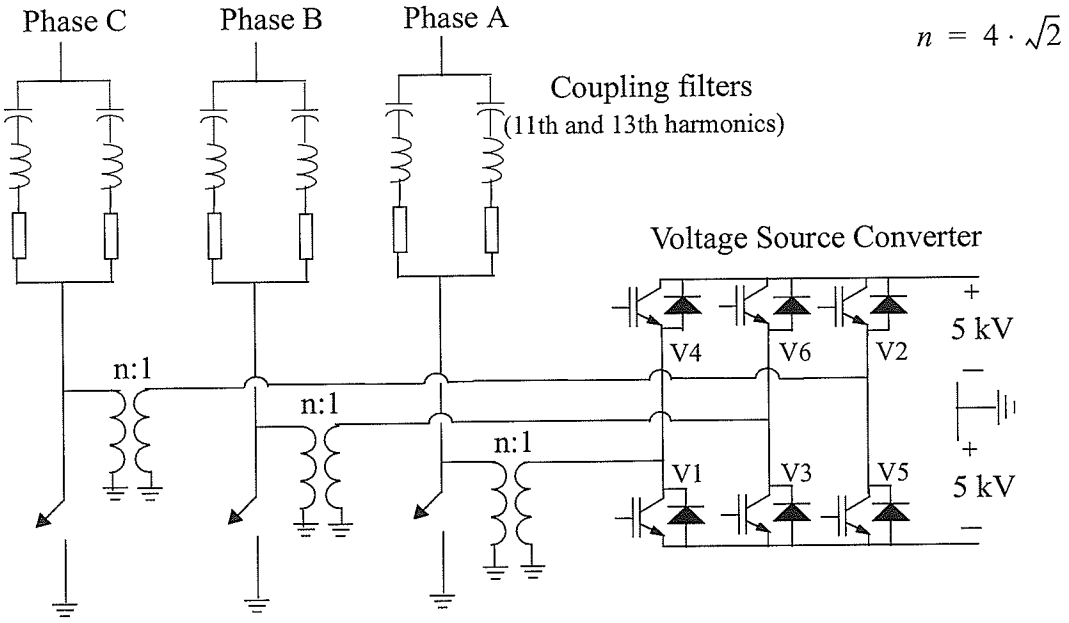

Figure 6.3 The active filter topology.

This output voltage is boosted up by a transformer and connected to the ac-bus through a coupling filter. The active filter can be bypassed by closing the switch on the secondary (network) side of the transformer so that only the coupling filter is connected to the ac-network. The primary voltage of the transformer is the VSC side voltage.

6.3.2 The control system

Figure 6.4 shows the algorithm used to generate the voltage order signal to the switching devices for phase A in the active filter. The active filter generates an output voltage that is derived with the objective of controlling the real and imaginary part of the harmonic voltage to zero. The measurement of the bus voltage in phase A, V_a, is supplied to a Fast Fourier Transform (FFT) block, which extracts the magnitude and phase of both the 11th (V_{11a},θ_{11a}) and 13th (V_{13a},θ_{13a})

harmonics. The control system re-calculates each harmonic voltage into a real and an imaginary part (i.e. $V_{11a}\cos\theta_{11a}$ and $V_{13a}\cos\theta_{13a}$), each of which is controlled to zero by a PI-controller. The output from each of the two PI-controllers is transformed back to time-domain quantities and then added to form the ordered voltage $f_{11}(t)$ to the active filter. A similar control system, indicated in the lower part of Fig. 6.4, is used to calculate the voltage-order $f_{13}(t)$ related to the 13th harmonic. Finally, these two voltage orders are added together to form the total voltage-order f(t) for phase A. The phase reference (i.e. cos(11ωt) and sin(11ωt)) used in the FFT as well as the signal reconstruction is obtained using a phase locked loop. Because of the feedback nature of the controller, any delays in the system voltage measurement are automatically compensated.

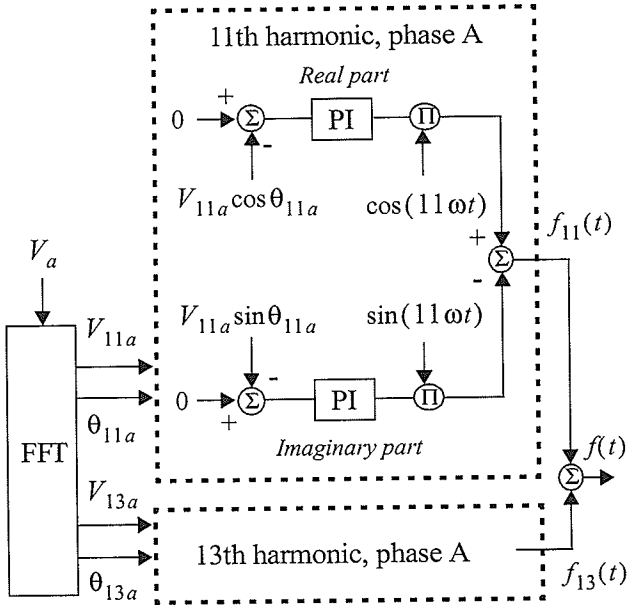

Figure 6.4 The control system for phase A.

An identical algorithm is used to calculate the voltage-order both in phase B and C. As shown in Fig. 6.2, the triangular fixed-amplitude carrier waveform is compared with the ordered voltage signal and appropriate firing pulses are generated for the IGBTs.

6.3.3 The coupling filter

The coupling filters consist of two parallel single-tuned bandpass filters with a quality-factor of 200, and are tuned to the 11th and 13th harmonic frequency, respectively. The component values are selected to provide reactive power of about 5 % of the converter's rated dc power for each of the filter branches (11th and 13th) respectively. The general expression for the resonant angular frequency ω_0 in these filters is given as follows:

$$\omega_0 = \frac{1}{\sqrt{L \cdot C}} \tag{6.1}$$

The voltage effort required by the active filter increases with the degree of de-tuning in the coupling filters. An expression for the de-tuning δ of this passive coupling-filter may be derived from (6.1), resulting in:

$$\delta = \frac{\Delta\omega_0}{\omega_0} = -\frac{\Delta C}{2C} \tag{6.2}$$

Using (6.2), it is clear that 10 % change in the capacitor size results in 5 % de-tuning from the resonant frequency. The tuned and de-tuned (5 %) impedances for the 11th harmonic coupling filter with respect to harmonic frequency are plotted in Figure 6.5.

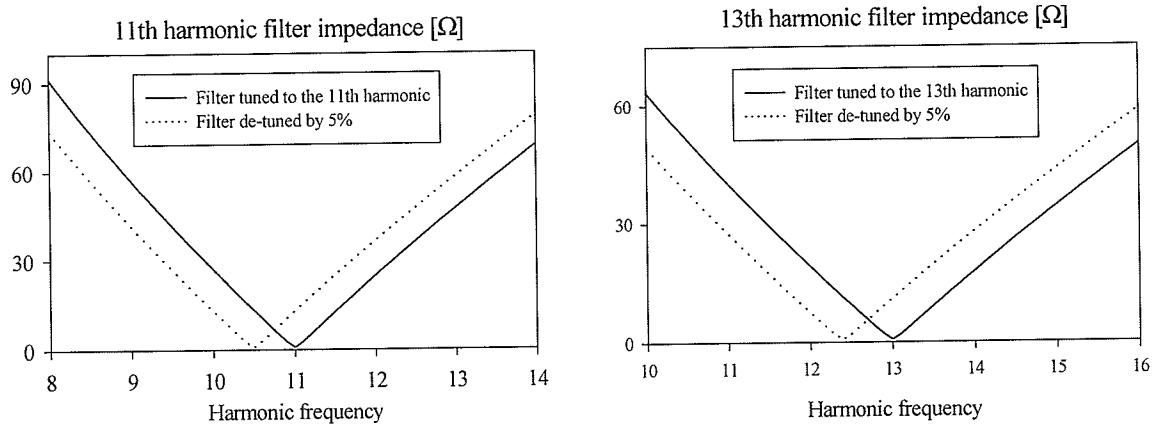

Figure 6.5 Impedance plot of tuned and de-tuned coupled filters.

It shows that the de-tuning increases the coupling filter impedance at the resonant frequency, resulting in a poorer filtering performance in the absence of any active filtering. This is evident also from the impedance plot for the 13th harmonic coupling filter.

6.4 OPERATING WAVEFORMS

The basic operation of the active filter is illustrated by an arrangement similar to that in Fig. 6.1, but the CCC replaced with a current source that injects fundamental frequency current as well as the largest characteristic harmonic current (i.e. the 11th). The injected 11th harmonic current magnitude is one-eleventh (205 A) of that of the fundamental (2.25 kA). The performance is investigated using electromagnetic transient simulation. The harmonic single-phase diagram of the circuit is shown in Fig. 6.8.

The coupling filter at this harmonic frequency is intentionally de-tuned by 5 % in phase A. The inverter is connected to a relatively weak ac-network, represented by an RL-type equivalent with a short-circuit-ratio (SCR) equal to 2.05. The damping angle at fundamental frequency is 85 degrees, which results in a predominantly inductive network impedance.

Figure 6.6a and b plots the injected current from the current source and the filtered current flowing into the ac-network in phase A. Figure 6.6c shows that the harmonic content of the current entering the ac network in the de-tuned phase A, is initially substantially larger than in the tuned phases. Due to the relatively large magnitude of fundamental frequency ac current, this distortion is only just visible in Fig. 6.6b. When the active filter is turned on, the control system calculates its steady-state voltage order to about 0.4 pu, shown in Fig. 6.6d. This causes the active filter to generate a voltage that reduces the harmonic current content to an even lower level than in the two tuned phases as seen in Fig. 6.6c

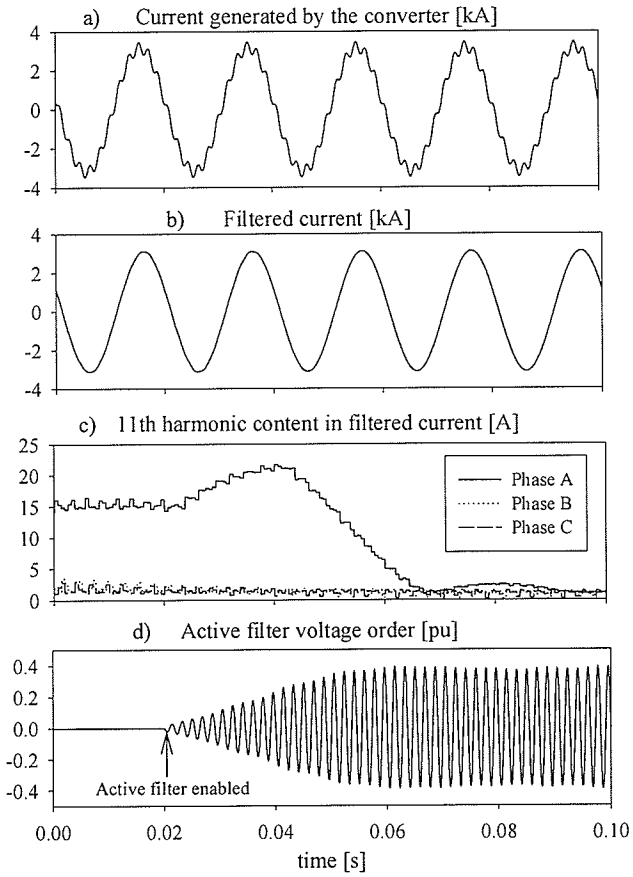

Figure 6.6 Impact on the harmonic current entering the ac-network when the ative filter is turned on.

Figure 6.7a shows the triangular carrier and ordered voltage signal during the steady-state. The corresponding output voltage generated by the active filter is shown in Fig. 6.7b.

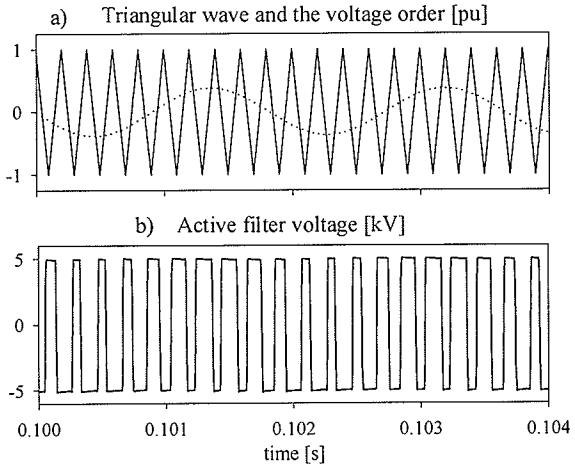

Figure 6.7 Sinusoidal PWM waveforms during steady-state conditions.

6.5 DESIGN CONSIDERATIONS

The actual ratings of the various elements in the active filter are dependent primarily on the level of system harmonics to be removed and on the expected degree of de-tuning in the coupling filters. The voltage effort required by the active filter, as a function of de-tuning, was investigated both theoretically and by simulation (PSCAD/EMTDC). The 11th and the 13th harmonic currents were injected in sequence by the current source, with a magnitude of one-eleventh (205 A) and one-thirteenth (173 A) of the fundamental, close to their expected maximum values.

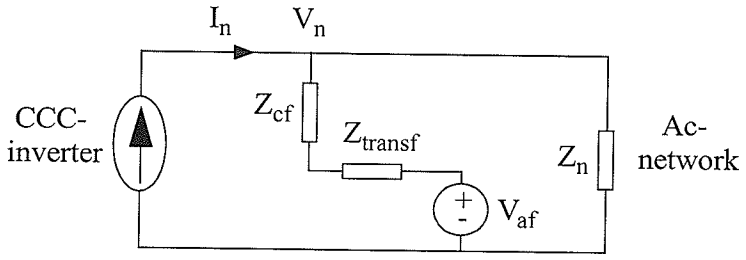

Figure 6.8 Harmonic single-phase impedance diagram of a CCC-inverter connected to an ac-network.

Equation 6.3 gives the theoretical expression for the voltage effort required by the active filter to reduce a given harmonic voltage to a value V_n (note that $V_n = 0$ means total elimination). The expression is derived from the impedance diagram in Fig. 6.8, where I_n stands for the nth harmonic current generated by the converter.

$$V_{af} = -I_n \cdot [Z_{cf} + Z_{transf}] + V_n \cdot \left[1 + \frac{Z_{cf} + Z_{transf}}{Z_n}\right] \tag{6.3}$$

Referring to (6.3), Z_{cf} is the coupling filter impedance, Z_{transf} is the filter transformer impedance and Z_n is the ac-network impedance. The expression for the voltage effort in (6.3) simplifies to the one given in (6.4) when total harmonic removal (V_n=0) is assumed.

$$V_{af} = -I_n \cdot [Z_{cf} + Z_{transf}] \tag{6.4}$$

Equation 6.4 shows that the voltage effort, V_{af}, increases with the degree of de-tuning in the

coupling filter (i.e. increased Z_{cf}), but is independent of the ac-network strength (Z_n). The voltage rating for the secondary (network) side of the filter transformer is based on the expected voltage effort. Figure 6.9 plots the theoretical and simulated results for each of the two injected harmonic currents, assuming total harmonic voltage removal. Due to its harmonic content, the fundamental component of the square-wave voltage at the secondary side of the transformer is somewhat difficult to measure accurately. The simulated results are therefore based on the voltage order calculated by the control system.

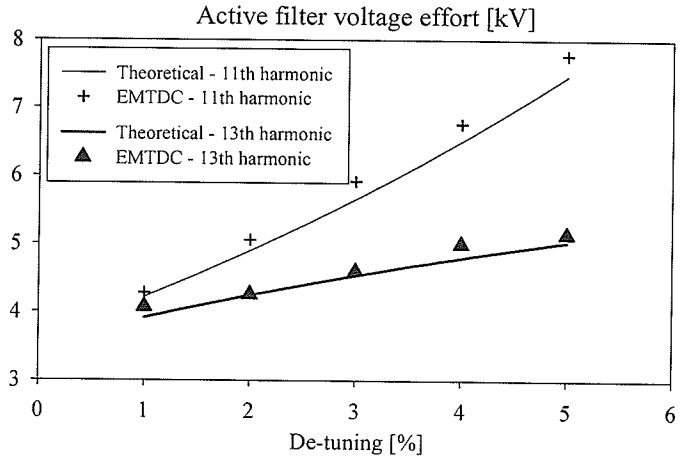

Figure 6.9 Active filter voltage effort vs. coupling filter de-tuning.

The results show that the theoretical and the simulated results agree well, thereby validating the simulation model. It is not practical to connect too many IGBTs in series because of the possible spread in turn-on and turn-off instants. The dc voltage is thus determined by the IGBT maximum voltage rating and is assumed to be 10 kV in this design. This also determines the voltage rating for the primary side of the filter transformer. It is also noteworthy that the active filter can work "too well". The filter can be overstressed in cases where it attempts to eliminate harmonics also from other sources than the one it was primarily built for. One possible solution is to purposely de-tune the active filter, i.e. allow a certain quantity of harmonics to enter the ac network. This aspect is however not covered here.

6.6 ACTIVE FILTER IN A CCC-APPLICATION

The active filter is now applied at the CCC-inverter ac-bus at the 1200 MW single-infeed HVDC-scheme described in Chapter 4. In this section, we will demonstrate that the active filter operates satisfactory both in the steady-state and under transient conditions.

6.6.1 Modelling of the HVDC-scheme

The rectifier is of the conventional type and is connected to a very strong ac-network. The dc-link, rated at 500 kV, 2.4 kA, is a 600 km long submarine cable terminating in an ac-network with an SCR of 2.05. The CCC-inverter operates in current control, whereas the rectifier operates in voltage control mode in normal operation, but switches into current control during fault recovery. The coupling filter arrangement consists of two band-pass filters tuned to the 11th and 13th harmonics. In addition to the coupling filter, there are two additional bandpass filter branches to remove the 23rd and 25th harmonics and a high pass filter to absorb higher order harmonics. The total reactive power installation at the converter bus is 174 Mvar, which is 14.5 % of the rated dc-power in the HVDC scheme. The 11th and 13th harmonic coupling filters are intentionally de-tuned by respectively +5 and –5 %. The inverter ac-network is represented by an RRL-type equivalent and has a damping angle of 85 degrees at fundamental frequency.

6.6.2 Steady state performance

It is desirable to have a low coupling filter impedance at their respective tuned frequency to achieve a good filtering performance and also to decrease the voltage requirements to the VSC. This can be accomplished by choosing a high quality factor which results in a low resistance component in the bandpass-filters. It is also preferable to select a high quality factor in order to minimise the losses at fundamental frequency. The drawback of choosing a high quality factor is a narrow bandwidth, which makes the filter more susceptible to detuning effects. This also results in a low damping capability which for instance means that the filter needs a long time to reach the steady state.

Our choice of a 2000 quality factor results in an individual voltage distortion of 1.15 % (1.99 kV) and 0.85 % (1.48 kV) for the 11th and 13th harmonics when the coupling filters are tuned and the active filter is disabled. Individual and total harmonic distortion (THD) are widely accepted indices of voltage distortion in ac networks. The internationally recommended levels of permitted voltage distortion [3,22] are 1 % for individual frequencies and 1.5 % for the total harmonic distortion (THD). This means that the voltage distortion in the tuned case coincide more or less with what is considered to be the maximum allowable according to these standards.

The individual voltage distortion in phase A for the 11th and the 13th harmonics are 3.77 % (6.5 kV) and 1.51 % (2.6 kV) respectively with 5 % detuning in the coupling filters. This distortion significantly exceeds that of the tuned phases (phase B and C) and also the recommended tolerance levels given in standards. As may be seen in Fig. 6.10, this harmonic distortion is reduced to well within acceptable margins when the active filter is enabled in phase A. In fact, the voltage distortion in the detuned phase A is brought to an even lower level than in the tuned phases, which thereby demonstrates the efficacy of the active filter under steady-state conditions.

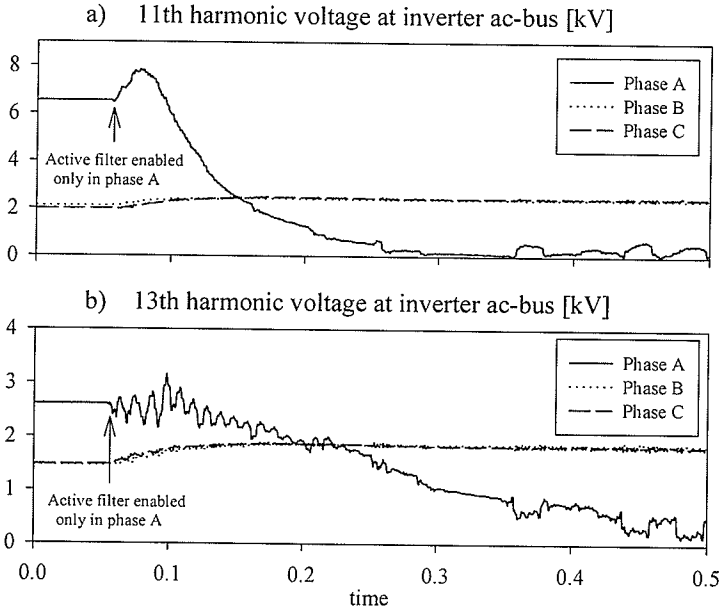

Figure 6.10 Active filter steady-state performance.

6.6.3 Transient performance

One of the concerns on the use of active filters at converter stations is the possibility of transient performance degradation. This could arise due to adverse interactions between the controllers of the HVDC converter and the active filter. Several transient simulations are carried out to examine this aspect and they all indicated that the active filter did not cause any adverse impact on the performance. It is, nevertheless, observed that the scheme demonstrated slightly less robustness against three-phase remote ac-faults. The results from two typical tests – a single-phase close-in fault and a control set-point change are presented in the following. The detuning in the 11th and 13th harmonic filter branches is now done in all three phases. The active filter thus operates in all three phases during the tests examined.

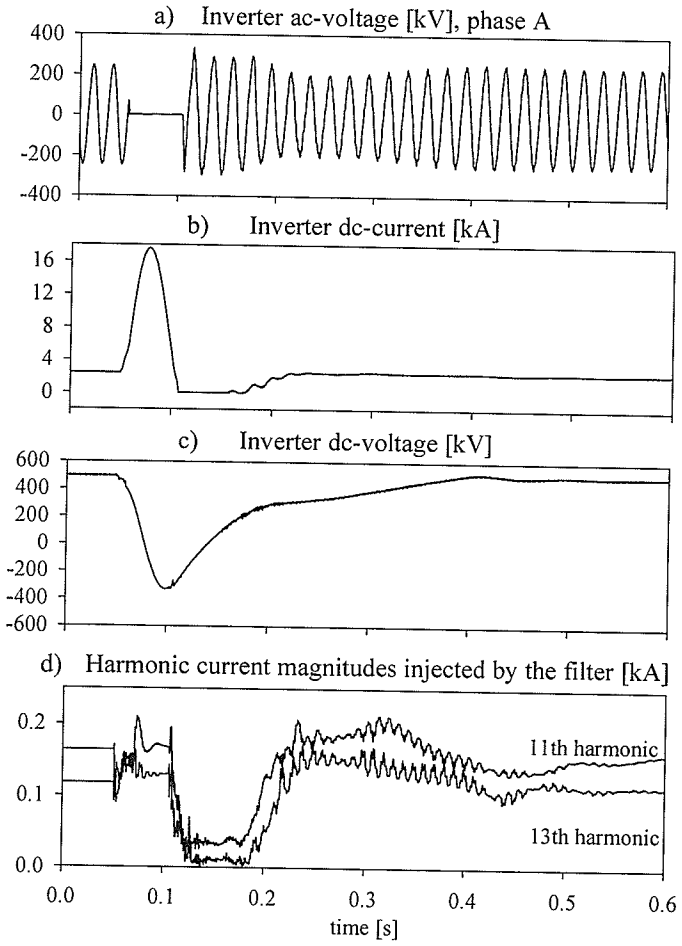

Figure 6.11 Single-phase to ground close-in fault applied at the inverter bus.

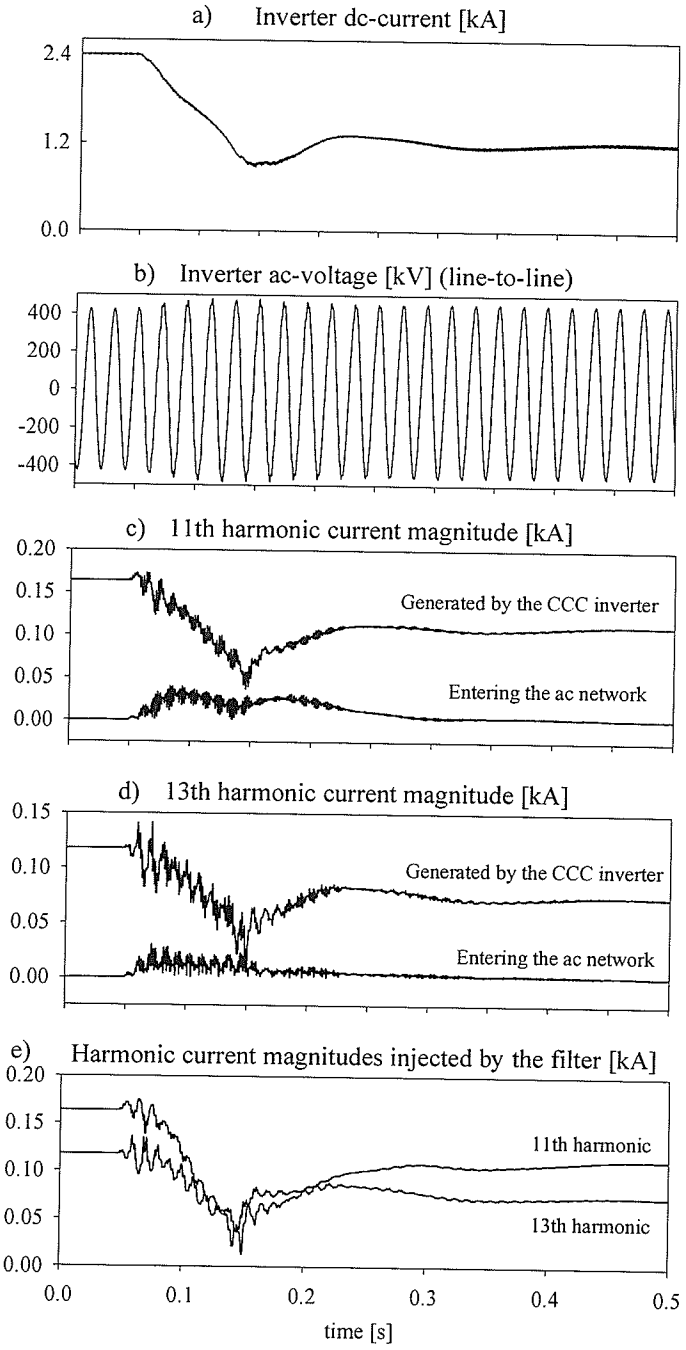

Figure 6.12 Step-decrease of 50 % in the dc-current order.

The recovery performance was investigated when a 50 ms single-phase to ground close-in fault was applied at the inverter ac bus. The recovery time is defined as the time from fault clearing to the instant at which 90 % of the power is restored. Figure 6.11 shows the dc-voltage and current, the ac-voltage at the CCC-inverter and the harmonic current magnitudes injected by the filter. The

recovery performance, e.g. recovery time of 240 ms, very similar to that found with perfectly tuned passive filters in Chapter 5.

In another test, the dc-current order was reduced from 1 pu to 0.5 pu. The simulation results are plotted in Fig. 6.12. Figure 6.12c and d show that the amount of 11th and 13th harmonic current generated by the CCC-inverter drops due to the reduction in the dc-current order. In the same graph, it may be seen that most of this current is compensated by the active filter, so that only a very small part of it enters the ac-network. Figure 6.12e shows clearly that the harmonic content of the current injected by the filter decreases with a step-decrease in the dc-current. The inverter 300 kV ac inverter bus voltage increases due to the lower voltage drop across the network impedance, as seen in Fig. 6.12b. Again, no adverse effects due to the active filter are observed.

6.7 CONCLUDING REMARKS

This chapter has introduced an active filter concept for application at the inverter ac side in a capacitor commutated converter based HVDC scheme.

- An active filter, including its topology, control system and coupling filter to the ac-network, has been developed.
- The operation of the active filter was illustrated by using electromagnetic transient simulation. When the coupling filters were detuned, the active filter reduced the level of harmonic current flowing into the ac network to a level well within acceptable limits. In fact, the active filtering performance was even better than the filtering of the coupling filters in tuned condition.
- The rating of the filter is primarily dependent on the level of harmonic current to be removed and the expected degree of de-tuning in the coupling filters. The primary side of the filter transformer is determined by the voltage ratings of the IGBT switching devices in the VSC.
- The active filter was used at a 1200 MW CCC inverter in a long cable HVDC scheme. The filter removed as expected, the 11th and the 13th harmonics in the steady-state operation. No adverse interactions between the active filter and the HVDC-controls were revealed.

The active filter did not significantly change the inverter's transient performance, with the exception of a slightly lesser robustness against three-phase remote faults.

The proposed active filter should therefore be attractive in the view of the expected application of near-unity-power-factor converters such as the CCC. The main portion of the results reported here, have also been submitted for publication in [35].

Chapter 7

MODELLING OF MULTI-INFEED LONG CABLE HVDC-SCHEMES

7.1 PRIMARY FOCUS

An ac-network which contains infeed from several HVDC links in close electrical proximity of each other is, in the following, named as a multi-infeed HVDC-scheme. One of the concerns in such a scheme is the occurrence of mutual interactions between the HVDC-schemes following a disturbance in the common ac-network. These interactions may deteriorate the performance of the overall multi-infeed scheme in comparison to a situation where each HVDC-scheme operates separately. Some aspects of such interactions have already been discussed in literature [36,37,38,39]. It is for instance reported that adjustments of the control settings in one of the HVDC-schemes, affect the performance of the other schemes. The reason for this finding is relatively obvious since the HVDC-converters practically share the same ac bus.

A particularly interesting scenario arises when all of the HVDC-links are feeding power into the ac-network. All of the HVDC-converters connected to the ac-network operate now as inverters, which makes them more susceptible to commutation failure in comparison to rectifier operation. The application of CCC inverters may, due to their higher robustness to most disturbances, enhance the performance of the multi-infeed scheme.

The primary objective is to evaluate whether the application of CCC inverters improves the performance of long cable multi-infeed HVDC-schemes. With this view, this chapter describes the modelling of three multi-infeed alternatives, whereas the next chapter investigates their steady-state and transient performance.

7.2 THE NORWEGIAN POWER SYSTEM

Multi-infeed HVDC-schemes are, as pointed out in Chapter 1, becoming increasingly popular in today's deregulated power system environment. The Scandinavian grid is a very good example of such a system since it is connected to the central European or the so-called UPCTE grid, through seven HVDC-connections as indicated by the solid-drawn lines in Fig. 7.1.

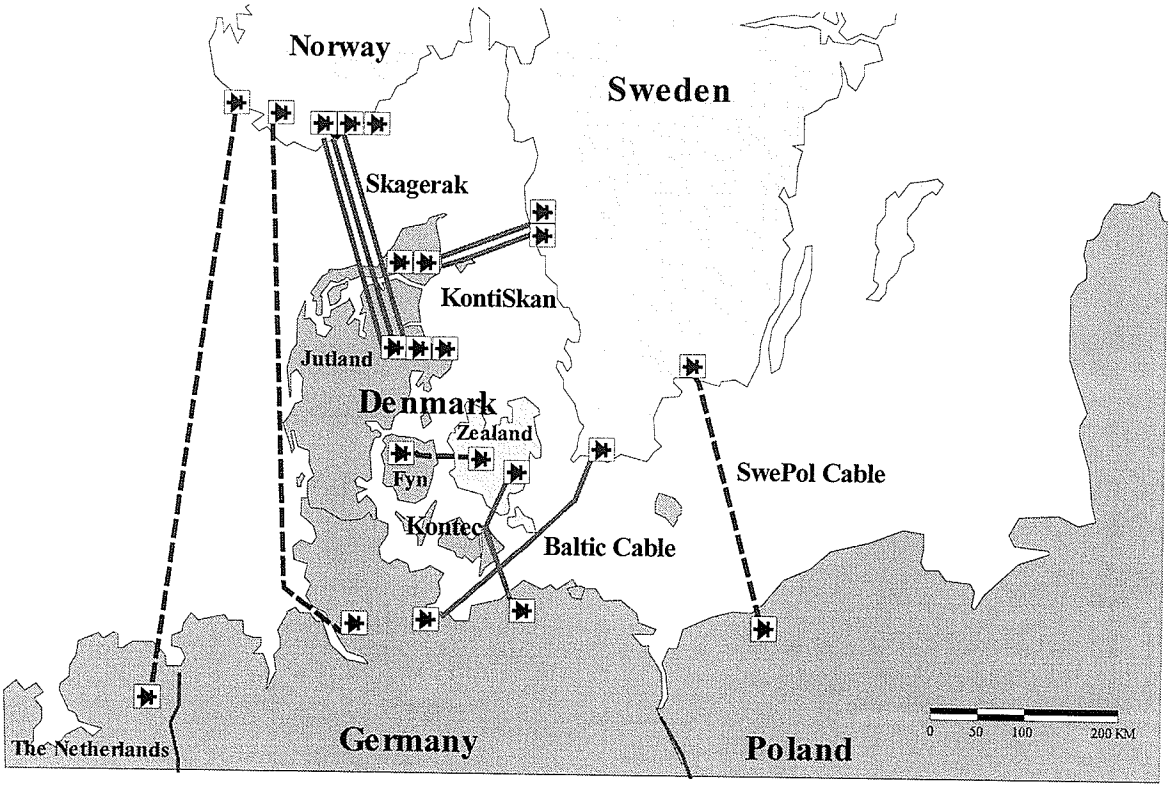

Figure 7.1 Existing and planned HVDC-links between the Scandinavian grid and the UPCTE-grid. (Courtesy: Statnett SF, Oslo Norway)

The Scandinavian transmission grid, also called the Nordel-grid [41], comprises the national transmission networks in Norway, Sweden, Finland and Denmark as well as several ac and dc interconnections between them. This grid is thus synchronous with a common frequency except the Jutland peninsula and the island of Fyn in Denmark, which are connected to the UPCTE-grid.

The HVDC-connections between the synchronous part of the Nordel-grid and the UPCTE-grid consist mainly of subsea cables that involves lengths up to 220 km; Skagerak 1, 2 and 3 run from

the south of Norway to the northern part of the Jutland peninsula in Denmark, which is synchronous with the UPCTE-grid. KontiSkan 1 and 2 run from the south-western part of Sweden and terminate in the Jutland peninsula as well. Kontec runs from the island of Zealand in Denmark to Rostock in Germany, whereas Baltic Cable runs from the far south of Sweden to Lübeck, also in Germany. Baltic Cable, with its 220 km cable, was the world's longest and most powerful submarine HVDC-cable when it was commissioned in 1996.

In addition to these existing HVDC-connections, there are several new HVDC-projects in the planning stage, indicated by dashed lines in Fig. 7.1. The SwePol Link, connecting Sweden to Poland, is scheduled to come into operation during the spring of 2000. The Norwegian Power Grid Company (Statnett SF) and their central European counterparts are currently investigating the incorporation of three submarine 550 km long cable HVDC connections from Norway to Germany and the Netherlands [31]. The Scandinavian grid is one of the best examples of so-called multi-infeed HVDC-systems. A listing of existing and planned HVDC-connections between the Scandinavian and the UPCTE-grid is given in Appendix 5.

The Norwegian electricity production is by close to 100 % based on environment-friendly hydropower. The central European power system also named as the UCPTE (Union for the Coordination of Production and Transmission of Electricity) is, on the contrary, mainly supplied by a mix of fossil and nuclear fuelled power generation. These include the highly controversial nuclear plants as well as oil, gas and coal fired plants, which use non-renewable energy and could have significant pollution levels. Technical, economical and environmental aspects makes it unfavourable to regulate these thermal plants rapidly to follow the daily variations in the load. The access to fast-acting hydro power for this purpose is therefore appealing for utilities in central Europe. As it was put in the words of a Norwegian utility official: *Norwegian hydro is like a environment-friendly speedy Lamborghini with a small gas tank, whereas thermal power in central*

Europe is like a highly pollutive slow Lada with a large gas tank. In central Europe, shortage of power is the main problem, not shortage of energy.

The Norwegian system rarely experiences a shortage of energy but extreme dry years occur occasionally. Statnett was in fact very close to be forced to shut off customers in the spring of 1996. The increased transmission capacity to central Europe, will therefore improve the reliability of energy supply and may also postpone or illuminate the need for increased generation in Norway. Shortage of energy is more critical than shortage of power in Norway.

The general difference in the nature of the power generation and the development into a competitive power market in Norway, are the main incentives to further increase the transmission capacity between the two systems. Scandinavia has positioned itself to become one of the most well-functioning power markets in the world. This process was initiated by the deregulation in the power sector following the Norwegian Energy Act, which was put into force in 1991. The new proposed HVDC-connections are therefore expected to be both economically and environmentally favourable for the areas in either end of the connections.

Multi-infeed HVDC schemes where several dc-transmission links terminate electrically very close to each other in a common ac-network, present special problems that have not been investigated in sufficient detail in literature. Several problems can potentially arise in such multi-infeed networks, including transient problems such as contagious commutation failures. These problems will be critical in the Norwegian grid, because it will most likely import power with a low SCR during night-time. The Nordel-grid is operated to withstand a maximum power loss of 1200 MW, based on the N-1 criterion. This criterion means no single-contingency shall result in unacceptable consequences. A contiguous commutation failure causing the tripping of several HVDC-links in a cascading process, may therefore result in a too large energy loss and subsequently lead to blackouts of portions of the Nordel-system. This potential scenario is naturally of great concern to

the system operators in the Nordel-grid.

7.3 THE MULTI-INFEED HVDC CONFIGURATION

Three multi-infeed HVDC-alternatives are developed, each being a simplified representation of the existing and planned HVDC-connections in the Norwegian power grid. Each alternative consists of two long cable dc links with rated power of 1200 MW and 1600 MW respectively, feeding power into a common ac-network in close electrical vicinity of each other.

The three multi-infeed HVDC alternatives are very similar with the exception that they have different inverter types as illustrated in Table 7.2.

- A scheme, termed as the conventional multi-infeed HVDC scheme, where both the 1200 MW and the 1600 MW link use conventional inverters.
- A scheme, termed as the mixed multi-infeed HVDC scheme, where the 1200 MW link uses CCC inverters and the 1600 MW link uses conventional inverters.
- A scheme, termed as the CCC multi-infeed HVDC scheme, where both the 1200 MW and the 1600 MW link use CCC inverters.

Table 7.2 Overview of the inverter types employed in each multi-infeed HVDC alternative.

Dc-link	Multi-infeed alternative		
	Conventional	Mixed	CCC
1200 MW	Conventional	CCC	CCC
1600 MW	Conventional	Conventional	CCC

Each of the three multi-infeed alternatives use conventional rectifiers at both their 1200 MW and the 1600 MW links, which are connected to a very strong sending ac-network. The two inverter terminals are separated by an impedance, which represents a 250 km long 300 kV transmission line. The inverters operate at an extinction angle (conventional) and real extinction angle (CCC) of 22 degrees. These operating points are obtained by adjustments in the inverter side network

voltage for each dc-links. Operation at the same extinction angle is necessary in order to make a meaningful comparison between the multi-infeed alternatives. The addition of the transmission line between the inverter terminals results in a different operating point which requires slightly different settings in the inverter network voltages. The mixed multi-infeed HVDC alternative is shown in Fig. 7.2.

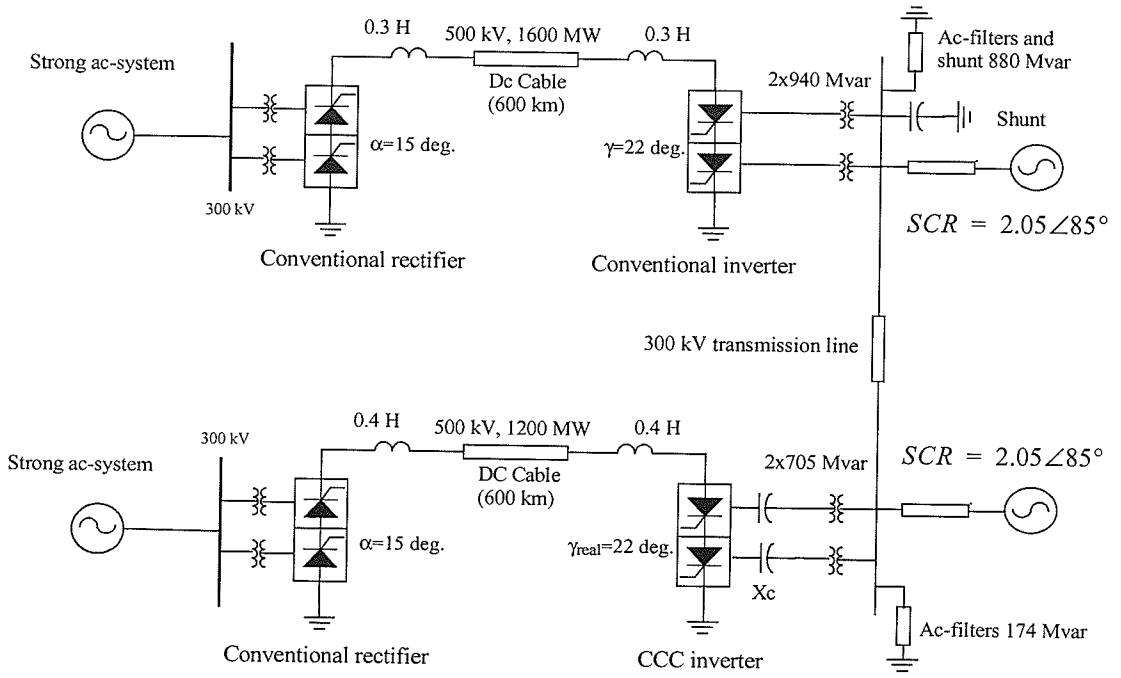

Figure 7.2 Mixed multi-infeed HVDC-alternative.

The 1200 MW conventional and CCC single-infeed HVDC-links, described in Chapter 4, were employed in the multi-infeed schemes. Two additional 1600 MW links are required in order to complete the modelling of the dc transmission in the multi-infeed schemes. These two links are generated by simply scaling up the 1200 MW links to 1600 MW power rating. The scaling is made so that the 1600 MW and the 1200 MW dc-links have identical pu-behaviour when they employ the same inverter type. The scaling of both the dc-links and their associated controls are described in detail in section 7.4. All the links are operated at control option 1 (rectifier in voltage control and inverter in current control) due to its superior performance in comparison to control option 2

(rectifier current control and inverter voltage control).

The multi-infeed alternatives represent a situation where the Norwegian power system imports power at low SCR during night-time. Hence, the alternatives are only examined with a uni-directional power flow in the links. A more extensive study should also include a scenario where on link is exporting and the other links is exporting power from the common ac-network. This requires a modification of the present controls to also allow bi-directional power flow. Such a study is, although interesting, not within the scope of this thesis.

7.4 SCALING HVDC-SCHEMES WITH DIFFERENT POWER RATING

The components and the control settings in the 1600 MW schemes are obtained by scaling the 1200 MW schemes to 1600 MW power rating. This ensures that the 1200 MW and the 1600 MW scheme, with the same inverter type, exhibit identical pu-behaviour. This section describes how the scaling is done. The resulting component values and control settings for the multi-infeed HVDC schemes are given in Appendix 9 and 10 respectively.

7.4.1 Component values

Let us first consider the relationship between the pu base impedances (Z_{base1} and Z_{base2}) in an HVDC-scheme 1 (1200 MW) and a scheme 2 (1600 MW). Since the rated voltage is equal in the two schemes, the relationship can be expressed as:

$$\frac{Z_{base2}}{Z_{base1}} = \frac{P_{base1}}{P_{base2}} \tag{7.1}$$

where P_{dc1} and P_{dc2} are the base power in the two schemes. An equal pu-impedance for any given component in the two schemes combined with (7.1), leads to the following relationship between the real impedance values (Z_{real1} and Z_{real2}):

$$Z_{real2} = Z_{real1} \cdot \frac{Z_{base2}}{Z_{base1}} = Z_{real1} \cdot \frac{P_{base1}}{P_{base2}} = Z_{real1} \cdot \frac{1200MW}{1600MW} = Z_{real1} \cdot \frac{3}{4} \tag{7.2}$$

This relationship is used to obtain values for the ac-network equivalent, ac-filter, shunt capacitor, converter transformers, series capacitance, dc-smoothing inductor and dc-cable in the 1600 MW HVDC schemes.

The ac-network on the inverter side in the 1600 MW scheme is represented similarly to that of the 1200 MW scheme, as shown in section 4.2. This means an RRL-type equivalent with a 2.05 SCR with a damping angle of 85 degrees at fundamental frequency.

The ac-filter components and the shunt capacitors were also obtained by scaling the corresponding 1200 MW components using the same quality factor in the filters. As a result, the reactive power installation at the inverter terminals increased by 4/3. The total ESCR for each multi-infeed alternative can be calculated using equation 7.3, neglecting the transmission line impedance connecting the inverter terminals.

$$ESCR = SCR - \frac{Q_c}{P_{dc}} \tag{7.3}$$

The total power rating P_{dc} of the multi-infeed HVDC schemes is now 2800 MW. Each alternative has different ESCR as the sum-Mvar (Q_c) installed in the filters and shunt capacitors at the two inverter terminal is different in the three schemes.

Table 7.3 SCR and ESCR in each multi-infeed alternative.

Multi-infeed HVDC alternative	Dc-links	Mvar-generation	SCR	ESCR
Conventional	1200 MW 1600 MW	660 Mvar 880 Mvar	2.05	1.5
Mixed	1200 MW CCC 1600 MW Conv.	174 Mvar 880 Mvar	2.05	1.67
CCC	1200 MW 1600 MW	174 Mvar 232 Mvar	2.05	1.905

The calculated ESCR for each multi-infeed HVDC alternative is given in Table 7.3, which shows that the use of CCC-inverters increases the ESCR. It is anticipated that the multi-infeed HVDC-

schemes employing CCC-inverters should exhibit a higher degree of robustness against disturbances in the ac-network.

The 250 km long 300 kV transmission line separating the inverter terminals is represented by a duplex Parrot with a resistance and reactance of respectively 0.0207 Ω/km and 0.308 Ω/km and. The capacitance (0.012 μF/km) introduced additional oscillations and was therefore simplicity reasons not included. The transmission line was included in order to examine the multi-infeed HVDC-schemes also with some impedance between their inverter terminals.

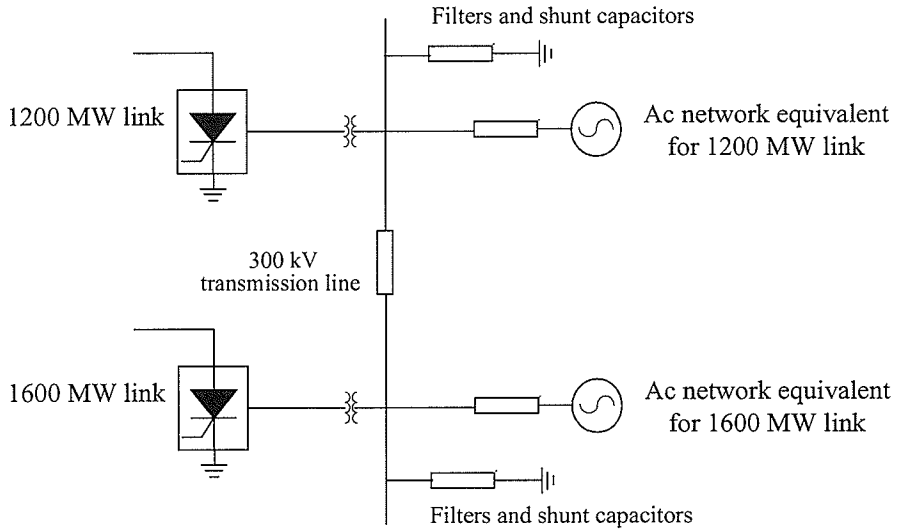

Figure 7.3 Configuration of a multi-infeed HVDC scheme.

7.4.2 Control parameters

Due to its superior performance, both links in each multi-infeed HVDC alternative are operated using control option 1 (rectifier voltage control and inverter current control). As mentioned in Chapter 4, the controllers at both the rectifier and the inverter use pu-quantities - a standard feature in modern HVDC-schemes. This is convenient since the control system becomes independent on power rating, i.e. it can be used in schemes of different power rating and still demonstrate the same pu-behaviour. This means e.g. that a given pu-error fed into the current controller results in the same change in firing angle regardless of the scheme's power rating. The controller gains and

time-constants of the 1200 MW and the 1600 MW dc-links are, thus, identical when they employ the same converter types. The rated dc-voltage is 500 kV in both schemes, which means that their rated current orders are 2.4 (1200 MW link) and 3.2 kA (1600 MW link), respectively.

Appendix 10 gives the control settings for each multi-infeed HVDC alternative, including the slopes limiting the rate-of-change (one for increase and one for decrease) in the VDCOL-generated current order. The slopes are stated in time-units. They correspond to the time required to increase the current order from zero to rated value, and similarly to decrease the current order from rated value to zero. The controller gains and time-constants in the multi-infeed alternatives are identical to those used in the single-infeed schemes.

The mixed alternative required modifications in these VDCOL-slopes, most likely due to the different nature of its inverter types. It was also necessary to adjust the slopes in the CCC multi-infeed alternative. The details are described in Appendix 10.

7.5 HARMONIC INSTABILITY

One of the concerns in HVDC-systems are the potential danger of harmonic instability between the ac and the dc side, which results in amplification of the second harmonic voltage on the ac side. The presence of a small second harmonic voltage on the ac-side generates a fundamental voltage component at the dc-side. If there is an anti-resonance (low impedance) near fundamental frequency on the dc-side, this would result in a relatively large fundamental current on the dc side. This current, in turn, generates a second harmonic as well as a dc current component on the ac-side, which would amplify the initial second harmonic ac-voltage if a second harmonic resonance (high impedance) is present at the ac-side. This will eventually saturate the converter transformer cores, generating additional harmonic in the magnetising current. The saturation is asymmetrical due to the dc-current flowing through the transformer, which will generate even more second harmonic current on the ac side. The amplification is self-sustaining since it continues even after

the initial source of the second harmonic voltage is removed. This scenario is particularly of concern since ac-faults often introduce a dc current which may lead to asymmetrical saturation of the converter transformer.

The multi-infeed alternatives should, hence, be examined to determine whether the conditions for harmonic instability are present. One often considers each side (ac and dc) separately in order to determine whether they resonate at the critical above-mentioned frequencies. Earlier work [40] has revealed that harmonic instability may not occur even though these critical resonances are present on the ac and the dc side of an HVDC-scheme. This approach is thus an approximation of the conditions that are required to generate harmonic instability since the ac and dc sides, in reality, are interconnected through the converter.

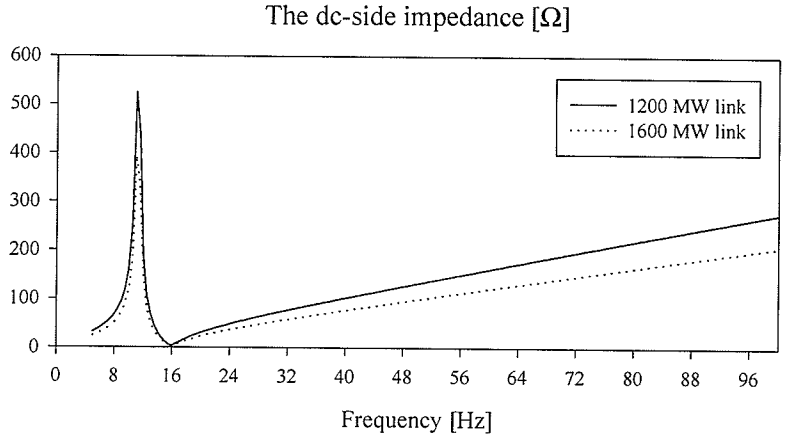

Figure 7.4 The dc side frequency response for the 1200 MW and 1600 MW HVDC-scheme.

The dc-side impedances for the 1200 MW and 1600 MW have both an anti-resonance at 16 Hz, as shown in presented in Fig. 7.4. This is far away from the critical fundamental frequency (50 Hz) and the conditions for harmonic instability are therefore not present in any of the multi-infeed alternatives, regardless of resonant frequencies appearing on the ac-side.

However, a growing oscillation at roughly 68 Hz is observed in the inverter dc current at rated conditions in both dc-links of the conventional multi-infeed alternative. The oscillation eventually

resulted in commutation failure in steady-state operation. This is avoided by eliminating this harmonic component in the dc current measurement, using a bandstop 4th order Butterworth filter, before it is supplied to the control system. It is sufficient to employ this filter in only one of the inverter dc-currents in order to damp the oscillation in both dc-links. This demonstrates the mutual interactions which exist between the two links.

Chapter 8

TRANSIENT BEHAVIOUR OF MULTI-INFEED LONG CABLE HVDC-SCHEMES

8.1 INTRODUCTION

The primary focus in this chapter is to evaluate the suitability of CCC-inverters a network configuration where two long cable HVDC-links terminate in a common ac-network in electrical vicinity of each other. This is done by investigating the transient performance of the three multi-infeed HVDC-schemes modelled in the previous chapter, using electromagnetic transient simulation. Each scheme consists of a 1200 MW and a 1600 MW HVDC-link feeding power into a common ac-network, but with different combinations of inverter types: the first scheme consists of conventional inverters in both links, the second is a mix of the conventional and CCC types and the third is a scheme using CCC inverters in both links. The performance of each scheme was examined when various faults were applied in the inverter ac network and when setpoint changes were made in the controls. Some of the preliminary results of this research can be studied in [33,34].

The two inverter terminal commutation buses are connected by a transmission line, which is represented by a small impedance. It is therefore evident that events (e.g. commutation failures or simply adjustments of the control settings) occurring in one link, also affect the commutation voltage at the other inverter. In other words, the performance of each HVDC-scheme mutually affects the other scheme since the two practically share the same inverter commutation bus voltage. One of the concerns in such schemes is, thus, the occurrence of mutual interactions between the HVDC-schemes following a disturbance. These interactions may deteriorate the

performance of the overall multi-infeed scheme in comparison to a situation where each HVDC-scheme operates separately. This is of particular concern since both the HVDC-converters connected to the ac-network operate as inverters, which makes them more susceptible to commutation failure in comparison to rectifier operation.

Some aspects of such transient interactions between HVDC-schemes have already been discussed in literature [37,38,39]. However, only [38] has addressed the configuration where several HVDC-links are *feeding* power into a common ac-network. One finding in this reference is that the mutual interactions between the dc links depends on the ac-network strength at each inverter terminal. Limited interactions should occur when the SCRs are high, whereas strong interactions are experienced under lower SCR operating conditions. This requires a coordinated design of the controllers in order to achieve good performance. It is for instance found that a good recovery performance of the dc-links can be obtained by coordinating the VDCOL slopes. Problems originating in one link may, hence, be solved by taking adequate control actions in other dc links. It is also reported that, for the same SCR conditions, the likelihood of commutation failure occurrence increases as the inverter terminals are more closely electrically connected.

The HVDC-scheme under study here, with closely neighboured multiple inverter infeed to a weak ac network, should therefore experience strong interactions between the dc links. These interactions may degrade the overall performance of the multi-infeed HVDC scheme. It is surmised that the presence of CCC inverter in one or more of the dc links would lessen this degradation. The primary objective is to evaluate whether the presence of CCC inverters improves the performance of long cable multi-infeed HVDC-schemes. With this view, the steady-state and the transient behaviour of three multi-infeed schemes are investigated in the succeeding sections. The multi-infeed alternatives are examined both when the inverters share a common ac-bus and when they are connected by a transmission line (as indicated in Fig. 7.3).

8.2 INVERTER LOAD REJECTION

Table 8.1 presents the overvoltages for each multi-infeed alternative following a permanent block and bypass at the 1200 MW and the 1600 MW inverters respectively. It is convenient to distinguish between the faulty and the healthy inverter bus when the inverters are separated by a transmission line. The faulty bus is the blocked inverter's commutation bus, whereas the healthy bus is the neighbouring inverter's commutation bus. The overvoltages at the healthy inverter bus are given in brackets. The results demonstrate that the presence of the CCC has the effect of lowering the steady-state overvoltage following an inverter block. This shows, as expected, that the main finding in the single-infeed HVDC study also holds true for the multi-infeed situation. The presence of the CCC contributes to significantly lower the inverter load rejection overvoltages due to the lower Mvar installation in its ac filters. This effect is expected to be even more evident for weaker ac networks.

Table 8.1 Inverter block overvoltages.

Electrical distance between inverter terminals	Blocked link	Multi-infeed HVDC alternative (1 pu = 300 kV)		
		Conventional	Mixed	CCC
Common ac-bus	1200 MW:	1.19 pu	1.08 pu	1.05 pu
	1600 MW:	1.26 pu	1.19 pu	1.08 pu
Transmission line	1200 MW:	1.32 pu / (1.09 pu)	1.11 pu / (1.04 pu)	1.11 pu / (1.02 pu)
	1600 MW:	(1.12 pu) / 1.40 pu	(1.07 pu) / 1.35 pu	(1.03 pu) / 1.12 pu

For instance, the overvoltage following the blocking of the 1600 MW conventional inverter is smaller in the mixed multi-infeed alternative (1.19 pu) in comparison to the conventional alternative (1.26 pu). This indicates that the presence of a CCC-inverter has an advantageous effect on the conventional inverter. The addition of the transmission line between the inverter terminal buses worsens the overvoltage at the faulty inverter bus, but improves it at the healthy inverter bus. This finding supports the argument that the addition of the transmission line has the effect of

lowering the SCR at the faulty inverter bus and increasing the SCR at the healthy inverter bus.

The results also show that the blocking of one inverter does not cause commutation failure in the remaining inverter when they share a common ac bus. This holds true for all three multi-infeed alternatives regardless of whether the blocked inverter is of the conventional or CCC type. The addition of a transmission line between the inverter terminals buses (as indicated in Fig. 8.1) changes this behaviour. The blocking of one inverter now results in commutation failure in the remaining inverter for all three multi-infeed alternatives, except in one case: the 1600 MW conventional inverter does not experience commutation failure following the blocking of the 1200 MW CCC inverter in the mixed alternative. The performance deterioration observed indicates that the addition of the transmission line has the effect of decreasing the SCR at the inverter buses. If the remaining inverter suffers commutation failure, it recovers nicely regardless of being of the CCC or of the conventional type.

It is evident that the blocking of a CCC inverter imposes a less severe voltage transient on the remaining inverter in comparison to the blocking of a conventional inverter. The results do not, however, clearly reveal an increased likelihood of commutation failure occurrence at the remaining inverter.

8.3 ROBUSTNESS AGAINST REMOTE AC-FAULT

A single-phase as well as a three-phase fault was applied at the two inverter buses in all three multi-infeed alternatives with the view to compare their robustness against these faults. The duration of both faults is 200 ms (10 cycles) and they are applied at one inverter bus at a time. The faults are simulated by connecting a single-phase or a three-phase shunt reactor at each of the ac-inverter buses. This is a standard practice for studies carried out on Transient Network Analysers (TNAs). As indicated in Fig. 8.1, the inverter bus where the fault is applied is referred to as faulty, whereas the nearby inverter bus is referred to as healthy. The minimum value of fault inductance

under which the system remains operating without commutation failure in neither of the two inverters, was identified by trial and error. Any fault with more severity (lower inductance) than this value causes commutation failure. As a low inductance corresponds to a more severe fault, the lower the limiting inductance, the more robust is the scheme.

The inverter's robustness against the remote fault is very sensitive to their extinction angle. Both inverters, in each of the multi-infeed alternatives, are therefore operated at 22 degrees extinction angle γ (γ_{real} in the case of the CCC) so that a meaningful comparison between the alternatives can be made.

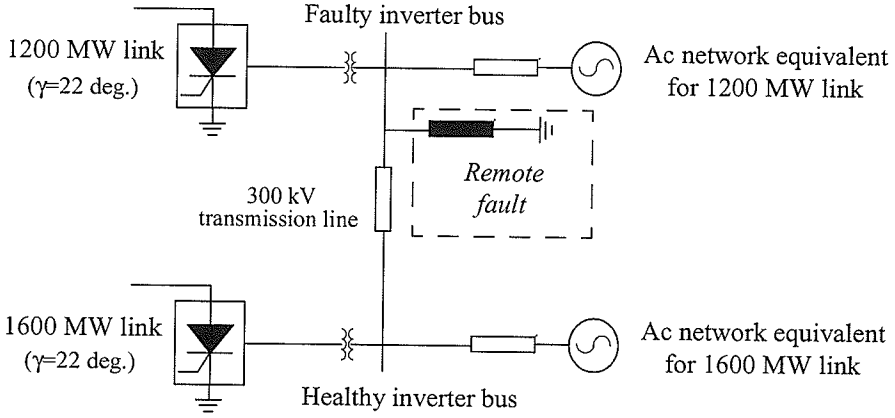

Figure 8.1 A remote fault applied in a multi-infeed HVDC-scheme.

The results for the single-phase remote fault are given in Table 8.2. They indicate, similarly to the single-infeed situation, that the CCC in general demonstrates a lesser degree of robustness against this fault in comparison to the conventional converter.

Table 8.2 Limiting (minimum) inductance simulating a single-phase remote fault.

Distance between inverter terminals	Faulty inverter bus	Multi-infeed HVDC alternative		
		Conventional	Mixed	CCC
Common ac-bus		0.33 H	0.33 H	0.46 H
Transmission line	1200 MW:	0.57 H	0.71 H	0.70 H
	1600 MW:	0.47 H	0.39 H	0.59 H

As pointed out in section 5.3, applying a three-fault remote fault causes the inverter bus voltage to drop in magnitude and to shift the phase angle in the leading direction. Both these effects bring the inverters closer to commutation failure. The CCC demonstrated the smallest change both in terms of voltage amplitude and phase angle, and was therefore more robust against the fault compared to the conventional inverter in the single-infeed situation. Therefore, it is expected that the use of CCC in a multi-infeed scheme would enhance its robustness against three-phase remote faults. The results presented in Table 8.3 clearly indicate that the CCC multi-infeed alternative demonstrates a larger degree of robustness in comparison to the conventional alternative. This is particularly evident when the inverters are connected by a transmission line. This finding is similar to that of the single-infeed situation.

However, the results from the mixed alternative with a common ac bus do not agree with this theory. It has a poorer performance (0.70 H) in comparison to the alternative with both inverters as conventional (0.54 H). One possible explanation for this behaviour is that the different nature of the inverter types results in distortions in their common commutation voltage and thus performance deterioration. The results from the mixed alternative with a transmission line between the inverter terminals are more according to expectation since they are superior or very similar to those of conventional and consistently inferior to those of the CCC alternative.

Table 8.3 Limiting (minimum) inductance simulating a three-phase remote fault.

Distance between inverter terminals	Faulty inverter bus	Multi-infeed HVDC alternative		
		Conventional	Mixed	CCC
Common ac-bus		0.54 H	0.70 H	0.51 H
Transmission line	1200 MW:	1.00 H	0.88 H	0.80 H
	1600 MW:	0.78 H	0.79 H	0.68 H

The addition of the transmission line between the inverter terminals has the effect of lowering the multi-infeed HVDC alternatives' robustness against both types of remote faults.

8.4 RECOVERY FROM CLOSE-IN AC-FAULTS

The recovery performance is investigated when a 50 ms (2.5 cycles) close-in fault is applied at each inverter ac bus in the three multi-infeed alternatives. The fault is first applied at the 1200 MW bus and then at the 1600 MW inverter bus. As indicated in Fig. 8.2, the inverter bus where the fault is applied is referred to as faulty, whereas the neighbouring inverter bus is referred to as healthy. The recovery performance following both a single-phase and a three-phase to ground fault was examined. The recovery time is defined as the time from fault clearing to the instant at which 90 % of the power is restored.

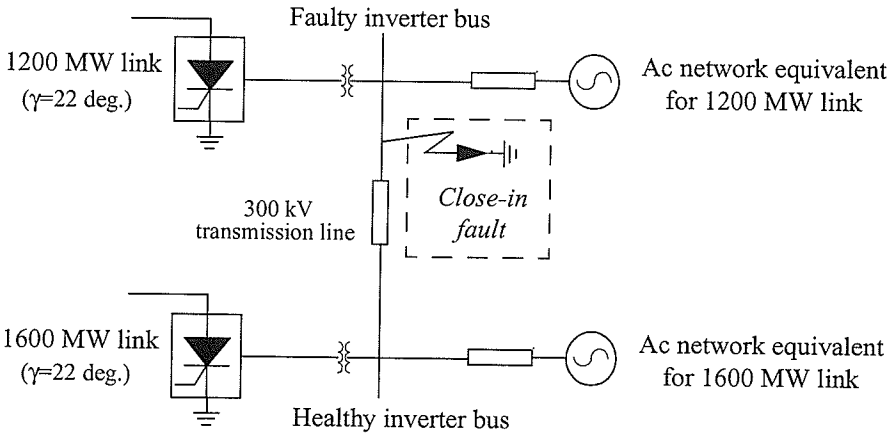

Figure 8.2 A close-in fault applied in a multi-infeed HVDC scheme.

The recovery performance in each multi-infeed alternative for the single-phase and the three-phase faults are reported in Table 8.4 and 8.5 respectively. The included quantities are the transient dc-current peak at the rectifier and the inverter as well as the dc-power recovery time in both dc-links. The results for the healthy dc-link are given in brackets.

First, let us consider the performance of the multi-infeed alternatives when their inverters share a common ac-bus (no interconnecting transmission line). The conventional and CCC multi-infeed alternatives did not require any adjustments in the control settings compared to those in the single-infeed configuration. Their 1200 MW and 1600 MW dc-links therefore demonstrate identical pu-

behaviour to the single-infeed schemes. This holds true for the application of the single-phase as well as the three-phase fault. The dc-links in the conventional multi-infeed alternative recover after 150 ms for both fault types. The corresponding recovery times for the CCC multi-infeed alternative were 245 (single-phase fault) and 90 ms (three-phase fault). The mixed multi-infeed alternative required a few control modifications compared to those of the single-infeed scheme in order to successfully recover from close-in faults. The modification consisted of a reduction of the maximum allowable rate-of-rise of the VDCOL-generated dc-current order in both links. This clearly indicates that the different nature of the inverter types requires a coordinated control design in order to accomplish satisfactory recovery performance. The results for the mixed multi-infeed alternative show that its 1600 MW conventional dc-link recover recovers after 170 ms (single-phase fault) and 165 ms (three-phase fault), which is slightly larger than those of the single-infeed scheme. The 1200 MW CCC dc-link recovers somewhat quicker after the single-phase (210 ms), but slower after the three-phase fault (280 ms) in comparison to the single-infeed scheme.

Table 8.4 Recovery performance for the 1200 MW link (first line) and the 1600 MW link (second line) following a single-phase to ground close-in fault.

Distance between inverter terminals	Fault applied at:	Multi-infeed HVDC alternative *(Dc-current peak at the rectifier/inverter [kA]- recovery time [ms])*		
		Conventional	Mixed	CCC
Common ac-bus		7.9/17.9 kA-150 ms 10.6/23.9 kA-150 ms	4.9/12.5 kA-210 ms 10.8/24.5 kA-170 ms	5.5/17.6 kA-245 ms 7.4/23.4 kA-245 ms
Transmission line	1200 MW bus:	7.9/18.0 kA-150 ms (4.8/23.5 kA-270 ms)	4.8/17.5 kA-205 ms (4.8/23.7 kA-295 ms)	4.7/17.6 kA-190 ms (4.6/16.7 kA-280 ms)
	1600 MW bus:	(3.6/17.6 kA-270 ms) 10.6/24.0 kA-145 ms	(3.4/12.0 kA-295 ms) 10.7/24.1 kA-165 ms	(3.5/11.7 kA-250 ms) 6.5/23.4 kA-190 ms

The recovery performance is somewhat different when the transmission line is included since it introduces a certain impedance between the inverter terminals. It should be pointed out that the mixed and CCC multi-infeed alternatives require control modifications, which are described in full detail in Appendix 10. One important aspect to be realised is that both types of close-in faults

result in commutation failure not only at the faulty inverter, but also at the healthy inverter. In other words, the neighbouring, healthy inverter suffers commutation failure resulting from transient voltage distortions caused by the commutation failure in the faulty inverter. This holds true for both the single- and the three phase fault in all three multi-infeed alternatives under study. The faulty dc-links recover in the 145 to 205 ms range when being subjected to the single-phase fault at their inverter bus. They recover within 145 to 230 ms when the applied fault is of the three-phase type. These recovery times are of the same order as those found in existing HVDC-schemes. Thus, the recovery performance is considered to be acceptable for the faulty dc-links.

Table 8.5 Recovery performance for the 1200 MW link (first line) and the 1600 MW link (second line) following a three-phase to ground close-in fault.

Distance between inverter terminals	Fault applied at:	Multi-infeed HVDC alternative *(Dc-current peak at the rectifier/inverter [kA]- recovery time [ms])*		
		Conventional	Mixed	CCC
Common ac-bus		7.9/18.0 kA-150 ms 10.6/24.1 kA-150 ms	4.3/10.1 kA-280 ms 10.6/24.1 kA-165 ms	4.3/10.5 kA-90 ms 5.8/14.2 kA-90 ms
Transmis-sion line	1200 MW bus:	8.0/18.1 kA-145 ms (10.6/23.9 kA-150 ms)	4.1/10.5 kA-160 ms (4.8/23.8 kA-290 ms)	4.1/10.5 kA-230 ms (4.6/19.6 kA-280 ms)
	1600 MW bus:	(8.0/18.0 kA-150 ms) 10.7/24.1 kA-145 ms	(3.5/11.6 kA-275 ms) 10.6/24.2 kA-160 ms	(3.5/11.6 kA-275 ms) 5.4/14.1 kA-155 ms

It is, however, observed that the voltage at the healthy inverter terminal bus is often not sufficiently suppressed (less than 230 kV) to utilise the adaptive slowing down of the rectifier controls during recovery (described in section 4.4.3). This results in a lowering of the rectifier dc-current but, more importantly, it unfavourably prolongs the recovery. It should, however, be realised that the healthy dc-link in the multi-infeed alternatives recovers in the 250-295 ms range, which is within the internationally accepted 300 ms restoration time [43]. It is, nevertheless, surprising that the healthy dc-link experiences a longer recovery time than the faulty link. The only exception is when the conventional multi-infeed alternative is subjected to a three-phase fault. In this particular case, the voltage reduction at the healthy inverter bus is sufficient in order to enable

the adaptive slowing down of the rectifier controls. The recovery performance of the healthy dc-link was therefore as good as that of the faulty dc-link.

One possible way to achieve a quicker recovery at the healthy dc-link is to use the minimum of the healthy and the faulty inverter bus voltages to enable the adaptive slowing down of the rectifier controls. This strategy will, however, require communication between the inverter terminals, which may be considered unreliable.

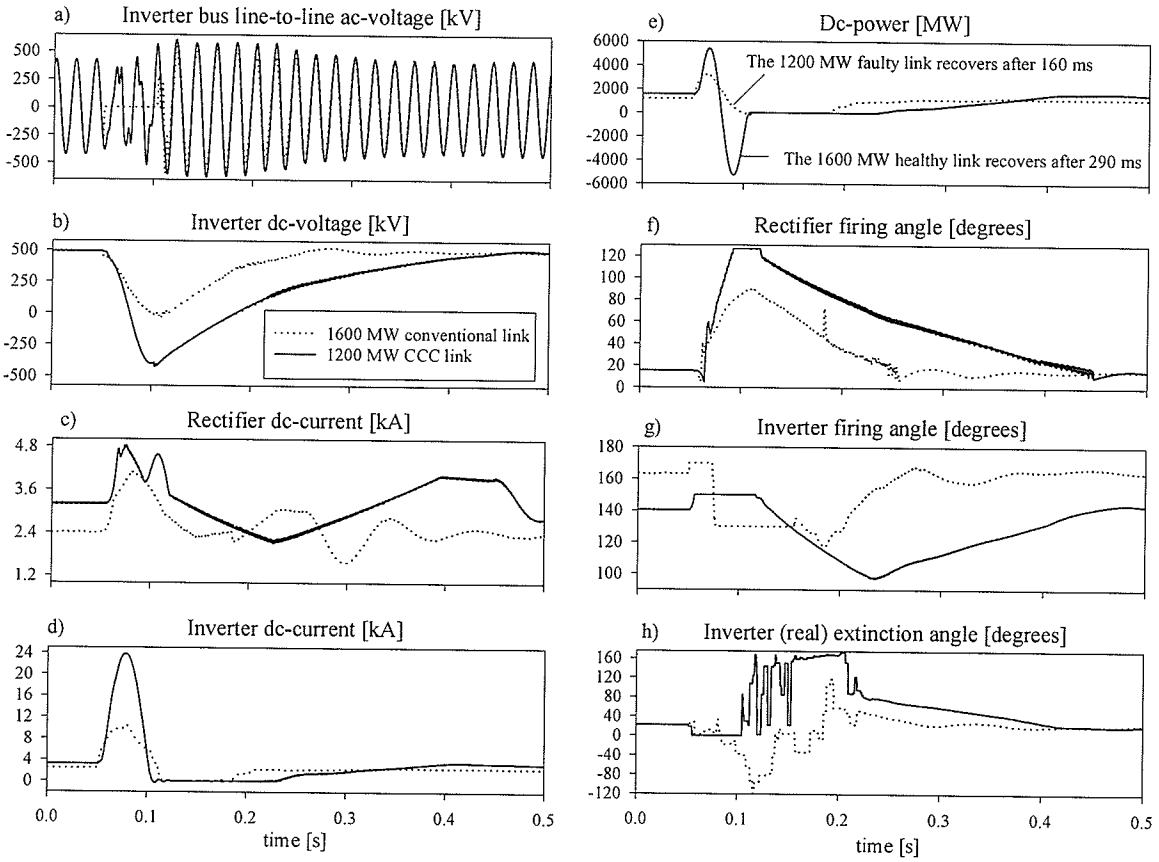

Figure 8.3 Three-phase to ground close-in fault applied at the 1200 MW inverter bus in the mixed multi-infeed HVDC alternative.

Figure 8.3 shows the transient performance of the mixed multi-infeed HVDC alternative when it is subjected to a three-phase close-in fault at the 1200 MW inverter bus. The ac-voltage at the healthy 1600 MW inverter is maintained to a certain extent, although it is suppressed during the fault and it experiences an overvoltage shortly after fault clearing, as seen in Fig. 8.3a. The

1600 MW conventional inverter suffers, nevertheless, commutation failure. Figure 8.3e shows that it has a significantly longer recovery time since the adaptive slowing down of the rectifier control is not utilised. The 1200 MW CCC inverter demonstrates much faster (160 ms) recovery. It may be observed from Fig. 8.3d that the dc-current is considerably smaller at the CCC inverter 10.5 kA (i.e. 4.4 pu) in comparison to the conventional 23.8 kA (i.e. 7.4 pu). This is favourable since it reduces the surge of current into the ac-network.

The conventional multi-infeed alternative demonstrates recovery times of 145-150 ms for the single-phase and three-phase fault. The results from the mixed and CCC alternatives indicate that the presence of the CCC-inverter has the effect of slightly increasing the recovery times. It is also evident that the use of the CCC-inverter demonstrates a lower transient current peak at the rectifier when recovering from single-phase close-in faults. For three-phase faults, the presence of the CCC-inverter has the effect of reducing the current peak not only at the rectifier, but also at the inverter. The results show that a coordinated control design is necessary to achieve satisfactory performance. It is also evident that the electrical distance between the inverter terminals has a significant impact on the optimal control settings.

8.5 SETPOINT CHANGES IN THE CONTROLS

The motivation for the investigation of this particular disturbance, is to examine the multi-infeed HVDC schemes' robustness against step-changes in the control settings. A step-change is made in the ordered dc-current, which essentially means a step-change in the ordered dc-power. A step-increase and -decrease are made at each link individually and then at both links simultaneously when the inverters operate at rated conditions. The results, reported in Table 8.6, present the maximum allowable step-changes that could be made without resulting in commutation failure. It is realised that although step-increases of as high as 72 % may be possible for some alternatives, they may not be applied in practice due to the ceiling in the controls. The purpose here is to

evaluate robustness and the multi-infeed alternative that survives a larger step-change is considered more robust. A generally accepted performance level is that the dc-links should be able to follow a 10 % change in the current order. All the alternatives meet this specification, albeit with varying margins.

The response to the step-change was investigated before any actions take place in the ac network. It should be realised that changes in the network configuration, such as filter tripping and transformer tapping, may eventually be required in order to reach the new permanent operating point.

Table 8.6 Maximum step-increase in the dc-current order.

Distance between inverter terminals	Step-increase applied at:	Multi-infeed HVDC alternative		
		Conventional	Mixed	CCC
Common ac-bus	1200 MW link:	30 %	72 %	40 %
	1600 MW link:	24 %	20 %	28 %
	Both links:	16 %	15 %	23 %
Transmission line	1200 MW link:	21 %	45 %	50 %
	1600 MW link:	20 %	21 %	37 %
	Both links:	16 %	18 %	24 %

A larger percentage step-increase should be possible at the 1200 MW than at the 1600 MW dc-link, due to the inverse linear relationship between dc-power and SCR. The results from all three multi-infeed alternatives agree with this theory both when the inverters share a common ac bus and when they are connected by a transmission line.

The results for the multi-infeed alternatives with a transmission line between the inverter terminals clearly demonstrate that the use of CCC results in a larger allowable step-increase in the dc-current order. This also agrees with the single-infeed situation. The mixed alternative performance is superior to the conventional alternative and inferior to the CCC alternative regardless where the

step-increase is made. For instance, a 45 % step-increase is possible in the 1200 MW dc-link in the mixed multi-infeed alternative, which is a considerably larger than in the conventional option (21 %) but less than in the CCC option (50 %). This finding holds true also when the inverters share a common ac-bus, except in the mixed multi-infeed alternative for step-changes made at the 1200 MW or the 1600 MW link. This may, again, be explained by the different nature of the inverter types results in distortions in their common ac voltage and hence in performance deterioration.

A step-decrease was, similarly to the step-increase, made at the the 1200 MW link, the 1600 MW link or at both links simultaneously. Each multi-infeed alternative allows a 98 or 99 % step-decrease in the current order. During the tuning of the controls, it became clear that the results related to step-decrease are highly dependent on the maximum allowable decrease of the VDCOL-generated current order. The observed performance is considered acceptable since most HVDC-schemes have an operational current order limit of 0.1 pu.

8.6 PERFORMANCE EVALUATION SUMMARY

The main objective in this chapter is to investigate the suitability of CCC-inverters in multi-infeed HVDC-schemes. Their performance which was examined in the preceding sections, is now summarized below.

It is evident that the inverter load rejection overvoltages are significantly reduced due to the presence of CCC-inverters in comparison to the conventional type. This favourable impact can be explained by the lower amounts of Mvar installed in the ac-filters and shunt capacitors at the CCC-inverter bus. It is strictly a steady-state effect and is, thus, independent of the control settings. Larger electrical distance between the inverter terminals confines the overvoltages to a greater extent to the part of the system where the load rejection is applied.

It is important to be aware that the transient behaviour is highly dependent on the control setting as

well as the ac-network configuration. The controls were originally developed and tuned for single-infeed applications. They were thereafter modified for use in the multi-infeed configuration with the view to enhance their transient performance. The evaluation of the multi-infeed alternatives is, thus, based on the particular control settings selected here. Most attention is paid to the configuration where the multi-infeed inverters are connected by a transmission line, since this is considered to be a more realistic application.

With regard to remote faults, the results indicate that the presence of the CCC-inverter worsens the multi-infeed HVDC-scheme's robustness against single-phase faults regardless of electrical coupling between the inverter terminals. The results also indicate that the CCC-inverter in general contributes to improved robustness against three-phase faults. These two findings agree with those of the single-infeed situation. Larger electrical distance between the inverter terminals results in a lesser degree of robustness against both types of remote faults examined here. This trend holds true regardless of which converter type that is employed at the inverter.

The multi-infeed HVDC alternatives demonstrates satisfactory recovery performance following single-phase as well as three-phase close-in faults. The presence of CCC-inverters generally results in slightly longer recovery times in comparison to conventional inverters. The mixed and the CCC multi-infeed alternatives exhibit a lower transient current peak at the rectifier when recovering from close-in faults. For three-phase faults, they demonstrate a reduction of the current peak not only at the rectifier but also at the inverter.

The results for the multi-infeed alternatives with a transmission line between the inverter terminals clearly shows that the presence of the CCC-inverters results in a larger allowable step-increase in the current order.

The results for the mixed multi-infeed alternative with a common ac-bus do not always agree with the conclusions made above. The inconsistent results might arise due to the different dynamic

characteristics of the two inverter types. The mutual interactions between the dc-links are particularly strong when the electrical coupling between their inverter terminals is low. Although considerable control modifications are carried out, which results in excellent performance for some disturbances (i.e. Table 8.6), they did not uniformly improve the performance for all types of disturbances (i.e. Table 8.3).

The presence of the CCC-inverter has a favourable impact on the multi-infeed HVDC scheme's performance when being subjected to inverter load rejections, three-phase remote faults and step-increases in the current order. The surge of current was significantly reduced after the occurrence of a three-phase close-in fault. The only severe deterioration identified was a lower robustness against single-phase remote faults. The results also indicate that the conventional multi-infeed HVDC scheme demonstrates satisfactory performance with proper control settings. This alternative should therefore be particularly interesting if the load rejection overvoltages are not of critical importance due to availability of fast-acting voltage regulating equipment, such as SVCs, located in close proximity to the inverter buses.

Chapter 9

CONCLUDING REMARKS

9.1 CONCLUSIONS

The primary focus in this thesis was originally to evaluate the suitability of the CCC-inverter in a multi-infeed HVDC configuration. It was, however, necessary to investigate several other CCC-related aspects in the process of establishing the electromagnetic transient simulation models required to conduct such a study. The author therefore feels that the work reported in this thesis contains four main contributions including the findings obtained from analysing the multi-infeed HVDC configuration.

- The derivation of an analytical steady-state formulation for the CCC and the implementation of a solution algorithm for this formulation in a computer program.
- The development of two alternative control strategies for long cable HVDC transmission which could be used both for the conventional and CCC-converter type.
- The design of a new ac active filter for use at near-unity-power-factor converters, such as the CCC.
- An evaluation of the suitability of the CCC-inverter in a multi-infeed HVDC scheme.

These contributions will be elaborated on in the following.

Analytical steady-state formulation for the CCC:

This thesis derives an analytical steady-state formulation for the CCC and implements a solution algorithm for this formulation in a Fortran-program. The program can be used to compare the steady-state behaviour of the conventional and the CCC converter types when they operate in various control modes. It is evident from the results that the CCC has both a larger maximum

available power transfer capability and a larger dc-current stability limit in comparison to the conventional converter in the constant power control mode.

The development of two new control strategies for long cable HVDC-transmission:

The traditional control strategy, with the rectifier operating in current control and the inverter operating in extinction angle control, was found unsuitable in long cable (600 km) HVDC transmission. Two new control strategies were developed in order to handle the unique characteristics of the large cable capacitance. The first option uses voltage control at the rectifier and current control at the inverter, whereas the second utilises current control at the rectifier and voltage control at the inverter. The suitability of CCC-inverters in a long cable HVDC-scheme was examined when operated by each of the two control options developed. The results indicated that the CCC-option demonstrates the better performance when subjected to various disturbances with the exception of single-phase remote and close-in faults. The presence of the CCC resulted in a significant reduction of surge of current into the ac-network after the application of a three-phase fault. It was also evident that the first control option (voltage control at the rectifier and current control) at the inverter resulted, although not uniformly, in the better performance.

The design of a new ac active filter for the CCC:

The ac-filters at near-unity-power-factor converters, such as the CCC, have a narrow bandwidth and which makes them sensitive to de-tuning effects. They therefore require some mechanism of on-line tuning to ensure satisfactory filtering performance during frequency drift or when component values change due to e.g. aging. An active filter, based on a voltage source converter using IGBTs as switching devices, was designed to target the most significant lower order characteristic harmonics (e.g. 11th and 13th). The active filter's topology, controls and coupling filters to the ac-network were developed in detail. The operation of the active filter was demonstrated at a 1200 MW CCC-inverter bus using electromagnetic transient simulation. No

adverse interactions between the active filter and the HVDC-controls were revealed. The application of the active filter at the CCC-inverter's ac bus did not significantly change its transient performance. The proposed filter should therefore be attractive in the view of the expected application of near-unity-power-factor converters in the future.

Evaluation of the CCC-inverter for use in a multi-infeed HVDC-scheme:

The suitability of CCC-inverters in a network configuration was evaluated in a multi-infeed HVDC-scheme where two long cable dc-links terminate in a weak ac-network. With this objective, the scheme's transient performance was investigated following the occurrence of various faults and disturbances. The results indicate that the presence of the CCC-inverter has a favourable impact on the performance when being subjected to inverter load rejections, three-phase remote faults and step-increases in the dc-current order. The scheme demonstrated, however, a lesser degree of robustness against single-phase remote fault. With regard to close-in faults, the use of the CCC did not uniformly enhance the performance. The surge of current into the ac-network after the occurrence of a three-phase fault was favourably reduced, whereas the recovery times for both the single- and three phase-fault were generally somewhat longer.

Any event that transiently lowers the inverter ac-voltage results in a surge of current into the ac-network when the large dc-cable capacitance discharges. The presence of the CCC-inverter in long cable HVDC-schemes was therefore believed to be very favourable, because its series capacitors act like a current-dependent voltage source. These capacitors will contribute to maintain the commutation voltage when such events takes place, which would limit the surge of current into the ac-network. The results obtained, both from the single- and multi-infeed configuration, agree with this theory for three-phase remote and close-in faults. It is, however, evident that this does hold true only for three-phase faults and not for single-phase faults. The CCC-inverter demonstrates, for instance, a lesser degree of robustness against single-phase remote faults. These findings indicate

that the proper commutation of the thyristor valves in the CCC is sensitive to imbalances between its series-capacitor voltages. The series capacitors, thus, appears to introduce additional dynamics which, though favourable for balanced conditions, are adverse in the presence of major asymmetrical disturbances such as single-phase faults. Further investigations are therefore needed in order to examine this aspect.

Finally, it should be noted that both the single-infeed and the multi-infeed long cable HVDC schemes demonstrated satisfactory performance regardless of the converter type employed at the inverter. Therefore, the conventional option also appears to be a feasible converter topology for use in long cable HVDC transmission, particularly if the higher load rejection overvoltages are not of critical importance, due to the presence of fast-acting voltage regulating equipment such as SVCs.

9.2 FURTHER RECOMMENDATIONS

The study of the single-infeed and the multi-infeed HVDC configurations were conducted with the assumption of certain conditions in the receiving ac-network. Recommendations for a more extensive study of the suitability of the CCC-inverter in these type of applications are outlined in the following.

The control strategies presented for use in long cable HVDC-transmission were developed and tuned for weak inverter ac-network (SCR=2.05). It would be of interest to examine both the single-infeed and the multi-infeed HVDC configuration with different levels of SCRs for the two inverter networks.

The impact of the presence of fast-acting voltage regulating devices close to the multi-infeed HVDC inverter terminals is another aspect that deserves attention. It is anticipated that this will reduce the interactions between the dc-links resulting from voltage fluctuations in the inverter commutation voltages.

The multi-infeed HVDC alternatives were examined without any significant power flow in the transmission line between the inverter terminal buses. The study could be extended to examine how various loading levels in this transmission line will affect the performance of the multi-infeed HVDC-schemes.

Uni-directional power flow was assumed in both dc-links in the multi-infeed HVDC-schemes due to the situation in the Norwegian grid. It would be of interest to investigate a situation where one link is importing and the other is exporting power from the ac-network. Such a study requires substantial modifications in the controls so that bi-directional power flow is allowed.

The presence of the CCC-inverter resulted in performance deterioration for both the single- and multi-infeed HVDC configuration when being subjected to single-phase faults. It is believed that this vulnerability is due to imbalances or dc-components in the series capacitor voltages due to dc-components. One possible way to improve the CCC-performance is to introduce some mechanism of continuous tuning to minimise these imbalances by slightly adjusting the firing for the valves.

Finally, a theoretical study of the likelihood of commutation failure occurrence in the CCC resulting from unbalanced- and balanced voltage reductions, could be conducted. Such a study could be similar to that already presented for the conventional HVDC converter [29].

REFERENCES

[1] E. W. Kimbark, "*Direct current Transmission*", Vol. 1, John Wiley & Sons, Inc. 1971.

[2] J. Arrilaga, "*High Voltage Direct Current Transmission*", Peter Peregrinus Ltd., London, UK, 1983.

[3] N. Mohan, T.M. Undeland, W.P. Robbins, "*Power Electronics: Converters, Applications and Design*", John Wiley & Sons, Inc. 1989.

[4] P. Kundur, "Power system stability and control", McGraw-Hill, Inc. 1994.

[5] A.R. van C. Warrington, "Protective Relays, their theory and practice", Vol. 2, Chapman and Hall, 1969, p. 151.

[6] W. Skene, "*Delusions of power - Vanity, folly and the uncertain future of Canada's hydro giants*", Douglas & McIntyre Ltd., Vancouver, British Columbia, Canada, 1997.

[7] F. Busemann, "*Economic Supply of Reactive Power for Inverter Stations*", Direct Current, June 1954, pp. 8-15.

[8] V.P.L. Bakharerski and A.M. Utevski, "*A Circuit for 2 Stage Artificial Commutation of an Inverter*", Direct Current, June 1957, pp. 153-159.

[9] J. Reeve, J.A. Baron and G.A. Hanley, "*A Technical Assessment of Artificial Commutation of HVdc Converters*", IEEE Trans. PAS, Vol. PAS-87, No. 10, pp. 1830-1840, Oct. 1968.

[10] V.K. Sood and J.P. Bowles, "*Forced Commutated HVDC Inverters*", Paper prepared for presentation at the System Planning & Operating Section CEA Spring Meeting, March 1979, Vancouver.

[11] A.M. Golé and R.W. Menzies, "*Analysis of Certain Aspects of Forced Commutated HVdc Inverters*", IEEE Transactions PAS, Vol. PAS-100, No. 5, pp. 2258-2262, May 1981.

[12] T. Jonsson and P. Björklund, "*Capacitor Commutated Converters for HVDC*", Proc. of the Int'l Symp. on Electric Power Engineering, Stockholm Power Tech, pp. 44-51, June 1995.

[13] K. Sadek, M. Pereira, D.P. Brandt, A.M. Golé, A. Daneshpooy, "*Capacitor Commutated Converter Circuit Configurations For Dc Transmission*", IEEE Transactions on Power Delivery, Vol. 13, No. 4, pp. 1257-1264, October 1998.

[14] J.D. Ainsworth, A. Gavrilovic and H. L. Thanawala, "*Static and synchronous Compensators for DC Transmission connected to Weak AC systems*", Paper 31-0, Cigré General Session 1980, Paris, France.

[15] A. E. Hammad, K. Sadek and J. Käuferle,"*A New Approach for the Analysis of and Solution of DC Voltage Stability Problems at HVDC terminals*", Proceedings of International Conference on DC Power Transmission, pp. 164-17, June 4-8 1984, Montréal, Canada.

[16] B. Frankén and G. Andersson, "*Analysis of HVDC converters connected to weak AC-systems*", *IEEE Transactions on Power Systems*, Vol. 5, No. 1, pp. 235-242, February 1990.

[17] O.B. Nayak, "*Dynamic performance of static and synchronous compensators at an inverter bus in a very weak AC-system*", Ph.D.-thesis at the University of Manitoba, Canada, 1993.

[18] O.B. Nayak, A.M. Golé, D.G. Chapman and J.B. Davies, "*Control Sensitivity Indices for Stability Analysis of HVdc Systems*", *IEEE Transactions on Power Delivery*, Vol. 10, No. 4, October 1995.

[19] A.M. Gole, V.K. Sood and L. Mootoosamy, "*Validation and Analysis of a Grid Control System using d-q-z Transformation for Static Compensator Systems*", Canadian Conference on Electrical & Computer Engineering (Congrès Canadien en génie Électrique et Informatique), Proceedings pp. 745-748, Montréal, PQ, Canada, September 17-20, 1989.

[20] D.L.H. Aik and G. Andersson, "*Voltage stability analysis of multi-infeed HVDC systems*", IEEE Transactions on Power Delivery, Vol 12, No. 3, July 1997.

[21] D.L.H. Aik and G. Andersson, "*Power stability analysis of multi-infeed HVDC systems*", IEEE Transactions on Power Delivery, Vol 13, No. 3, July 1998.

[22] CIGRE WG 14.30, "*Guide to the specification and design of ac filters for HVDC systems*", *1998.*

[23] M. Pereira and K. Sadek, "*Application of Power Active Filters for Mitigation of*

Harmonics", Proceedings of the International Symposium on Electric Power Engineering, Stockholm Power Tech, pp. 219-224, June 1995.

[24] C. Wong, N. Mohan, S.E. Wright and K.N. Mortensen, "*Feasibility study of AC- and DC-side active filters for HVDC converter terminals*", IEEE Transactions on Power Delivery, Vol. 4, No. 4, pp. 2067-2075, October 1989.

[25] W. Zhang, G. Asplund, Å. Aberg, U. Jonsson, O. Lööf, "*Active DC-filter for HVDC system - A test installation in the Konti-Skan DC link at Lindome converter station"*, IEEE Transactions on Power Delivery, Vol. 8, No. 3, pp. 1599-1605, July 1993.

[26] A. Plaisant and J. Reeve, "*An Active Filter for AC Harmonics from HVDC Converters - Basic Concepts and Design Principles*", pp. 395-400 Vol. 1, Conference Proceedings, IEEE PES Summer Meeting 1999, Edmonton, Alberta, Canada, July 1999.

[27] F.Z. Peng, H. Akagi and A. Nabe, "*A New Approach to Harmonic Compensation in Power Systems - A Combined System of Shunt Passive and Series Active Filters*", IEEE Transactions on Industry Applications, Vol. 26, No. 6, pp. 983-990, Nov/Dec. 1990.

[28] R. Arora and V.K. Sood, "*Development of EMTP-Based Active Filter Model for Distribution System Studies*", The 11th Canadian Conference on Electrical & Computer Engineering (Congrès Canadien en génie Électrique et Informatique), Conference Proceedings, Vol. 1, pp. 77-80, Waterloo, ON, Canada, May 1998.

[29] C.V. Thio, J.B. Davies and K.L. Kent, "*Commutation failures in HVDC transmission systems*", IEEE Transactions on Power Delivery, Vol. 11, No. 2, April 1996.

[30] O. Gjerde, I. Glende, G. Nilsen, L. Nesse, "*Coordination of power system operation in a competitive power market environment*", CIGRE 1994, 39-204, Paris, France.

[31] T.H. Carlsen, D. Lysheim, T.R. Time, J. Rittiger, W. Schultz, D. Tröger, R. Witzmann, *Feasibility Study for Increased Power Exchange Between Norway and Continental Europe by New HVDC Links*, IEE 6th International Conference on AC and DC Power Transmission, Conference Publication Number 423, pp. 100-105, April/ May 1996.

[32] T. Karlsson and G. Liss, "*HVDC transmissions with extremely long dc cables control strategies*", Proceedings of the International Symposium on Electric Power Engineering, Stockholm Power Tech, pp. 24-29, June 1995.

[33] M. Meisingset, A.M. Golé, R. Burton, T.R. Time, P.O. Eide and R. Fredheim, "*Impact of*

capacitor commutated converters in ac-systems with multiple dc infeed", Proceedings on the 13th PSCC (Power Systems Computation Conference) in Trondheim Norway, Vol. 1, pp. 516-522, June/July 1999.

[34] M. Meisingset, A.M. Golé, R. Burton and T.R. Time, "*Application of Capacitor Commutated Converters in multi-infeed HVDC-schemes*", submitted in March 1999 for publication in IEEE PES Transactions.

[35] A.M. Golé and M. Meisingset, "*An ac active filter for use at Capacitor Commutated HVDC Converters*", submitted in December 1999 for publication in IEEE PES Transactions.

[36] H.P. Lips, "*Aspects of multiple infeed of HVDC inverter stations into a common a.c. system*", IEEE Transactions on Power Apparatus Systems, Vol. 92, pp. 775-779, 1973.

[37] L.X. Bui, V.K. Sood and S. Laurin, "*Dynamic interactions between HVDC systems connected to ac buses in close proximity*", IEEE Transactions on Power Delivery, Vol. 6, No. 1, January 1991.

[38] M. Szechtman et. al.,"*The behaviour of several HVDC links terminating in the same load area*", CIGRE 1992.

[39] J. Reeve and S.P. Lane-Smith, "*Multi-infeed HVDC transient response and recovery strategies*", IEEE Transactions on Power Delivery, Vol. 8, No. 4, October 1993.

[40] X. Jiang and A.M. Gole, "*A frequency scanning method for the identification of harmonic instabilities in HVDC systems*", IEEE Trans. on Power Delivery, Vol. 10, No. 4, Oct. 1995.

[41] NORDEL, "*Annual report 1998*", Statnett SF, Postboks 5192, Majorstua, 0302 Oslo, Norway.

[42] CIGRE SC 14, "*Compendium of HVDC schemes throughout the world*", 1996.

[43] CIGRE Working Group 14.07, IEEE WG 15.05.05, "*Guide for planning DC links terminating at AC systems locations having low short-circuit capacities, Part I: AC/DC interaction phenomena*", pp. 10.1-10.9, June 1992.

[44] Manitoba HVDC Research Centre, "*EMTDC User's Manual*", #400-1619 Pembina Highway, R3T 3Y6, Winnipeg, MB, Canada, 1988.

APPENDICES

APPENDIX 1

GLOSSARY SUMMARY

This appendix gives a brief explanation of some of the technical terms and expressions that are used in this thesis. The main portion of them describes or relates to components and applications in the field of HVDC and power electronics.

- High Voltage Direct Current (HVDC) transmission is normally used to transfer power over long distances, with the dc-connection as either overhead line or cable. The dc current is flowing in one direction only, which is determined by the valves. Most schemes have full control features that permit bidirectional dc power flow. The power flow is controlled by adjusting the dc voltage.
- A rectifier is the converter at the sending end in terms of dc power, whereas an inverter is the converter at the receiving end. Whether a converter is operating as rectifier or inverter, is therefore decided by the direction of the dc-power.
- The monopolar HVDC-scheme has one dc conductor (one pole) and the return current flows through earth or water.

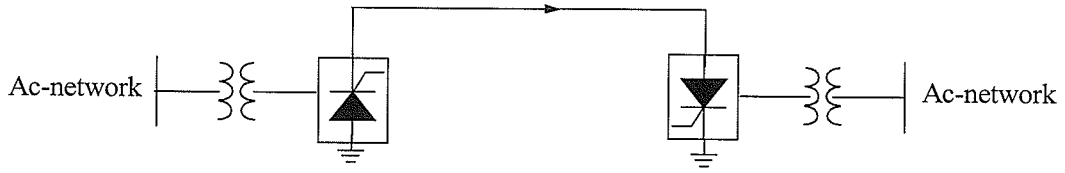

Figure A.1 Monopolar HVDC-scheme.

- A bipolar HVDC-scheme has two dc conductors (one positive pole and one negative pole), which normally operate at equal current. Thus, the total voltage between the conductors is the sum of the voltage across each pole. The earth return current related to each pole will be equal in magnitude but opposite in direction, resulting in zero total earth return current.

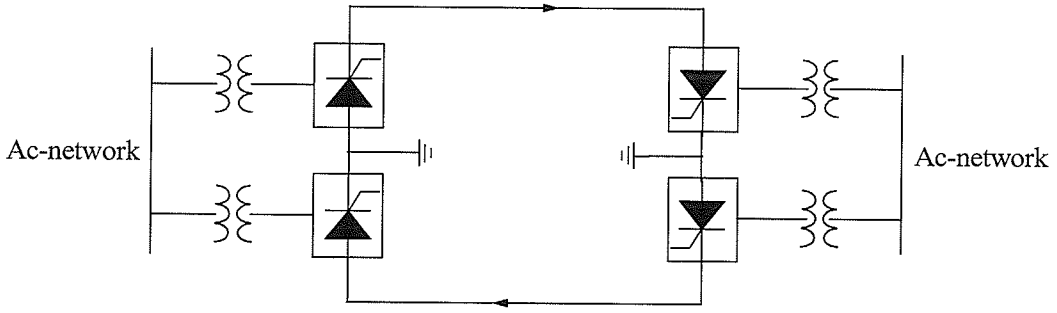

Figure A.2 Bipolar HVDC-scheme.

- Balanced bipolar operation means that the return current flows in the cable.
- One important feature with the HVDC-concept is its ability to connect ac-networks with different frequencies.
- The mercury-arc valve operates similarly to the principles of a vacuum tube except that the mercury in the valve has the capacity of passing high currents with low voltage drop.
- The thyristor valve is a solid-state version of the mercury arc type.
- A valve is consists of several (e.g. 80) series-connected thyristors. There are 6 and 12 valves in a 6 and 12-pulse converter respectively.
- A valve-group consists of 6 valves (two valves in each of the three phases). Thus, a 12-pulse bridge consists of two valve-groups.
- The four valve units in one phase of a 12-pulse converter are normally stacked together vertically to form a *quadruple* valve or a *quadri*-valve. Three quadri-valves constitute a 12-pulse converter.
- Commutation is the process of turning off a thyristor.
- Natural commutation: If the commutation voltage is ac, the thyristor current goes through a natural zero, and a reverse voltage appears across the thyristor. The device is then turned off due to the behaviour of the source voltage. This is known as natural commutation and has been traditionally used in HVDC-schemes.
- Forced commutation: In circuits where the commutation voltage is dc and the forward current of the switching devices is forced to zero and hence turned off by an additional circuit called the commutation circuit. This technique is referred to as forced commutation and is normally applied to dc-dc converters (choppers) and dc-ac converters (voltage source converters). The switching signals may e.g. be generated by the Pulse Width Modulation (PWM)-technique.
- Voltage source converters (VSC) have been applied in FACTS applications such as (Flexible AC Transmission System), STATCOMs (STATic synchronous COMpensator) and UPFCs (Unified Power Flow Controller). The VSC requires switching devices with turn-off capability, such as the IGBT and the GTO. The application of VSC, so-called VSC-transmission, has been introduced also in HVDC transmission in the recent years. The fast development of the switching devices such as the IGBT, has made VSC possible for low power dc-transmission. This makes the concept suitable to supply weak ac-networks such as islands with few rotating machines. Each valve consists of series-connected IGBTs with an anti-parallel diode. The switching devices in VSC-transmission are, contrary to the traditional HVDC topology, forced-commutated.

APPENDIX 2

DERIVATION OF THE STEADY-STATE EQUATIONS FOR THE CCC

The steady-state solution of the CCC shown in Fig. 3.1 may be described by 14 equations and the 18 variables listed below. Four of these unknown variables have therefore to be pre-determined in order to obtain a solution. The solution may be reached by using non-linear equation solving techniques such as the Newton Raphson method. The 14 steady-state equations for the CCC are derived in the following.

LISTING OF THE VARIABLES

I_d, V_d	Dc current and voltage.
$\alpha, \gamma_{app}, \mu$	Firing, apparent extinction angle and overlap angle for the bridge.
$\Delta v_1, \Delta v_2$	Increase in capacitor voltages during the overlap interval for incoming and out-going phase, respectively.
B	Constant resulting from the solution of the overlap differential equation
n	Turns ratio of transformer (primary/valve side)
$V_{lp}\angle 0°$	Transformer primary side ac line-to-line voltage
$I_{ap}\angle\phi_a$	Magnitude and phase of ac current in transformer (primary side)
$I_f\angle\phi_f$	Magnitude and phase of current in ac-filter from the ac-network
$I_s\angle\phi_s$	Magnitude and phase of system current from converter to network
$V_s\angle\delta_s$	Magnitude and phase of network equivalent voltage

LIST OF SYMBOLS

$E = \sqrt{2}V_{lp}/n$	Peak line-to-line voltage on valve side of transformer
L	Transformer leakage inductance (valve side)
C	Commutating capacitance
ω	Angular frequency of the ac source (i.e. $2\pi \times 50$ rad/s)
$\omega_o = 1/\sqrt{LC}$	Angular frequency of oscillation during overlap period
$Z_s = R_s + jX_s$	Ac-network impedance, where R_s and X_s are resistance and reactance, respectively
$Y_f = G_f + jB_f$	Admittance of ac-filters, where G_f and B_f are conductance and susceptance.

Let us consider a 6-pulse CCC converter shown in Fig. A.3, and examine the commutation interval $\omega t=[0,\mu]$ where the *in-coming* valve 3 takes over conduction from the *out-going* valve 1 in the upper part of the bridge. The valves in the converter are numbered in the order of firing. The *in-coming* valve 3 is in the process of igniting whereas the *out-going* valve 1 is extinguishing during the overlap interval. Valve 2 in the lower part of the bridge is conducting alone during the overlap interval. An expression for the current *i* in the off-going valve 1 will first be derived, which will lead to four equations specific for the CCC-converter.

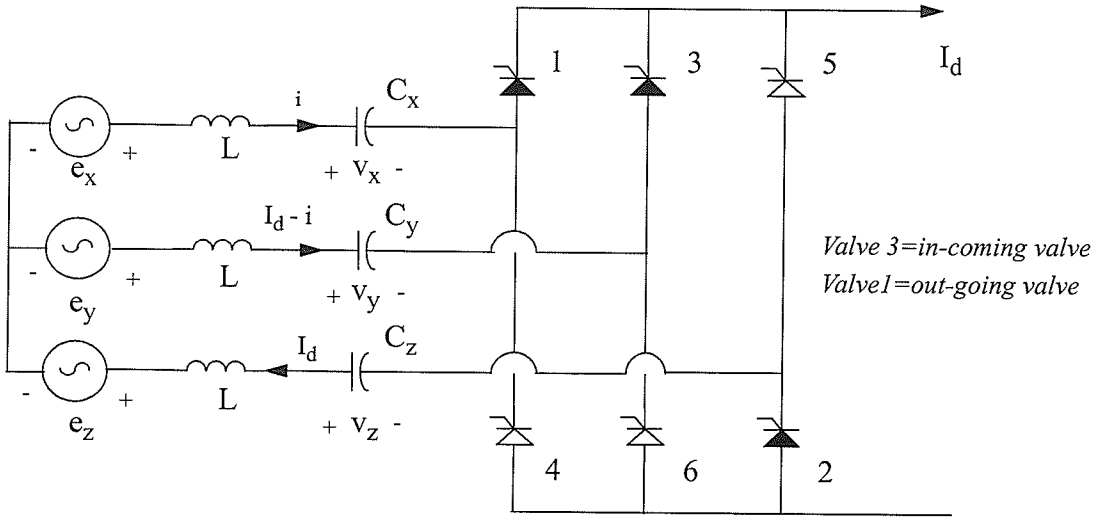

Figure A.3 The circuit during commutation from valve 1 to valve 3.

The initial current during the overlap is thus zero in valve 3 and I_d in valve 1. During the overlap interval, the charging of capacitor C_y and C_x is via currents I_d -*i* and *i*, respectively. Valve 3 is conducting alone in the remaining part of the conduction interval $\omega t=[2\pi/3-\mu]$, and is thereby linearly charging C_y with a slope of I_d/C_y. If we write the equations in terms of $\theta=\omega t$, we obtain for the total charging of capacitor y during turn-on, conduction and turn-off of valve 3:

$$(V_{max}-V_{min}) = \frac{1}{\omega C}\cdot\left[\int_0^{\mu}(I_d-i)d\theta+\int_{\mu}^{\frac{2\pi}{3}} I_d d\theta+\int_{\frac{2\pi}{3}}^{\frac{2\pi}{3}+\mu} i d\theta\right] = 2V$$

We have assumed by symmetry, that the capacitors charge to a maximum/minimum voltage of +V/-V. Evaluating the integral and solving for V, leads to:

$$V = \frac{I_d \pi}{3\omega C} \tag{A.4}$$

Capacitor y in the incoming phase is at voltage -V, whereas the capacitor x in the outgoing phase is at V-Δv_2 at the beginning of the commutating period. During the overlap period, the off-going capacitor x voltage is increased by an amount Δv_2. The in-coming capacitor y is charged from -V to -V+Δv_1, which is followed by a period of linear charging for the remaining of the $2\pi/3$ radians conduction interval. This may be observed in Fig. A.4.

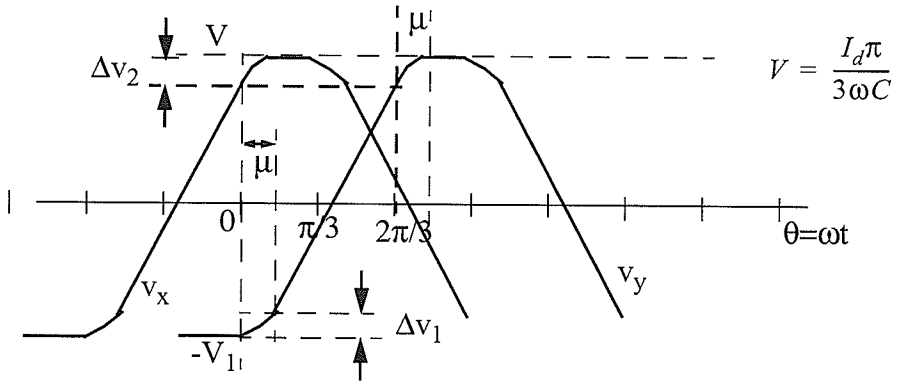

Figure A.4 Voltage waveforms for off-going C_x and on-coming C_y series capacitors.

The current equation during the overlap interval is:

$$e_{yx} = L\frac{d(I_d - i)}{dt} + v_y - \left[L\frac{di}{dt} + v_x\right] = -2L\frac{di}{dt} + v_y - v_x \tag{A.5}$$

where $e_{yx}=E\sin(\omega t+\alpha)$ leads to the following equation at the beginning of the overlap interval, $\omega t=\theta$:

$$E\sin(\omega t+\alpha) = -2L\frac{di}{dt}+\frac{1}{C}\cdot\int_0^{\frac{\mu}{\omega}}(I_d-i)dt+v_y(0)-\left[\frac{1}{C}\cdot\int_0^{\frac{\mu}{\omega}}idt+v_x(0)\right]$$

Taking the derivative of this equation with respect to t, results in:

$$E\omega\cos(\omega t+\alpha) = -2L\frac{d^2i}{dt^2}+\frac{1}{C}\cdot[I_d-i]-\frac{1}{C}\cdot i$$

This leads to the following differential equation:

$$\frac{d^2i}{dt^2}+\frac{1}{LC}\cdot i = \frac{I_d}{2LC}-\frac{E\omega}{2L}\cos(\omega t+\alpha) \qquad (A.6)$$

Solving (A.6), we obtain a solution including initial-condition dependent-constants A and B.

$$i(\omega t) = A\cos(\omega_0 t)+B\sin(\omega_0 t)+\frac{I_d}{2}-\frac{E\omega}{2(\omega_0{}^2-\omega^2)L}\cos(\omega t+\alpha) \qquad (A.7)$$

To determine the constants A and B, we use the initial conditions in the out-going phase capacitor voltage $i(t=0) = I_d$ in (A.7), to get:

$$A = \frac{I_d}{2}+\frac{E\omega}{2(\omega_0{}^2-\omega^2)L}\cos\alpha \qquad (A.8)$$

and the final condition $i(t=\mu/\omega) = 0$ in (A.7), to get:

$$A\cos\left(\frac{\omega_0}{\omega}\cdot\mu\right)+B\sin\left(\frac{\omega_0}{\omega}\cdot\mu\right)+\frac{I_d}{2}-\frac{E\omega\cos(\mu+\alpha)}{2(\omega_0{}^2-\omega^2)L} = 0 \qquad (A.9)$$

Equation A.8 gives directly the value of A, whereas (A.9) is the first of four non-linear equations representing the full solution. To obtain three additional equations related to the overlap interval,

we substitute equation (A.7) into (A.5) and evaluate it at $\omega t=0$, which is the start of the overlap interval. After some re-arrangement and remembering that $v_y(t=0)=-V$ and $v_x(t=0)=V-\Delta v_2$, we obtain:

$$B+\frac{2V-\Delta v_2}{2L\omega_0}+E\sin\alpha\frac{\omega_0}{2(\omega_0^2-\omega^2)L}=0$$

Using (A.4), this second non-linear equation can be re-written as:

$$B+\frac{1}{2\omega_0 L}\left[\frac{2\pi I_d}{3\omega C}-\Delta v_2\right]+E\sin\alpha\left[\frac{\omega_0}{2(\omega_0^2-\omega^2)L}\right]=0 \qquad \text{(A.10)}$$

Equation A.11 is obtained in a similar manner by substituting (A.7) into (A.5), evaluated at the end of the overlap interval $\omega t=\mu$. Using $v_y(t=\mu/\omega) = -V+\Delta v_1$ and $v_x(t=\mu/\omega) = V$, we obtain the third main equation:

$$-A\cos\left(\frac{\omega_0}{\omega}\mu\right)+B\sin\left(\frac{\omega_0}{\omega}\mu\right)+E\cos(\mu+\alpha)\left[\frac{\omega_0}{2(\omega_0^2-\omega^2)L}\right]+\frac{2V-\Delta v_1}{2L\omega_0}=0$$

Using (A.4) again, this third non-linear equation may be re-written as:

$$-A\cos\left(\frac{\omega_0}{\omega}\mu\right)+B\sin\left(\frac{\omega_0}{\omega}\mu\right)+E\cos(\mu+\alpha)\left[\frac{\omega_0}{2(\omega_0^2-\omega^2)L}\right]+\frac{1}{2\omega_0 L}\left[\frac{2\pi I_d}{3\omega C}-\Delta v_1\right]=0 \qquad \text{(A.11)}$$

The fourth equation is obtained by realising that capacitor y initially has a voltage $-V+\Delta v_1$, and after charging linearly for an additional angle $2\pi/3-\mu$, is charged up to $V-\Delta v_2$. Thus:

$$V-\Delta v_2 = -V+\Delta v_1+\frac{1}{\omega C}\int_{\mu}^{\frac{2\pi}{3}} I_d d\theta$$

Using (A.4) once again, gives us the fourth non-linear equation:

$$\Delta v_1 + \Delta v_2 - \frac{I_d \mu}{\omega C} = 0 \qquad \text{(A.12)}$$

The equations A.9-A.12 (or equation 3.1-3.4 in the main report) provide four out of a total of 14 equations required to reach a solution. The four additional equations derived in the following.

The average dc-voltage in a cycle may be calculated by averaging the instantaneous dc-voltage over a interval of $\pi/3$ radians, as it is known that its waveform repeats itself six times in each cycle. The network phase voltages are chosen so that $\theta=\alpha$ corresponds to the firing instant of valve 3, which require the following voltages:

$$e_x(\theta) = \frac{E}{\sqrt{3}} \cdot \cos(\theta + \alpha + \pi/3),\ e_y(\theta) = \frac{E}{\sqrt{3}} \cdot \cos(\theta + \alpha - \pi/3) \text{ and}$$

$$e_z(\theta) = \frac{E}{\sqrt{3}} \cdot \cos(\theta + \alpha - \pi)$$

The $\pi/3$ radians interval consists of the commutation interval μ (where the on-coming valve 3 takes over conduction from the off-going valve 1), and the remaining $\pi/3$-μ interval (where valve 3 conducts alone). Valve 2 in the lower part of the bridge has already been conducting for $\pi/3$ radians, when valve 3 in the upper part of the bridge is fired and starts igniting at $\theta=\alpha$.

During the overlap interval $\theta \in [0, \mu]$, the instantaneous dc-voltage $V_{d\mu}$, may be expressed as:

$$V_{d\mu} = \frac{1}{2}\left[\left(e_y - L\frac{d(I_d - i)}{dt} - v_y\right) + \left(e_x - L\frac{di}{dt} - v_x\right)\right] - \left[e_z - L\frac{d(-I_d)}{dt} - v_z\right]$$

The instantaneous dc-voltage potential at the upper part of the bridge may be expressed either by the in-coming phase or the out-going phase. However, in order to make the calculation of $V_{d\mu}$

more convenient to solve, these two expressions are added together and then divided by two.

$$V_{d\mu} = \frac{e_y + e_x}{2} - \frac{[v_y + v_x]}{2} - e_z + v_z \text{ where}$$

$$v_y(\theta) = -\frac{I_d\pi}{3\omega C} + \frac{1}{\omega C}\int_0^{\theta}(I_d - i)d\theta \text{ and } v_x(\theta) = \frac{I_d\pi}{3\omega C} - \Delta v_2 + \frac{1}{\omega C}\int_0^{\theta} id\theta$$

$$v_z(\theta) = -\left[-\frac{I_d\pi}{3\omega C} + \Delta v_1 + \frac{I_d}{\omega C}\left(\frac{\pi}{3} - \mu\right) + \frac{I_d}{\omega C}\cdot\theta\right] = -\left[\frac{I_d}{\omega C}\cdot\theta - \Delta v_2\right] \text{ result in:}$$

$$V_{d\mu}(\theta) = \frac{E}{\sqrt{3}}\cdot\frac{\cos(\theta+\alpha)}{2} - \frac{1}{2}\left[-\Delta v_2 + \frac{I_d\theta}{\omega C}\right] - \left[\frac{E}{\sqrt{3}}\cdot\cos(\theta+\alpha-\pi)\right] - \left[\frac{I_d}{\omega C}\cdot\theta - \Delta v_2\right]$$

$$V_{d\mu}(\theta) = \frac{E\sqrt{3}}{2}\cos(\theta+\alpha) + \left[\frac{3}{2}\Delta v_2 - \frac{3}{2}\frac{I_d}{\omega C}\cdot\theta\right]$$

The instantaneous dc-voltage, V_{dcon}, in the conduction interval $\theta \in [\mu, \pi/3]$ where valve 3 conducts alone in the upper part of the bridge:

$$V_{dcon} = \left[e_y - L\frac{dI_d}{dt} - v_y\right] - \left[e_z - L\frac{d(-I_d)}{dt} - v_z\right] = e_y - e_z - v_y + v_z$$

$$v_b(\theta) = \left[-\frac{I_d\pi}{3\omega C} + \Delta v_1 + \frac{I_d(\theta-\mu)}{\omega C}\right] = \frac{I_d}{\omega C}\left(\theta - \frac{\pi}{3}\right) - \Delta v_2$$

$$V_{dcon}(\theta) = \frac{E}{\sqrt{3}}\cdot\left[\cos\left(\theta+\alpha-\frac{\pi}{3}\right) - \cos(\theta+\alpha-\pi)\right] - \left[\frac{I_d}{\omega C}\left(\theta - \frac{\pi}{3}\right) - \Delta v_2\right] - \left[\frac{I_d}{\omega C}\cdot\theta - \Delta v_2\right]$$

$$V_{dcon}(\theta) = \left[\frac{E\sqrt{3}}{2}\cdot\cos(\theta+\alpha) + \frac{E}{2}\cdot\sin(\theta+\alpha)\right] + \left[\frac{I_d}{\omega C}\left(\frac{\pi}{3} - 2\theta\right) + 2\Delta v_2\right]$$

The dc-voltage is calculated by averaging the expressions for the instantaneous dc-voltage over the $\pi/3$ radians overlap and conduction interval, which were derived above.

$$V_d = \frac{1}{\pi/3}\left[\int_0^{\mu} V_{d\mu}(\theta)d\theta + \int_{\mu}^{\pi/3} V_{dcon}(\theta)d\theta\right]$$

which results in:

$$V_d = \frac{3E}{\pi}\cdot\left[\frac{\cos\alpha + \cos(\alpha+\mu)}{2}\right] + \frac{3}{\pi}\cdot\left[(\Delta v_2 - \Delta v_1)\cdot\left(\frac{\pi}{3} - \frac{\mu}{4}\right)\right]$$

The first term in the equation above is identical to the expression for the dc-voltage in a conventional converter. There are two contributions from the series capacitance having an impact on the dc-voltage; the most significant one is represented in the first term because the capacitance lowers the overlap angle μ and thereby increases the dc-voltage. The contribution from the second term is negligibly small and is caused by a difference between the charging of the in-coming capacitor Δv_1 and the out-going capacitor Δv_2 during the overlap interval. This gives the next equation in the analytical formulation.

$$-V_d + \frac{3}{\pi}\cdot\frac{\sqrt{2}V_{lp}}{n}\cdot\left[\frac{\cos\alpha + \cos(\alpha+\mu)}{2}\right] + \left[\frac{3}{\pi}(\Delta v_2 - \Delta v_1)\cdot\left(\frac{\pi}{3} - \frac{\mu}{4}\right)\right] = 0 \qquad \text{(A.13)}$$

Equation A.14 is also valid for the conventional inverter, and simply gives the relationship between the amplitude of the ac-current at the transformer primary side and the dc-current.

$$nI_{ap} - \frac{\sqrt{6}}{\pi}I_d = 0 \qquad \text{(A.14)}$$

Equation (A.15) is also identical to the one valid for a conventional inverter.

$$\cos\phi_a + \frac{\cos\alpha}{2} + \frac{\cos(\alpha+\mu)}{2} = 0 \qquad \text{(A.15)}$$

Equation (A.16) is simply the well-known knowledge that the firing angle, overlap and the apparent extinction angle in each cycle adds up to π.

$$\pi - \alpha - \mu - \gamma_{app} = 0 \qquad \text{(A.16)}$$

The remaining 6 equations of the 14 required, are established by simply applying Ohm's Law on the circuit on the primary side of the transformer.

$$V_{lp} - V_s - \sqrt{3}Z_s I_s = 0 \qquad \text{(A.17)}$$

$$I_s - I_{ap} + I_f = 0 \qquad \text{(A.18)}$$

$$\frac{V_{lp} Y_f}{\sqrt{3}} - I_f = 0 \qquad \text{(A.19)}$$

where Z_s and Y_f are the ac-network impedance and the ac-filter admittance, respectively. The equations A.17-A.19 involve complex quantities, so each of them may be re-written as one real and one imaginary equation.

With these last six equations, there are in total fourteen equations established. Four of the 18 variables have to be pre-determined in order to reach a solution. The final problem involves then 14 unknown variables and 14 equations, which may be solved by a using a non-linear iterative technique, such as the Newton Raphson method.

To calculate the real extinction angle, we must record the angle γ_{real} from valve turn-off $\theta=\mu$ to the positive zero-crossing of the forward voltage across that valve. Considering the anode-cathode voltage across the off-going valve x after turn-off, this gives:

$$V_{AK}(\theta = \gamma_{real}) = -e_{yx} + v_y - v_x = 0$$

$$-E\sin(\gamma_{real} + \mu + \alpha) + \left[-V + \Delta v_1 + \frac{I_d \gamma_{real}}{\omega C}\right] - V = 0$$

Using (A.4) again and re-arranging the equation, we get:

$$\frac{\sqrt{2}V_{lp}}{n}\sin(\alpha + \mu + \gamma_{real}) + \frac{2\pi I_d}{3\omega C} - \Delta v_1 - \frac{I_d \gamma_{real}}{\omega C} = 0 \qquad \text{(A.20)}$$

APPENDIX 3

TECHNICAL DATA FOR THE 800 MW CCC-APPLICATION

V_{dbase}=500 kV	Rated dc-voltage at the converter
I_{dbase}=1.6 kA	Rated dc-current at the converter
V_{lpbase} = 300 kV	Rated primary side ac line-line voltage
V_{lbase} = 364 kV	Rated secondary side ac line-line voltage
SCR = 1.82 $\angle -75°$	Short Circuit Ratio
$Z_s = \frac{[V_{lpbase}]^2}{\lvert V_{dbase}\rvert \cdot \lvert I_{dbase}\rvert \cdot SCR}$	Impedance in system equivalent
R_s = 15.998 Ω	Resistance in the RL-type network equivalent
X_s = 59.707 Ω	Reactance in a RL-type network equivalent
TMVA = 850 MVA	Transformer MVA rating
$L = \frac{([V_{lbase}]^2 \cdot L_{pu})}{TMVA \cdot \omega}$ = 74.42 mH	Transformer leakage inductance as seen from valve /secondary side, where L_{pu} = 0.15 pu.
C = 48 μF	CCC series capacitance
ω = 314.1593 rad/s	Angular frequency of the ac source, $2\pi \cdot 50$ rad/s
$\omega_o = \frac{1}{\sqrt{LC}}$ = 529.096 rad/s	Angular frequency of oscillation during the overlap period
Q_c = 116 or 440 Mvar	Reactive power produced in the ac-filter for the conventional or the CCC option, respectively.
G_f = 0 Mho	Conductance in the ac-filter
$B_f = \frac{Q_f}{[V_{lbase}]^2}$ Mho	Susceptance in the ac-filter

APPENDIX 4

DEFINITION OF SCR AND ESCR

The strength of an ac-network at fundamental frequency is measured in terms of the Short Circuit Ratio (SCR). It is defined as the short-circuit MVA at the converter bus divided by the rated dc-power. A similar concept to the SCR is the Effective Short Circuit Ratio (ESCR), which also takes into account the installed Mvar Qc in the filters and any shunt capacitors at the converter bus. The filters are capacitive at fundamental frequency and have therefore the effect of increasing the load rejection overvoltage.

$$\frac{MVA_{ESCR}}{P_{dc}} = \frac{MVA_{SCR}}{P_{dc}} - \frac{Q_c}{P_{dc}} \tag{A.21}$$

$$\text{or} \quad ESCR = SCR - \frac{Q_c}{P_{dc}} \tag{A.22}$$

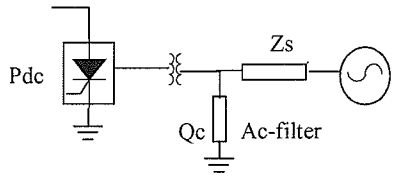

Figure A.5 Simple HVDC-scheme connected to an ac-network equivalent.

The ac-network equivalent Z_s is inversely proportional to the SCR. A network with an SCR smaller than 2.5 is considered to be a weak system. The damping angle at fundamental frequency is assumed to be 75 degrees, which means that Z_s is highly inductive.

$$Z_s = \frac{V_{lp}^2}{P_{dc} \cdot SCR} \tag{A.23}$$

APPENDIX 5

HVDC-CONNECTIONS BETWEEN SCANDINAVIA AND CENTRAL EUROPE

Table A.1 Existing HVDC-connections.

HVDC-links	Rated voltage [kV]	Transmission capacity [MW]	Total length of line [km]	Of which cable [km]	Commissioning year
KontiSkan 1 *Sweden-Jutland, Denmark*	250	270-290	176	88	1965
Skagerak 1 *Norway-Jutland, Denmark*	250	270	240	127	1976
Skagerak 2 *Norway-Jutland, Denmark*	250	270	240	127	1977
KontiSkan 2 *Sweden-Jutland, Denmark*	285	360-380	149	87	1988
Skagerak 3 *Norway-Jutland, Denmark*	350	500	240	127	1988
Baltic Cable *Sweden-Germany*	450	600	250	220	1994
Kontec *Zealand, Denmark-Germany*	400	600	166	166	1996

Most of the data in Table A.1 and Table A.2 are obtained from [41,42]. It should be pointed out that there is some uncertainty related to the commission dates for the planned connections between Norway and Germany/the Netherlands.

Table A.2 Planned HVDC-connections.

HVDC-links	Rated voltage [kV]	Transmission capacity [MW]	Total length of line [km]	Of which cable [km]	Expected year of commissioning
The SwePol Link *Sweden-Poland*	450	600	252	237	2000
Norway-The Netherlands	400-600	min. 600	ca. 550	ca. 550	ca. 2002
The Great Belt *Zealand-Fyn, Denmark*	400	500-600	70	70	2003
Norway-Germany (bipole)	400-600	min. 2 x 600	ca. 600	ca. 550	ca. 2004

APPENDIX 6

AC-FILTER DESIGN

The filters size and their quality are two basic concepts in filter design. The size of the filter, or its capacitance, is defined as the reactive power that the filter supplies at fundamental frequency. The quality of the filter is a measure of its sharpness of tuning. Filters are classified into two categories; tuned filters and damped filters.

- Tuned filters target a specific frequency or frequencies. They are characterized by a high quality factor which is necessary to achieve a good filtering performance. The drawbacks with these filters include low damping and a narrow bandwidth. The low damping means that the filter needs relatively long time to to reach steady state, whereas the narrow bandwidth makes the filter more sensitive to detuning effects. The filters are also referred to as bandpass or BP filter
- Damped filters provide a low impedance over a range of frequencies and are often used to eliminate higher order harmonics. These are also referred to as highpass or HP filters.

In the ac-filters used at the HVDC converter, single-tuned filters are used to target the lower order harmonics (i.e. 11th, 13th, 23rd and 25th) and a high pass filter is used for removal of higher order harmonics. These two filter types shown in Fig. A.6, are discussed in the following.

Figure A.6 Bandpass and highpass filter topology.

First, the capacitance value (C) is directly obtained from the reactive power (Mvar) that the filter should produce at fundamental frequency (ω_f). Here, the impact from the inductance on the installed Mvar is neglected, which is a reasonable assumption for harmonics of 11th or higher

order. Then, the inductance (L) is determined by the fact that the series-connected inductance and the capacitance should form a low-impedance path at the frequency (ω_r) targeted for elimination. Finally, the resistance (R) is given from the quality-factor that is chosen. This is illustrated in the equations below.

$$C = \frac{Mvar}{V_{ph}^{\ 2} \cdot \omega_f} \ , \ L = \frac{1}{\omega_r^{\ 2} \cdot C} \text{ and } R = \frac{\omega_r \cdot L}{Q} \text{ (BP) or } R = \omega_r \cdot L \cdot Q \text{ (HP)}$$

Figure A.7 plots the impedance for the filters used at the 1600 MW conventional converter as a function of harmonic frequency. The plot includes the bandpass filter targeting the 11th harmonic and the highpass filter with a cut-off frequency at the 36th harmonic. The other bandpass filters (13th, 23rd and 25th) have a similar characteristic as for the 11th plotted here. The bandpass filter has a 29.5 Mvar installed and a 2000 quality-factor, whereas the highpass filter has 34.0 Mvar installed and a 100 quality-factor. The nominal converter bus voltage is 300 kV.

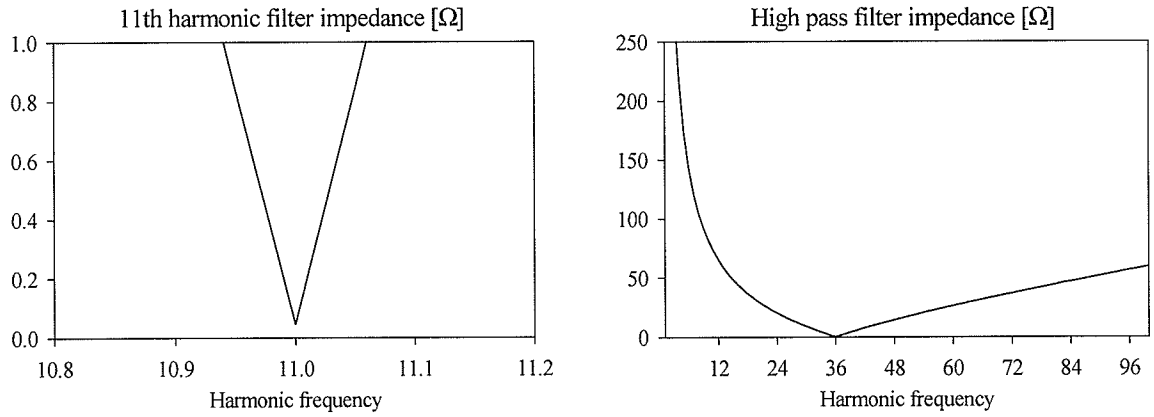

Figure A.7 Filter impedance plot for the bandpass and the highpass filter vs. harmonic frequency.

The relationship between bandwidth, Mvar-installation and filtering performance in the bandpass filter is discussed in the following. The primary task of the bandpass filter is to provide a satisfactory filtering performance under tuned conditions. It is therefore necessary to design a filter with a low impedance (i.e. small resistance) at the harmonic frequency targeted for elimination.

The derivation of the relationship between the installed Mvar and the quality factor/bandwidth for the bandpass filter, is presented in the following.

$$Mvar = V_{ph}^{\ 2} \cdot \omega_f \cdot C \Rightarrow C = \frac{Mvar}{V_{ph}^{\ 2} \cdot \omega_f} \tag{A.24}$$

$$L = \frac{1}{\omega_r^{\ 2} \cdot C} = \frac{1}{\omega_r^{\ 2}} \cdot \left[\frac{V_{ph}^{\ 2} \cdot \omega_f}{Mvar} \right] \tag{A.25}$$

Using the expressions for L and C in (A.24) and (A.25), we then calculate:

$$\sqrt{\frac{L}{C}} = \frac{V_{ph}^{\ 2} \cdot \omega_f}{Mvar \cdot \omega_r} \tag{A.26}$$

which we use to obtain an expression of the quality-factor:

$$Q = \frac{\omega_r \cdot L}{R} = \frac{1}{R} \cdot \sqrt{\frac{L}{C}} = \frac{1}{R} \cdot \left[\frac{V_{ph}^{\ 2} \cdot \omega_f}{Mvar \cdot \omega_r} \right] \tag{A.27}$$

The bandwidth of the filter is the region where its impedance is below $R \cdot \sqrt{2}$, which is the range between the following two frequencies:

$$\omega = \frac{\mp (R \cdot C) + \sqrt{(R \cdot C)^2 + 4 \cdot L \cdot C}}{2 \cdot L \cdot C} \tag{A.28}$$

From (A.28) it may de derived that this bandwidth (Bw) equals ω_r/Q, which clearly shows that a high quality-factor results in a narrow bandwidth. Now we use the relationship between bandwidth and quality-factor to find the expression for bandwidth as a function of installed Mvar in the filter.

$$Bw = \frac{\omega_r}{Q} = R \cdot \left[\frac{Mvar \cdot \omega_r^2}{V_{ph}^{\ 2} \omega_f} \right] \tag{A.29}$$

Let us assume that the resistance (R) is pre-selected in order achieve good filtering performance under tuned conditions. Equation (A.29) shows, under this assumption, that the only way to increase the bandwidth is to increase the reactive power installation (Mvar) in the filter. This is the reason why near-unity-power-factor converters, such as the CCC, need some mechanism of on-line tuning in its tuned filters. It is impossible to achieve the necessary bandwidth simply because of the low amount of Mvar installed in their filters.

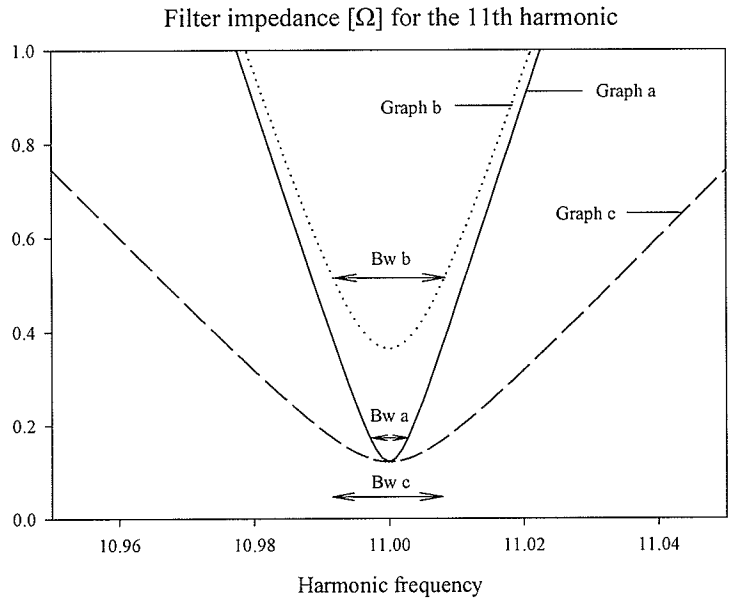

Figure A.8 The bandwidth of a high-pass filter.

Graph a in Figure A.8 shows the impedance plot for the 11th harmonic filter at the 1200 MW CCC inverter. The filter has a 11.25 Mvar reactive power installation and a 2000 quality factor, which results in a relatively narrow bandwidth (Bw a). This makes the filter sensitive to detuning effects and it is thus desirable to increase its bandwidth.

The quality-factor for the filter is now increased by a factor of three, but the Mvar installation is kept constant. This results in a three times larger bandwidth (Bw b) as may be seen in graph b. However, the filter's resistance is now increased (by a factor of three) resulting in a poorer filtering performance at tuned conditions.

The only way to increase the bandwidth and at the same time fulfil its primary task of good filtering at tuned conditions, is to increase the Mvar-installation in the filter. This may be learned from (A.29). Graph c plots the filter impedance in which the installed Mvar is increased by a factor of three and the resistance is kept constant compared to the filter plotted in graph a. This filter has now a wide bandwidth as well as a satisfactory filtering performance at tuned conditions.

APPENDIX 7

AC-NETWORK EQUIVALENTS

Figure A.9 shows the RRL and the RL-equivalents for the ac-network. Their magnitude and phase angle are plotted as a function of frequency in Fig. A.10 and Fig. A.11 respectively. Note that the graphs are plotted in a semi-log scale.

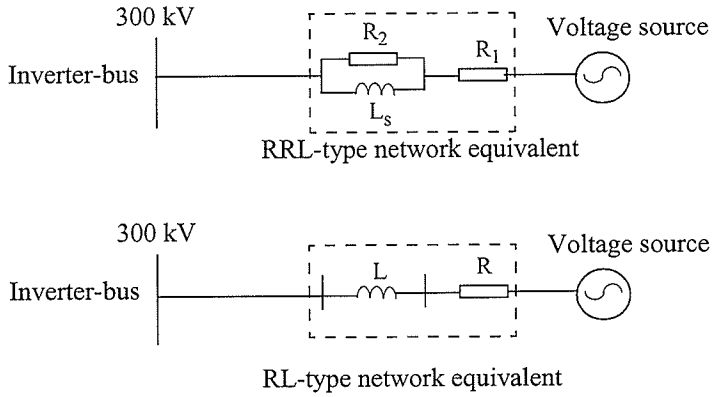

Figure A.9 The RRL and the RL ac-network impedances.

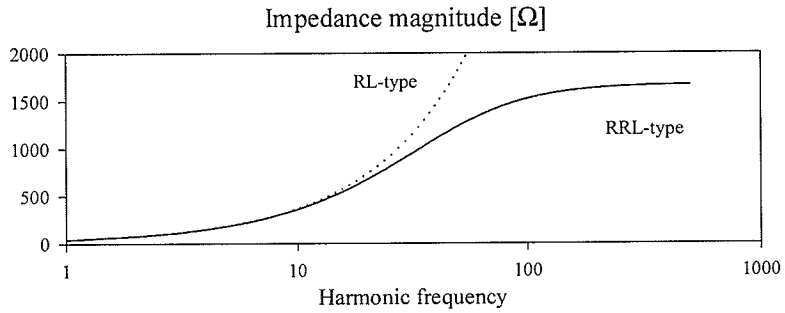

Figure A.10 Impedance magnitude for ac-network equivalent

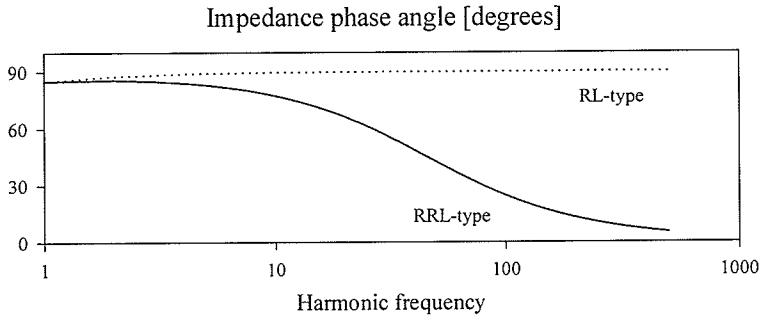

Figure A.11 Impedance phase angle for ac-network equivalent

APPENDIX 8

CONTROL SETTINGS FOR THE SINGLE-INFEED HVDC-SCHEMES

Table A.3 Control parameters using control option 1.

Single-infeed alternative	Rectifier					Inverter		
	Voltage Control		Current Control			Current Control		
	Gain	Time-constant [ms]	Gain	Time-constant [ms]	Current order slopes (up/down) [ms]	Gain	Time-const. [ms]	Current order slopes (up/down) [ms]
Conventional: 1200 MW	0.5	100	2.16	1042	160 /120	0.24	30	160 /120
CCC: 1200 MW	0.5	100	2.88	1042	160 / 25	0.3	40	160 / 25

Table A.4 Control parameters using control option 2.

Single-infeed alternative	Rectifier			Inverter				
	Current Control			Voltage Control		Current Control		
	Gain	Time-constant [ms]	Current order slopes (up/down) [ms]	Gain	Time-const. [ms]	Gain	Time-const. [ms]	Current order slopes (up/down) [ms]
Conventional: 1200 MW	0.86	104.2	106.7 / 25	2	20	0.384	20.83	106.7 / 25
CCC: 1200 MW	2.16	42	120 / 80	2	100	0.7	52	120 / 80

APPENDIX 9

COMPONENT VALUES FOR THE MULTI-INFEED HVDC SCHEMES

Table A.5 Component values in the inverter ac-network equivalent.

Dc-link	R_1	L_s	R_2
1200 MW	2.3926 Ω	0.1161 H	1669.51 Ω
1600 MW	1.794 Ω	0.08705 H	1252.13 Ω

Table A.6 Installed Mvar in ac-filters for each single-infeed scheme.

Dc-links	RLC	HP	Shunt capacitor	Total
1200 MW Conventional	22.1	25.55	106.0 (11.25 μF)	660
1600 MW Conventional	29.5	34.0	141.4 (15μF)	880
1200 MW CCC	11.25	13.0	None	174
1600 MW CCC	15	17.33	None	232

Table A.7 Component values in the dc-cable model.

Dc-power	Resistance [Ω]	Inductance [mH]	Capacitance [μF]
1200 MW	1.5	45	456
1600 MW	1.125	33.75	602.67

Table A.8 Other component values.

Dc-link	Converter transformers (2 units)	Smoothing inductance (One at each end of the dc-link)	Series capacitance (CCC)
1200 MW link	705 MVA	0.4 H	144 μF
1600 MW link	940 MVA	0.3 H	192 μF

APPENDIX 10

CONTROL SETTINGS FOR THE MULTI-INFEED HVDC SCHEMES

Table A.9 presents the controller gains and VDCOL-slopes for the three multi-infeed alternatives with the transmission line between their inverter terminals. The controller gains are identical to those of the single-infeed schemes. The slopes, stated in time-units, limit the maximum allowable rate-of-change (one for increase and one for decrease) of the VDCOL-generated current order. They correspond to the time required to increase the current order from zero to rated value, and similarly to decrease the current order from rated value to zero.

The conventional alternative did not require any adjustments in the VDCOL-slopes compared to those in the single-infeed HVDC scheme. This holds true both when the inverters share a common ac bus and when they are connected by the transmission line.

Table A.9 Control parameters for the three multi-infeed alternatives (including transmission line).

Multi-infeed HVDC alternative	Rectifier					Inverter		
	Voltage Control		Current Control			Current Control		
	Gain	Time-const. [ms]	Gain	Time-constant [ms]	Current order slopes (up/down) [ms]	Gain	Time-const. [ms]	Current order slopes (up/down) [ms]
Conventional: 1200 MW link + 1600 MW link	0.5 0.5	100 100	2.16 2.16	1042 1042	160 / 25 160 / 25	0.24 0.24	30 30	160 / 25 160 / 25
Mixed: 1200 MW CCC link + 1600 MW conv. link	0.5 0.5	100 100	2.88 2.16	1042 1042	100 / 40 200 / 25	0.3 0.24	40 30	200 / 40 200 / 25
CCC: 1200 MW link + 1600 MW link	0.5 0.5	100 100	2.88 2.88	1042 1042	100 / 40 100 / 40	0.3 0.3	40 40	160 / 40 160 / 40

The mixed alternative, on the other hand, required a few modifications when its inverters share a common ac bus in order to successfully recover from close-in faults. It was necessary to reduce the allowable rate-of-rise of the VDCOL-generated current order from 15 to 12 kA/s (1200 MW link) and from 20 to 16 kA/s (1600 MW link). This means that the VDCOL-slopes are increased from 160 to 200 ms. When the transmission line between the inverter terminals were included, the 1200 MW (CCC) links needed further modifications in VDCOL-slopes. The maximum allowable rate-of-decrease in the current order was tripled from 20 to 60 kA/s at both the rectifier and the inverter. As a result, the current order can be reduced from rated value to zero on 40 ms instead of 120 ms. The slope limiting the rate-of-rise in the rectifier's current order was increased from 12 to 24 kA/s. This means that the rectifier's current order is permitted to increase twice (100 ms) as fast as that at the inverter (200 ms).

The CCC multi-infeed alternative also required adjustments in the VDCOL slopes when its inverters are connected through the transmission line. Firstly, the disabling criterion for the adaptive slowing down of the rectifier controls was reduced from 45 to 30 degrees firing angle. This means that the controls are slowed down for a longer interval during recovery. Secondly, the slope limiting the rate-of-decrease was tripled from 20 to 60 kA/s (1200 MW) and from 26.67 to 80 kA/s (1600 MW link). This means that the current order is allowed to decrease from rated value to zero during 40 ms instead of 120 ms. Thirdly, the slope limiting the rate-of-rise in the current order at the rectifiers were increased from 15 to 24 kA/s (1200 MW) and from 20 to 32 kA/s (1600 MW). As a result, the current order at the rectifiers are allowed to increase somewhat faster (100 ms) than at the inverters (160 ms).

APPENDIX 11

RESULTING AC-NETWORK IMPEDANCE FOR MULTI-INFEED HVDC SCHEMES

The resulting ac-impedance, seen from the inverter terminal buses, is plotted for the conventional, the mixed and the CCC multi-infeed HVDC-scheme in Figure A.12 through A.14. This is done in order to illustrate the impact by the presence of the CCC type inverters on the frequency response. It is, however, realised that the conditions for harmonic instability are not present in any of the multi-infeed alternatives, since the dc side does not have an anti-resonant (low impedance) close to the fundamental frequency (50 Hz). The impedance seen from a common ac bus is also included so that the impact of the presence of the transmission line can be visualised.

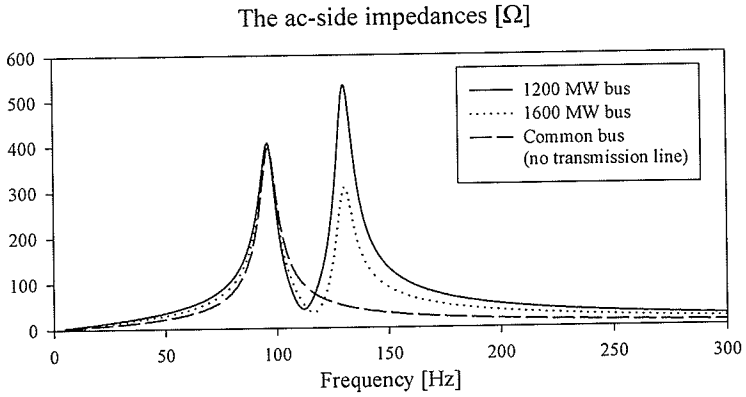

Figure A.12 The conventional multi-infeed HVDC-scheme.

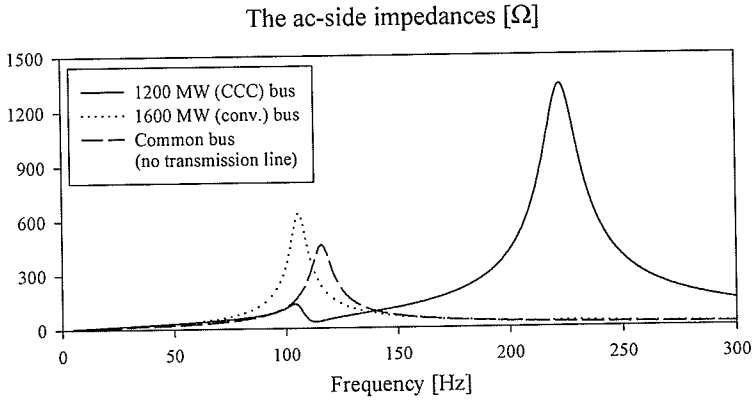

Figure A.13 The mixed multi-infeed HVDC-scheme.

Figure A.12 shows that the conventional multi-infeed alternative has a resonance at about 96 Hz when the dc-infeeds terminate regardless of if the inverter terminal buses are connected by a transmission line or if they share a common ac bus.

The mixed multi-infeed alternative resonates at about 116 Hz with a common inverter bus. The presence of a transmission line between the inverter terminal buses results in resonant frequencies at 104 Hz at the CCC inverter bus and at 106 Hz at the conventional inverter bus. This means that the resonance frequencies have moved closer to the critical second harmonic frequency. The impedance magnitude seen from the CCC inverter bus at the resonance frequency is, however, greatly reduced in comparison to being of the conventional type.

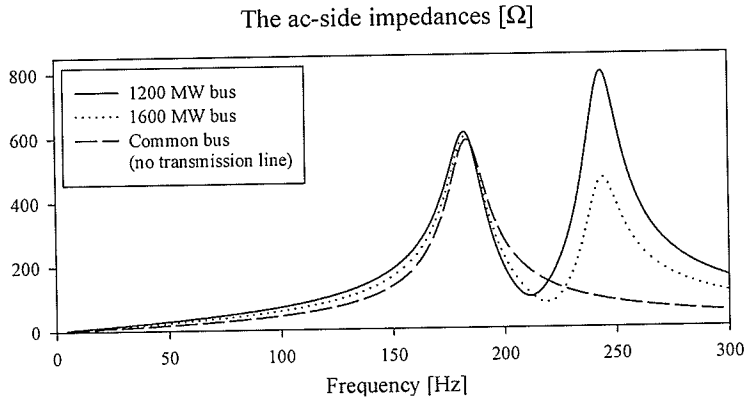

Figure A.14 The CCC multi-infeed HVDC-scheme.

The two inverter terminal buses in CCC multi-infeed alternative have both an impedance resonance at 183 Hz, which is far away from the second harmonic frequency and therefore considered harmless from the harmonic instability standpoint. The presence of the transmission line between the inverter terminals does not significantly move this resonance frequency.

The transmission line introduces an additional resonance at a higher frequency, which is not considered a problem in this context. The conventional and mixed (with transmission line) multi-infeed HVDC-schemes have resonant frequencies very close to the critical second harmonic frequency. The use of CCC in such multi-infeed HVDC schemes has, in general, the effect of

increasing the resonance frequencies at the ac-side impedance. Again, it should be reminded that the conditions for harmonic instability are not present since there is no anti-resonance at fundamental frequency on the dc side.